ISSN Print: 2518-4245
ISSN Online: 2518-4253
Vol. 61(1), March 2024

PROCEEDINGS
OF THE PAKISTAN ACADEMY OF SCIENCES:
A. Physical and Computational Sciences

PAKISTAN ACADEMY OF SCIENCES
ISLAMABAD, PAKISTAN

Proceedings of the Pakistan Academy of Sciences: Part A Physical and Computational Sciences

Proceedings of the Pakistan Academy of Sciences A. Physical and Computational Sciences is the official flagship, the peer-reviewed quarterly journal of the Pakistan Academy of Sciences. This open-access journal publishes original research articles and reviews on current advances in the field of Computer Science (all), Materials Science (all), Physics and Astronomy (all), Engineering Sciences (all), Chemistry, Statistics, Mathematics, Geography, Geology in English. Authors are not required to be Fellows or Members of the Pakistan Academy of Sciences or citizens of Pakistan. The journal is covered by Print and Online ISSN, indexed in Scopus, and distributed to scientific organizations, institutes and universities throughout the country, by subscription and on an exchange basis.

Annual Subscription: **Pakistan:** Institutions, Rupees 8000/-; Individuals, Rupees 4000/- (Delivery Charges: Rupees 300/-)
Other Countries: US$ 200.00 (includes air-lifted overseas delivery)

HEC Recognized; Scopus Indexed

Published by **Pakistan Academy of Sciences**, 3 Constitution Avenue, G-5/2, Islamabad, Pakistan
Email: editor@paspk.org; **Tel:** 92-51-920 7140 & 921 5478; **Websites:** www.paspk.org/proceedings/; www.ppaspk.org

Printed at **Graphics Point.,** Office 3-A, Wasal Plaza, Fazal-e-Haq Road Blue Area Islamabad.
Ph: 051-2806257, **E-mail:** graphicspoint16@gmail.com

PROCEEDINGS OF THE
PAKISTAN ACADEMY OF SCIENCES: PART A
Physical and Computational Sciences

CONTENTS

Volume 61, No. 1, March 2024 **Page**

Research Articles

Submission of Manuscripts: Manuscripts may be submitted as an e-mail attachment at editor@paspk.org or submit online at http://ppaspk.org/index.php/PPASA/about/submissions. Authors must consult the ***Instructions for Authors*** at the end of this issue or at the Website: www.paspk.org/proceedings/ or www.ppaspk.org.

Proceedings of the Pakistan Academy of Sciences: A Physical and Computational Sciences 61(1): 1-10 (2024)

ISSN (Print): 2518-4245; ISSN (Online): 2518-4253
https://doi.org/10.53560/PPASA(61-1)815

Pakistan Academy of Sciences

Research Article

Latent Factors of Sustainable Tourism Practices and Green Hospitality Measures in Gilgit Baltistan, North Pakistan

Muhammad Qasim[1*], Atta-ur-Rahman[1], Takaaki Nihei[2], and Zaheer Ahmed[2]

[1]Department of Geography and Geomatics, University of Peshawar, Pakistan
[2]Urban Environmental Sciences, Tokyo Metropolitan University, Japan

Abstract: The tourism activities and hospitality services are part and parcel to each other; therefore, adaptation of green management within hospitality services is inevitable for development of tourism in sustainable way. The current study therefore determines the factors responsible for development of tourism in sustainable way and green management within hospitality entities throughout Gilgit Baltistan (GB) region. Quantitative data through a structured set of questionnaires is acquired from the registered hospitality units of the study area including hotels and guest houses. Yamane's formula is used to specify the sample size from the targeted population. Following the result of applied formula, 177 hospitality managers out of 499 total registered hospitality units are approached from all the three divisions of Gilgit Baltistan. To determine the latent factors, factor analysis is applied on the data through statistical software. To ensure the appropriateness of the statistical analysis, Kaiser-Mayer-Olkin (KMO) and Bartlett's test is applied initially. KMO sampling adequacy of 0.626 and Bartlett's test of sphericity with most significant value of ($p < 0.001$) endorsed the appropriateness of the proposed analysis. Rotated Components Matrix through Kaiser Normalization concluded seven latent factors with different components of variances including six factors related to hospitality management services. Hence, green management in hospitality is necessary for sustainability in tourism.

Keywords: Factor Analysis, Green Management, Hospitality Units, Quantitative Data, Rotated Matrix.

1. INTRODUCTION

Sustainable tourism encompasses the conservation and expansion of tourism. It addresses the present requirements and needs of both tourists and the local community, with a focus on future sustainability [1]. The conception of sustainability in tourism materialized with the goal of mitigating and minimizing the discouraging effects of tourism activities [2, 3]. This also aims to ensure the satisfaction of both local and international tourists at their destinations. Moreover, itis simultaneously contributing to the improvement of host communities and their income levels. Furthermore, the protection of local traditions and cultural landscapes is considered an essential and integral aspect of sustainable tourism development [4, 5]. The initial framework for sustainable tourism approaches can be categorized through: tourists, hospitality managers, operators and the community [6, 7]. The three initial domains in which sustainable tourism approaches are elucidated are Economy, society and environment [8-10].

The reality as well as integrity of the overall process of sustainable tourism cares all the aspects of nature and anthropogenic involvement through protected travel [11]. The stakeholders' take the course of actions in such a way that the fulfillment of the criteria under the umbrella of sustainable tourism is guaranteed [12]. To make the tourism activities sustainable at the tourists' destinations, the participation of people within the proximity of a destination is given utmost importance in decision making process for the defined domains of sustainable tourism [13, 14]. Sustainability in tourism is the utmost need of the time as this industry has now become second largest industry after petroleum industry world widely [15-17].

Green Hospitality Management (GHM) is an innovative and remarkable progression in the field

Received: May 2023; Revised: December 2023; Accepted: March 2024
*Corresponding Author: Muhammad Qasim <qasimskardu@uop.edu.pk>

of hospitality management, specifically designed to address environmental concerns related to hotel services [18]. GHM incorporates various practices such as the utilization of renewable power possessions, substitute technologies, green services in hospitality, and the implementation of sustainable actions [19]. Additionally, GHM focuses on promoting and utilizing local brands in hospitality services, while also emphasizing the financial benefits associated with such practices [20].

Tourism activities and hospitality management are intrinsically interconnected due to the essential part of hospitality services in facilitating guests at the destinations and making their access to resorts [21, 22]. The arrangement of conveyance, lodging, and food, collectively referred to as hospitality services, is crucial for the commencement, persistence, and progress of tourism in every locality [23, 24]. Consequently, Green Hospitality Management has emerged as a recent alternative term encompassing sustainable hospitality measures. The relationship between sustainable tourism and green hospitality management is directly proportional, as sustainable tourism development cannot be achieved without implementing sustainable hospitality measures [25].

Through Green Hospitality Management, eco-friendly practices are implemented within hotels and other accommodation arrangements including; waste reduction and recycling, water and energy conservation, and mitigation of harmful emissions [26, 27]. The environmental initiatives, which are preferred by tourists, are the key components of responsible measures adopted in this management approach [28-30]. The main aim of this research is to determine the factors which are necessary to cope with tourism sustainable economically, socially and environmentally and to specify the dynamics to green hospitality management in the study area.

2. THE STUDY AREA

The previously known northern area of Pakistan and currently Gilgit Baltistan region is the study area for this research. The study area is located between 32º 10′ 0″ to 37º 20′ 0″ N latitude, 72º 40′ 0″ to 80º 50′ 0″ E longitude (Figure 1).

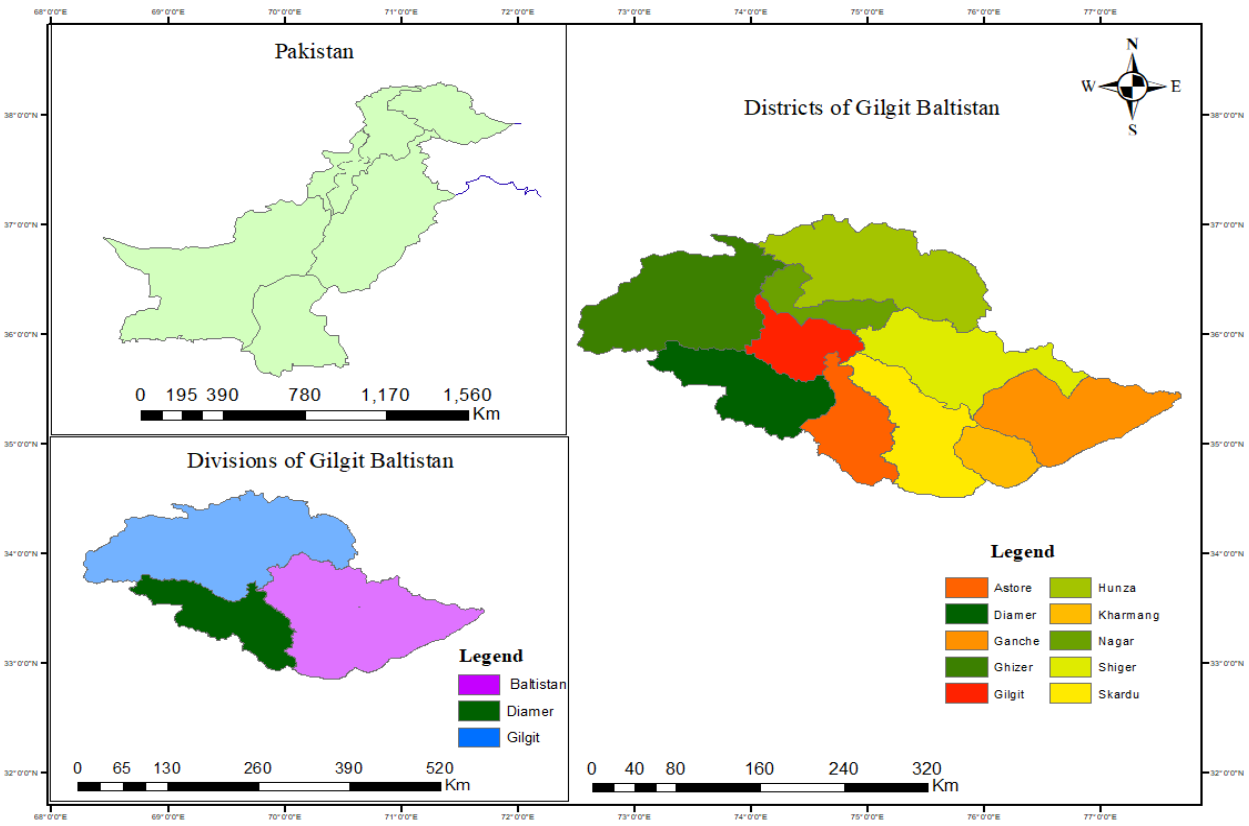

Fig.1. Location Map, Gilgit Baltistan.

3. MATERIALS AND METHODS

To determine the latent factors of sustainable measures in development of tourism and green practices in hospitality are the central theme of this research. This study is based on quantitative method of research. Primary data using a structured questionnaire is used to get the responses of targeted respondents. Among all the stakeholders of tourism and hospitality management in Gilgit Baltistan, the registered hospitality units are selected as Population. The sample size is finalized through "Yamane Formula" [31].

$$\text{Formula:} \quad n = \frac{\mathrm{N}}{1 + \mathrm{N(e)}^2}$$

Where,

n = The sample size
N = The Population size
e = The acceptable sampling error

The data acquisition from Directorate of Tourism, Gilgit Baltistan revealed that total registered hospitality units in the region are 499. The application of formula on the total registered hospitality units proposed 177 hospitality service providers as sample size. Therefore 177 hospitality managers are approached randomly to get responses on questionnaire from all the three administrative divisions of Gilgit Baltistan; Diamer, Gilgit and Baltistan division. The collected data is analyzed quantitatively through SPSS using Data Reduction method [32].

4. RESULTS AND DISCUSSION

4.1. Factor Analysis: Responses of Hospitality Managers of Gilgit Baltistan

Factor analysis is utilized to identify the influential factors in the sustainable development of tourism activities and the green services in hospitality management. The factors examined here reflect the perspectives of hospitality managers who oversee various accommodations such as hotels, guest houses, camping sites, and huts, catering to both domestic and international tourists. The data collected from these hospitality managers is obtained through a structured questionnaire featuring nominal variables. The inclusion of factors is based on the principles of "green hospitality management," allowing for an assessment of the habitual practices of hotel managers in relation to these principles. Additionally, the crucial factors for the sustainable growth of tourism practices are also determined.

To streamline the factors and address the issue of high variability, associated statistical tests are employed alongside factor analysis. These tests help consolidate the numerous factors into a smaller set based on the co-linearity within the specified variables. This co-linear amalgamation of many variables facilitates the identification of hidden or underlying factors related to sustainable tourism development (STD) and green hospitality management (GHM). By focusing on these latent factors, it becomes possible to achieve sustainability in tourism and hospitality services.

4.2. Application of KMO and Bartlett's Test for Data Suitability in Study Area

The Kaiser-Mayer-Olkin (KMO) is utilized to appraise the aptness of data reduction analysis for the given data [33]. The mentioned test examines the proportional values of variances among the given variables. The suitability statistics ranged from 0-1, with a higher value indicating greater suitability for factor analysis. A minimum value of 0.5 is generally required for reduction of values, while 0.5 to 0.8values are defined as adequate without the need for remedial action. Typical values for suitability fall within the range of 0.8 to 1.

"Bartlett's-Test" is an essential part of the KMO-test in the "Data Reduction" part of the analysis portion in the statistical software. This test is also essential for shaping the usefulness of the acquired data for "factor analysis". The significance level of the test ensures the data adequacy. Values exceeding the particular range may need corrective measures to tackle the flaws in given data before applying factor analysis.

In the case of the data collected from hospitality managers in Gilgit Baltistan, the KMO test was performed to assess its appropriateness for factor analysis. The "KMO Sampling Adequacy measure" for the existing data is accounted as 0.626, which indicates that the given data suits this analysis. Additionally, the "Bartlett's-sphericity test" yielded a highly considerable value with ($p < 0.001$) for the given variables (Table1).

Table 1. Hospitality Managers' Responses and KMO-Bartlett's Test.

Kaiser-Meyer-Olkin Sampling Adequacy Measures		0.626
Bartlett's-Sphericity Test	Chi-Square Approx.	2687.132
	Df.	300
	Significance	0.000

4.3. Sustainability in Tourism and Green Management: Scree Plot

The Scree-plot or the Scree-test is a diagrammatic demonstration of multivariate data in statistical form. It authenticates the specification of related variables that shows co-linearity base on their values (eigen) in data reduction analysis. The Scree plot also helps in determining the appropriate sets of factors to be retain. It visualized the eigen values for each factor in a descending line or curve, providing an ordering from highest to lowest characterization. In the case of the responses obtained from hotel managers focusing sustainable activities in tourism and green practices in the hotel industry, the Scree plot resulted in the retention of five factors. These factors were determined based on the eigen values associated with the 25 variables. The extracted eigen values ranges from 5.2 to 0.049 approximately (Figure 2).

4.4. Explained Total Variance

In the current section, the response of hotel managers is represented by a total of 25 variables (Table 2, variables; Table 3, Total values). The percentage of variance is computed for each of these linear components based on their eigen values. Upon analyzing the initial eigen values, it is determined that exactly seven components (1 - 7) out of the total 25 have eigen values exceeding one, while the remaining 18 variables (8-25) have below one eigen values (Table 2). The eigen value ranges; above and below one disclosed that the variables with greater than one eigen shows a higher percent of variances compared to those with eigen values below one. The eigen values for the components exceeding one range from 5.249 to 1.296, with cumulative percentages ranging from 20.996% to 72.055%. On the other hand, the eigen values below one ranges from 0.989 to 0.049. In order to reach a cumulative percentage of 100%, the cumulative percentage for eigen values below one starts with 76.011%. Additionally, the eigens and variance percentage are calculated with the squared loadings of rotated sums (Table 2).

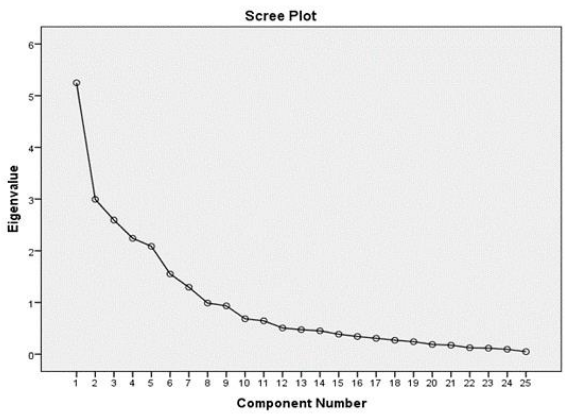

Fig.2. Hospitality Managers' Perception: Scree Plot.

4.5. Tourism Sustainability and Green Hotel Management: Factor Analysis

The perceptions of hotel managers in Gilgit Baltistan (GB) have led to the identification of seven distinct factors, each consisting of various components. Except for factor five, which has a different composition, all other factors encompass three or more components that necessitate analysis. The extraction method used is "Principal Component-Analysis," employing "Varimax with Kaiser-Normalization" during the extraction process. The objective is to find out the hidden factors related to sustainability of tourism and Green hotel management. In this approach, each and every variable within a component is measured as a factor, and a suitable comprehensive label is assigned to encompass all the variables as essential components.

4.5.1. Unsustainable consumption: Factor I

The reduced variables in this factor are; burden on hospitality services, 0.808, visit with personal vehicles, 0.759, plastic product usage, 0.754 and increase in emission of harmful substance, 0.681.

In this factor there are four linear variables that contribute to a latent factor aimed at achieving sustainable tourism activities and hospitality services. These four variables collectively focused on minimizing the discouraging impact on the natural environment. The first variable raises awareness about the increasing demand

Table 2. Explained Total Variance: Hospitality Managers' Responses.

Variables	Initial values of Eigens			Extraction-Sums: Squared Loadings			Rotation-Sums: Squared Loadings		
	Total	Percent of Variance	Cumulative Percent	Total	Percent of Variance	Cumulative Percent	Total	Percent of Variance	Cumulative Percent
1	5.249	20.996	20.996	5.249	20.996	20.996	3.624	14.498	14.498
2	2.995	11.979	32.975	2.995	11.979	32.975	2.889	11.554	26.052
3	2.594	10.377	43.352	2.594	10.377	43.352	2.725	10.900	36.952
4	2.242	8.967	52.319	2.242	8.967	52.319	2.393	9.571	46.524
5	2.087	8.346	60.665	2.087	8.346	60.665	2.261	9.044	55.567
6	1.552	6.208	66.873	1.552	6.208	66.873	2.169	8.676	64.243
7	1.296	5.182	72.055	1.296	5.182	72.055	1.953	7.812	72.055
8	0.989	3.956	76.011						
9	0.935	3.740	79.751						
10	0.685	2.741	82.492						
11	0.646	2.584	85.076						
12	0.508	2.030	87.106						
13	0.474	1.898	89.004						
14	0.452	1.808	90.812						
15	0.386	1.544	92.356						
16	0.343	1.371	93.727						
17	0.308	1.230	94.957						
18	0.270	1.081	96.038						
19	0.242	0.968	97.006						
20	0.189	0.755	97.760						
21	0.174	0.698	98.458						
22	0.125	0.499	98.958						
23	0.117	0.468	99.426						
24	0.095	0.379	99.805						
25	0.049	0.195	100.000						

Extracted Method: Principal Component Matrix.
Source: Field Survey.

for resources used in the hospitality industry to provide adequate services. The influx of tourists poses challenges to these resources, as sustainable resource management becomes essential. The use of personal vehicles by tourists contributes to an increase in private transportation within the tourism sector, leading to various environmental issues such as pollution. Another significant concern is the lack of sufficient parking facilities for the large number of vehicles, particularly in guest houses and majority of hotels (Table 3).

The excessive use of plastic products, which is known to contribute to significant environmental degradation, is a major concern in the tourism and hospitality management industry. It is imperative to reduce or eliminate the use of plastic bags as part of sustainable and eco-friendly practices. Additionally, limiting or completely eliminating harmful substances, particularly carbon emissions, is crucial in achieving sustainability objectives (Table 3).

4.5.2. Unfamiliarity with sustainable approaches: Factor II

The 2nd factor extracted the following variables; non-renewable resources usage, 0.794, waste recycling practice, 0.728, familiarity of green practices, 0.687, familiarity of sustainable tours, 0.670 and reservation on services, 0.563.

This factor specified five variables to disclose one of the significant hidden factors for tourism sustainability and Green management in the study area. All variables loaded in the given factor based from the lack of familiarity of hotel managers with sustainable practices. The usage of non-renewable resources is an important hurdle towards sustainable development of tourism. Therefore, shifting of hospitality measures focus towards renewable and eco-friendly resources. Given that waste generation is inherent in the hospitality industry, recycling measures are essential to mitigate the waste generated through tourism services. It is crucial for hospitality management to prioritize recycling initiatives within the study area (Table 3).

To address unsustainable day-to-day practices, it is essential for hospitality managers to be familiar with green practices within guest houses, hotels and other hospitality entities [34]. Tourism officials can raise awareness among hospitality managers through dedicated sessions on this subject. Since hospitality managers cater to both the local and non-local tourists for lodging, awareness with sustainable tourism is of key importance. Tourists generally expect the provision of top-quality services based on the capacity and capability of hospitality establishments. When the standard of services is compromised, tourists' express reservations. Green management practices evaluate the quality of services based on environmental measures (Table 3).

4.5.3. Monitoring the hotel services: Factor III

Variables extracted in 3rd factor according to "Principal-Component-Analysis" are; organic foods availability, -0.807, food wastage -0.760, Natural environment disturbed, 0.667 and deviation of local culture, 0.613.

In order to determine the third hidden aspect of sustainable practices in tourism and environmentally-friendly practices in the hospitality sector, the survey data from hospitality managers in the area were examined for four interrelated factors. These factors encompass various aspects of monitoring sustainability within hospitality services. The initial two factors within this aspect encompass the fundamental components of environmentally-conscious management in the hospitality field. Giving prominence to offering organic food to visitors and minimizing or eradicating food waste hold significance in the context of green hospitality management (Table 3).

Undoubtedly, hospitality services have influence over the natural landscape [35]. The fundamental objective of implementing green management practices in hospitality is to minimize negative impacts and maximize encouraging impacts to the nature. To preserve the cultural heritage of the region, particular attention is given to upholding local customs and traditions (Table 3).

4.5.4. Eco–consciousness within hospitality entities: Factor IV

The variables included in 4th factor are; suggestions to tourists, -0.797, disposal of wastes, -0.751 and drinking water wastage, 0.622.

Latent factor IV consists of three variables that exhibit linear coherence and are integral to green practices in the region. The given variables have direct association with the environmental awareness of hotel managers. Environmentally familiar managers suggest tourists to prefer sustainable practices within the hospitality units and during the entire tour. Demonstrating this consciousness, these managers ensure proper waste disposal arrangements within the hospitality units. Additionally, they actively discourage the wastage of drinking water among both staff and tourists (Table 3).

4.5.5. Tourists' responsible behavior during the tour: Factor V

The extracted variables in 5th factor are local products usage, 0.751 and security/safety issues, -0.655.

Factor V carries only 02 variables, which is concerned with the responsible practices of the tourists towards sustainable practices during their tours in the study region. This specified factor shows the responsibilities of visitors in promotion of sustainable actions. Responsible tourists prioritize and appreciate local products during their accommodations at the destination. By favoring local brands and products, they contribute to the economic advancement and empowerment of the hosting people. The enhancing interests of tourists

in local products stimulate the participation of locals in economic activities. Furthermore, responsible tourists refrain from engaging in behaviors that compromise safety or security, demonstrating their responsible conduct [36]. Both variables are crucial for the social as well as economic sustainability of tourism practices in the region (Table 3).

4.5.6.Sustainable practices and perceptions of hospitality managers: Factor VI

The extracted variables along 6th factor are; solid waste accumulation, 0.740, energy saving products, 0.697, reduction in non-renewable, 0.645 and inorganic foods and materials, 0.565.

Factor VI revealed four variables derived from the feedback of sustainability-conscious hospitality managers in the tourism and GHM sector. These variables encompass the sustainable practices that should be implemented by hotel and accommodation staff as part of their sustainability initiatives. Local hospitality managers are well aware that solid waste accumulation becomes

Table 3. Perceptions of Hospitality Managers: Rotated Matrix.

	Components						
	01	**02**	**03**	**04**	**05**	**06**	**07**
Burden on hospitality services	0.808	-0.160	0.155		0.151	0.269	
Arrival of tourists with private vehicle	0.759		-0.200	-0.121			0.171
Needless usage of plastic products	0.754	-0.104			0.189	0.172	
Increase in harmful-emissions	0.681	-0.135	0.178		-0.145		-0.203
Non-renewable resources		0.794	-0.413				
Waste recycling	-0.305	0.728		-0.233			0.105
Awareness about Green management	-0.142	0.687	0.344	0.428	-0.163	-0.187	
Familiar with Sustainability in tourism	-0.114	0.670		0.582	-0.153	-0.161	-0.133
Reservations regarding services	-0.293	0.563	0.240	0.166	0.303	-0.266	
Offering organic food	-0.179		-0.807		0.168		
Food wastage in hotels	0.154	0.267	-0.760	0.285			
Natural environment disturbance	0.305	0.209	0.667		0.383		0.190
Deviation to local customs		0.181	0.613	0.151	-0.508		-0.215
Sustainable tour suggestions to the tourists	0.207	0.131	0.167	-0.797		-0.110	0.264
Disposal the wastes		-0.149		-0.751	0.205		-0.272
Drinking water wastage	-0.176		-0.118	0.622	0.553		-0.361
Use of local products	0.258				0.751		-0.173
Security or safety issues					-0.655		
Accumulation of solid waste	0.262	-0.157			-0.215	0.740	0.126
Energy saving practices	-0.201			-0.191		0.697	-0.354
Reduction in resource usage	0.479	-0.144				0.645	0.153
Inorganic food in hotels	0.532	-0.118			0.377	0.565	
local food availability		0.196		-0.126			0.819
Water conservation	0.370	-0.331	-0.356			0.293	0.565
Allergen features	-0.291	-0.152	0.178		-0.231		0.542

Source: Field Survey.

prevalent during the tourism season, presenting a direct challenge to sustainability in tourism and hospitality establishments. To tackle this issue, alternative sources and proper waste disposal methods can be employed. Apart from waste management, hospitality managers also need to prioritize the conservation of energy resources within hotels, restaurants, and guest houses. This objective can be accomplished by utilizing energy-efficient appliances and minimizing excessive energy consumption (Table 3). Undoubtedly, resources are essential for providing proper services in hotel management. However, to ensure resource sustainability, managers can reduce their usage by identifying and minimizing needless areas [37]. The usage of inorganic foods for serving tourists in hospitality services is also evaluated in terms of green management. In this regard, hospitality managers can substitute inorganic materials with local and organic products (Table 3).

4.5.7 Green management within hospitality units: Factor VII

The 7th factor extracted the given variables; offering local food 0.819, conservation of water, 0.565 and allergen issues in hotels, 0.542.

Factor VII loaded three variables associated with the green management practices that should be prioritized in hospitality services in the GB region. One aspect of green management is the offering of local foods, which not only adds uniqueness and distinction to the hospitality service but also promotes endemic brands and preserves the customs of the region. Regional foods provide benefits to both the locals and the food seekers. Another initiative of green management in hospitality services focuses the reduction of water wastage, regardless of its abundance. It is crucial to prevent water wastage in the hosting units. Additionally, green practices prioritize the health concerns of tourists [38] with the availability of non-allergic features within guest houses and other hospitality centers [39] including the hotels (Table 3).

5. CONCLUSIONS

Reduction of factor was applied using SPSS to specify the hidden factors contributing towards tourism sustainability and green practices in the hospitality entities based on sustainable measures. The data for this analysis was collected through questionnaires administered during a field survey, and all relevant tests associated with the analysis were conducted. The adequacy of the data collected from hospitality managers was assessed using the "KMO-Measures for Sampling-adequacy," which carried the value having 0.626, indicating sufficient data for factor analysis. Additionally, the "Bartlett's-sphericity test" showed a greatly significant statistics of ($p < 0.001$). The scree plot revealed five factors from the 25 components, as indicated by the eigen numbers. Furthermore, the total variance showed the interdependent factors based on the eigens, identifying seven out of the 25 components. These seven latent factors include unsustainable consumption, lack of familiarity with sustainable measures, monitoring the services of hotels, environment-consciousness of hospitality managers, tourists' friendly behavior, sustainable practices carried out by hotel managers, and green measures within hospitality entities. The integration of sustainability in tourism activities and the implementation of green hospitality management are crucial for the advancement of sustainable tourism development.

6. CONFLICT OF INTEREST

The authors declare no conflict of interest.

7. REFERENCES

1. M. Carrillo, and J.M. Jorge. Multidimensional Analysis of Regional Tourism Sustainability in Spain. *Ecological Economics* 140: 89-98 (2017).
2. R. Sharpley. Tourism and Sustainable Development: Exploring the Theoretical Divide. *Journal of Sustainable Tourism* 8(1): 1-19 (2000).
3. R. Sharpley. Rural tourism and sustainability – A Critique. In: New directions in rural tourism, D. Hall, L. Roberts, and M. Mitchell (Eds.). *Ashgate Publishing Limited, Aldershot, UK* (2003).
4. G. Helgadóttir, A.V. Einarsdóttir, G.L. Burns, G.O. Gunnarsdóttir, and J.M.E. Matthíasdóttir. Social sustainability of tourism in Iceland: A qualitative inquiry. *Scandinavian Journal of Hospitality and Tourism* 19(4-5): 404-421 (2019).
5. A.I.P. Nugraheni, T.K. Priyambodoac, B. Sutiknoa, and H.A. Kusworoa. Defining Social Sustainability and Socially Conscious Tourist in Sustainable Tourism Development. *Journal of Business on Hospitality and Tourism* 5(2): 264-276 (2019).

6. J. Cukier, and H.D. Haas. Small Scale Tourism and Sustainability in Niue. *Pacific Tourism Review* 4(1): 1-6 (2000).
7. D.F.V. Uzun, and M. Somuncu. Evaluation of the Sustainability of Tourism in Ihlara Valley and Suggestions *European Journal of Sustainable Development* 4(2): 165-174 (2015).
8. R.W. Butler. Tourism and the environment: A geographical perspective. *Tourism Geographies: An International Journal of Tourism Space, Place and Environment* 2(3): 337–358 (2000).
9. P. Peeters, and G. Dubois. Tourism travel under climate change mitigation constraints. *Journal of Transport Geography* 18(3): 447-457 (2010).
10. C.H. Lui, G.H. Tzeng, M.H. Lee, and P.Y. Lee. Improving metro–airport connection service for tourism development: Using hybrid MCDM models. *Tourism Management Perspectives* 6: 95-107 (2013).
11. Y. Jabareen. A New Conceptual Framework for Sustainable Development. *Environment Development and Sustainability* 10(2): 179-192 (2008).
12. T. Tiwari, and A. Abrol. A Research Paper on Eco-Tourism-its sustainability in India. *International Research Journal of Commerce, Arts and Science* 6(9): 22-29 (2015).
13. A.N. Candrea, and A. Hertanu. Developing ecotourism destinations in Romania. A case study approach. *Economic Sciences* 8(2): 163-174 (2015).
14. O. Filiposki, M. Ackovska, N.P. Angelovska, and D. Mtodijeski. Socio economic impacts of tourism. *Economic Development* 18(1-2): 125-155 (2016).
15. D.A. Fennell (Ed.). Ecotourism, 5th Edition. *Taylor and Francis, Routledge* (2003).
16. N.D. Sausmarez. Crisis Management, Tourism and Sustainability: The Role of Indicators. *Journal of Sustainable Tourism* 15(6): 700–714 (2007).
17. A.C. Hunt. "We Are Even Poorer, but there is more work" An Ethnographic Analysis of Ecotourism in Nicaragua. *Ph.D. Thesis, Texas A & M University, USA* (2009).
18. K. Peattie, and A. Crane. Green marketing: legend, myth, farce or prophesy. *Qualitative Market Research: An International Journal* 8(4): 357-370 (2005).
19. J. Grant. Green Marketing. *Strategic Direction* 24(6): 25-27 (2008).
20. J. Pickett-Baker, and R. Ozaki. Pro environmental products: marketing influence on consumer purchase decision. *Journal of Consumer Marketing* 25: 281-293 (2008).
21. X. Font, and R. Buckley (Eds.). Tourism ecolabelling: certification and promotion of sustainable management. *CABI Publishing, Wallingford, United Kingdom* (2001).
22. X. Font. Environmental Certification in Tourism and Hospitality: Progress, Process and Prospects. *Tourism Management* 23(3): 197-205 (2002).
23. E.S.W. Chan, and S. Wong. Motivations for ISO 14001 in the Hotel Industry. *Tourism Management* 27(3): 481-492 (2006).
24. E. Cavagnaro, and S.A. Gehrels. Sweet and Sour Grapes: Implementing Sustainability in the Hospitality Industry-A Case Study. *Journal of Culinary Science & Technology* 7(2): 181-195 (2009).
25. M.S. Moise, I. Gil-Saura, and M.E.R. Molina. The importance of green practices for hotel guests: Does gender matter? *Economic Research-Ekonomska Istraživanja* 34(1): 3508-3529 (2021).
26. A. Kasim. A Look at Tourists' Propensity Towards Environmentally and Socially Friendly Hotel Attributes in Pulau Pinang, Malaysia. *International Journal of Hospitality & Tourism Administration* 5(2): 61-83 (2004).
27. C.N. Chiu. Tourism expansion and economic development: Evidence from the United States and China. *Journal of China Tourism Research* 17(1): 120-111 (2021).
28. S. Ayuso. Comparing voluntary policy instruments for sustainable tourism: The experience of the Spanish hotel sector. *Journal of Sustainable Tourism* 15(2): 144-159 (2007).
29. J. Dawson, E.J. Stewart, H. Lemelinc, and D. Scott. The carbon cost of polar bear viewing tourism in Churchill, Canada. *Journal of Sustainable Tourism* 18*:* 319-336 (2010).
30. M. Qasim, and A. Rahman. Trends and Patterns of Temporal Tourism Growth in Gilgit Baltistan Region, Pakistan. *Journal of Development and Social Sciences* 3(3): 524-537 (2022).
31. M. Qasim, A. Rahman, and Z. Ahmed. Adventure Tourism in Gilgit Baltistan: Opportunities, Trends and Destinations. *Annals of Human and Social Sciences* 3(2): 44-54(2022).
32. M. Forina, C. Armanino, S. Lanteri, and R. Leardi. Methods of Varimax rotation in factor analysis with applications in clinical and food chemistry. *Journal of Chemometrics* 3(S1): 115-125 (2005).
33. R.R. Croes. A paradigm shift to a new strategy for small island economies: Embracing demand side economics for value enhancement and long term economic stability. *Tourism Management* 27(3): 453–465 (2006).
34. K. Dube, and G. Nhamo. Vulnerability of nature-based tourism to climate variability and change: Case of Kariba resort town, Zimbabwe. *Journal of Outdoor Recreation and Tourism* 29(1): 100281 (2020).
35. R. Durbarry. The economic contribution of tourism in Mauritiu. *Annals of Tourism Research* 29(3): 862-865 (2002).
36. R.G. Dyson. Strategic development and SWOT

analysis at the University of Warwick. *European Journal of Operational Research* 152(3): 631-640 (2004).

37. N. Faber, R. Jorna, and J.M.L. Engel. The sustainability of 'sustainability' - A study into the conceptual foundations of the notion of 'sustainability'. *Journal of Environmental Assessment Policy and Management* 7(1): 1-33 (2005).
38. B.H. Farrel, and L. Twinning-Ward. Re conceptualization Tourism. *Annals of Tourism Research* 31(2): 274-295 (2004).
39. J. Zoltan, and B. McKercher. Analyzing intra-destination movements and activity participation of tourists through destination card consumption. *Tourism Geographies* 17(1): 19-35 (2015).

Proceedings of the Pakistan Academy of Sciences: A Physical and Computational Sciences 61(1): 11-18 (2024)

ISSN (Print): 2518-4245; ISSN (Online): 2518-4253
https://doi.org/10.53560/PPASA(61-1)834

Pakistan Academy of Sciences

Research Article

An Artificial Neural Network Method for Forecasting the Stability of Soil Slopes

Zulkifl Ahmed[1], Sumra Yousuf[2*], Shuhong Wang[1], Shafiq ur Rehman[3,4], Mustabshirha Gul[5], and Muhammad Saqib Hanif[6]

[1]School of Resource and Civil Engineering, Northeastern University, Shenyang, China
[2]Department of Building and Architectural Engineering, Faculty of Engineering & Technology, Bahauddin Zakariya University, 60000 Multan, Pakistan
[3]Department of Computing and Information Technology, Mir Chakar Khan Rind University of Technology, Dera Ghazi Khan, Pakistan
[4]Department of Computer Science, Lasbela University of Agriculture, Water & Marine Sciences, Uthal, 90150, Pakistan
[5]Department of Mechanical Engineering, Faculty of Engineering & Technology, Bahauddin Zakariya University, 60000 Multan, Pakistan
[6]School of Civil Engineering, Southwest Jiaotong University, Chengdu 610031, China

Abstract: Artificial neural network (ANN) methods, based on sophisticated models, have been developed recently that can predict slope stability. In this study, we have developed a genetic algorithm (GA) based on ANN to assess the stability of soil slope. Firstly, an ANN-based genetic algorithm was trained for nonlinear input-output mapping of the slope. A total of 190 soil slopes with unique values of shear strength properties (friction angle, cohesion, and unit weight), geometric parameters (slope angle and slope height) and corresponding factor of safety (FS) have been collected to give a neural network training dataset. Then, a three-layer neural network model is established based on GA. The prediction and performance ability of the established model is assessed using the correlation coefficient (R^2). By the outcomes, the trained ANN model with the R^2 value of 0.98 is reliable, valid and simple for evaluating the soil slope stability and estimating the FS. Additionally, the proposed neural network model is applied to a case of soil slope from prior studies. Findings show that the developed ANN model can be versatile in studying the stability of soil slopes.

Keywords: Soil Slope, Cohesion (c), Genetic Algorithm (GA), Internal Friction Angle (ϕ), Slop Angle (θ).

1. INTRODUCTION

Researchers usually determine the soil slope stability and failure process to exactly categorise critical slip surfaces [1]. Several analytical methods are also documented to estimate the factor of safety (FS) of different slopes [2]. Because soil strength properties and slope profile affect the stability of loose slopes [3]. Therefore, the analysis evaluation of slope stability is of great engineering significance in the geotechnical field [3, 4]. A variety of slope stability analyzing and forecasting methods have been proposed, which can be divided into two categories: the extreme balance method and the numerical analysis method. Janbu method, Swedish division method, Sarma method, Bishop method and residual thrust method are well-known methods today. The advantage of these methods is that they are strictly based on the theory of slope geology. For example, the Bishop method assumes that the forces between the blocks are horizontal, and the Swedish assumes that the combined forces between the slices are parallel [3, 5]. These assumptions are often far from the actual physical and technical behaviour of the rock and soil material, and therefore their accuracy is greatly

Received: August 2023; Revised: February 2024; Accepted: March 2024
*Corresponding Author: Sumra Yousuf; <sumra.yousafrm@gmail.com>

reduced [6]. However, Finite element technique (FEM), distinct element approach (DEM), boundary element method (BEM) and particle flow method are much handy [2, 6]. The numerical analysis method is often based on some hypothesis about the physical properties of rock and soil material, and its accuracy is highly dependent on the slope model and input parameters (shear strength properties). Therefore, results from these numerical methods are often difficult to confirm the reality [7].

The method of judgment of the critical slip surface is directly connected to way of determining the minimum safety factor. Some scholars have used limit equilibrium techniques to evaluate FS and slip surface statically [8, 9], or numerically [10, 11]. To determine the minimum FS for a sliding surface, the limiting equilibrium technique may allow a precise and accurate evaluation method during large-scale stability investigations. Therefore, commonly used approaches are limiting equilibrium techniques; hence, cannot be used to locate CFS with general limit under composite conditions. On the other hand, optimisation techniques are considered as an effective tool to estimate FS for typical slip surfaces [12] and dynamic programming is used to allocate the non-circular slip surface [11]. Monte Carlo techniques can evaluate slope FS and critical slip surface [13]. Other researchers proposed a few conventional solutions for rock slope stability analyses [14, 15].

Many methods and techniques have been introduced previously to assess soil slope stability. Such as the Bishop method [8], Baker technique [16], extended Spencer method [17], and Morgenstern and Price approach [18] are well known today. The above techniques are not laborious [19], but numerical modelling techniques are time-saving and appropriate for slope stability investigation [20]. Some scholars presented key block [21] and fuzzy key-block [22] methods that can be used for slope failure analysis. Other used genetic algorithms [23] and optimization techniques [24] for non-circular sliding surface determination.

Recently, ANN based methods have emerged in the field of geotechnical engineering for slope stability prediction [25]. Previously, ANN models were established based on material strength properties ignoring slope profile.

In the present study, a high nonlinear artificial neural network (ANN) model is presented to predict soil slope stability. Firstly, a genetic optimization algorithm is established based on soil properties and slope profiles. The accuracy of the proposed model is judged through the correlation coefficient (R^2). Combined with case studies and the results from SLOPE/W software, the forecasting abality of the proposed ANN model is effective.

2. METHODOLOGY AND ANN METHOD

Studying soil slope stability is one of the most important kinds of research in the geology and geo-engineering fields. Many geotechnical researchers of the 20th century divided the sliding mass of the slope into several slices to calculate the accurate value of FS [8, 26, 27]. Furthermore, because of the rise of computer technology statistically more laborious equations can be solved easily to resolve soil and rock mechanics problems [28, 29]. Numerical models are not generally straightforward for operators and are considered supplementary means capable of delivering information helpful for stability analysis [28]. However, ANN-based models are powerful tools for tackling difficult stability issues [30].

ANN is an intelligence managing technique that can learn, generalise and recall from training records [31, 32]. ANN is a model established with the help of a set of several basic handling elements known as neurons. Neurons are rigorously interlinked computational components that can perform data representation and data processing using wide similar computation [31, 33]. The vigorous computational structure of ANN can be used to train a complex model [34, 35]**.** Numerous ANN designs have been previously used in civil and geotechnical engineering applications [34, 36] and soil slope stability prediction [33, 37].

ANN is a kind of nonlinear structure that has clear nonlinear planning capacity. ANN could also be used for nonlinear mapping without knowing the specific distribution of data [38]. Artificial neural networks are a self-learning technique that stores the outcomes in the upper limit of neurons by using the relation weight between nerve cells. After this, new engineering examples were entered, and the network used its nonlinear mapping capability to give heuristic inferences. To predict the slope

status and FS, based on slope parameters, a new ANN model is shown in Fig. 1. Many engineering experiences show that the main factors affecting the stability of slope are the physical and mechanical properties, slope geometry, groundwater, and external loads. As well as the properties of soil slope materials are mostly controlled by the weight of the rock and soil body. Cohesion (c), geometry and internal friction (ϕ) of the soil slope are mostly controlled by the slope angle (θ) and height (H). So, the modelling of slope for stability estimation can be founded by mapping the relationship (G).

$$y = G(\gamma, E, c, \phi, H, h, w) \quad (1)$$

In equation (1), the value of y (y is the safety value) ranges from 0-1, and if $y = 0$, then the slope will be thought-out unstable, and if $y = 1$, indicates that the slope is stable. G is highly nonlinear due to the complexity of the shear strength and geometric properties of the slope material. It is difficult to precisely describe G by mathematical equations. Given the high nonlinear mapping capability of neural networks, we have used neural networks to describe G, which can be affected by density (γ), Young's modulus (E), cohesion (c), angle of internal friction (ϕ), overall height (H), slope height (h), slope angle (θ) and weight of water (w =0). The prediction of slope stability by neural network can be divided into two stages: the first stage is the self-learning stage of the network. This stage was achieved by previous studies. The second stage is the prediction stage, which predicts the stability of the slope directly.

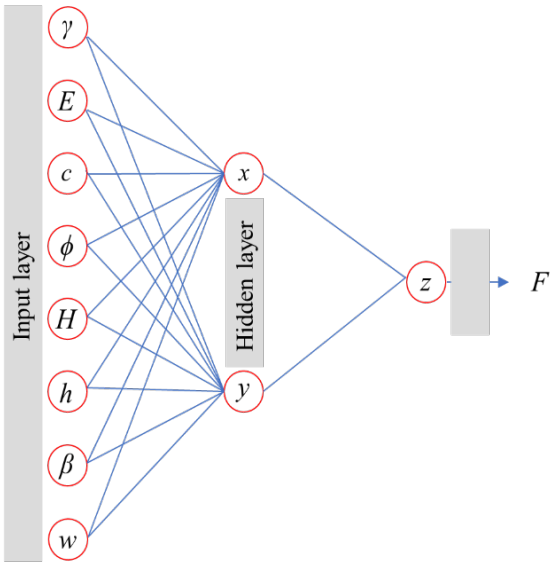

Fig. 1. Neural model for FS prediction.

3. STRUCTURE OF ANN

Because the slope stability problems are highly nonlinear, which requires the neural network to be used to map. The mapping relationship (G) can be as close to the objective reality as possible and ANN should have a strong enough generalization ability to get the correct results based on input parameters. The capacity and generalization ability of a neural network depends largely on the structure, of the structure of the neural network, including the connection mode of neurons in the network and the connection weight between neurons. The proper connection mode and optimized connection weight are important to neural networks' capacity and generalization ability.

The shortcomings of conventional neural network algorithms during the data optimization process are not obvious. The selection of connection mode and the weight of neural networks cannot be processed systematically. The conventional ANN technique determines the connection between neurons in the network according to the experience. Then the neural network samples rearrange the input data to make a proper connection between networks. Also, if the input data are not met, then all the optimization steps are repeated to find out optimal solution. Additionally, it is very difficult to find out the optimal network by using conventional method. So, the capacity of traditional ANN model is insufficient and the ability to generalize data is poor for solving large slope stability problems. In addition, the learning ability of the traditional ANN method is low, and it is not easy to fall into local extreme values.

Obviously, according to the characteristics of the problem, the number of neurons in the input layer are 6, corresponding to the 6 factors considered in this research, and the number of neurons in the output layer is 1, which corresponds to the final output result. The middle layer is set to m layer and each layer has n neurons. The connection of the neurons is a single-layer forward, i.e., the descending layer can only be connected to the neurons in the subsequent layer. For the convenience of calculation, the connection weights between neurons in each layer of the neural network and the thresholds of each neuron are deposited into a one-dimensional vector as:

$$X = (X_1, X_2, \ldots, X_N) = (W_1, W_2, \ldots, W_l, q_1, q_2, \ldots, q_k) \quad (2)$$

Where, W_1, W_2 and W_N are the connection weight in the neural network and q_1, q_2 and q_k are the threshold for neurons in ANN. The genetic algorithm does not directly influence the input parameters. However, on a particular encrypting of the input parameters, the current study utilizes dual encrypting by adjusting the vector as:

$$i_i = X_i \in [\varepsilon_{i\,\min} = \varepsilon_{i\,\max}] \quad (3)$$

While encrypting precision of a dual coding length (L_i) could be estimated through equation (4) as:

$$Li = int[log2\frac{x_{i\,max} - X_{i\,min}}{e} + 1] + 1 \quad (4)$$

To make the calculation simple, the undefined binary encoding length (L) of the variable is as:

$$L = max\,(L_i) \quad (5)$$

Total output error E of the network can be defined as:

$$E(i) = \frac{1}{2}\sum_{s=1}^{s}\left(Y^{s*} - Y^{s}\right)^2 \quad (6)$$

Where, Y^{s*} and Y^{s} are the expected and actual layers of the neurons for S group samples. Accordingly, the adaptability function of the genetic algorithm, F(i), can be defined as:

$$E(x) = C - E(x) \quad (7)$$

Where, C = const., and satisfied: $C > |E_{max}(i)|$, E_{max} (i) is the maximum output error for the network. The selected population size is N_p. Cross probability is P_C. When the above steps are completed, the structure of the neural network is tuned as follows: if a weight is 0 or the absolute value is small, there is no connection between the corresponding two neurons. If the input weight of a neuron is 0 or the absolute value is less than 1, the neuron is considered redundant, and the neuron is removed. After adjusting the structure of the neural network, let the network re-learn the sample and further adjust the weight of the network, because at this time the structure of the network is close to optimal, and the learning process will be completed quickly.

4. RESULTS AND DISCUSSION

4.1. Numerical Example

Several examples of slopes were collected from the literature [8, 27]. An extreme probability function (P) is obtained from the arithmetic hypothesis test. The numbers of soil slope stability controlling factors are not similar in different cases. Furthermore, dissimilarity cannot be helpful to the analysis of the ANN model. The reason is that the input parameters involved during the training of the model required to be processed and standardised, which can be done as:

$$h_i^* = \frac{2(h_i - h_{min})}{h_{max} - h_{min}} - 1 \quad (8)$$

Where, h_i and h_i^* are equivalence variables before and after soil slope failure, respectively. h_{min} and h_{max} are the lower and upper bounds of the variables, respectively. The parameters in equation (8) were assessed from the engineering examples.

In this study, three intermediate layers were initially selected by twelve neurons. The population size for the genetic algorithm was selected as N_P = l00, copy probability P_S = 0.6. Cross probability $P_{C=}$ 0.4, probability of variation P_m = 0.05, interval of the network connection weigh is taken -10 and 10. The threshold interval of neurons is taken as a sample of standardized slope engineering data. After the end of the learning process, delete the connection right absolute value of less than 0.1. Let the neural network re-learn the samples to obtain the optimal network structure. To test the effectiveness of the established method, the stability of the 10 soil slopes is forecasted in Table 1.

Table 1. Slope examples and input data.

Slope	γ (kN/m^3)	c (kPa)	ϕ (°)	θ (°)	H (m)	Status
1	19.6	0	25	18	6.9	Unstable
2	27.1	30	37	36	100	Stable
3	31.6	40	39	38	100	Stable
4	23.2	0	23	22	8	Unstable
5	18.1	14	30	36	25	Unstable
6	20.7	30	0	32	65	Unstable
7	29.2	8	35	35	77	Unstable
8	26.1	70	38	45	215	Unstable
9	23.1	45	35	50	285	Stable
10	28.8	35	35	48	355	Stable

Standardized data was used as inputs in the neural network and its stability was predicted. The actual situation of the slopes is shown in Table 2. From the results of Table 2, only the slope analysis results (stabilisation) of example six are inconsistent with

Table 2. Comparison in between current results and previous results of slopes.

Slope	Actual results	Studied results
1	Unstable	Unstable
2	Stable	Stable
3	Stable	Stable
4	Unstable	Unstable
5	Unstable	Unstable
6	Unstable	Stable
7	Unstable	Unstable
8	Unstable	Unstable
9	Stable	Stable
10	Stable	Stable

the actual situation (destruction). The accuracy of the proposed model is 97%, which shows that the forecast method proposed in the present study has a high forecast accuracy.

A comparison of FS values predicted from the ANN models and with that of the values obtained from the numerical analysis is depicted in Figure 2. The coefficient of correlation (R^2) between the simulated and predicted values reveals an outstanding forecast ability of the model. There is barely a meaningful contrast between the ability of the ANN training model. It can be understood that the ability of the training model did not change significantly when the amount of the input properties was decreased to 8. However, a significant change in R^2 value is observed during the testing phase (Figure 2).

4.2. Model Application

In this section, considering the key objective of the present research, the established artificial model is utilized for soil slope status and FS calculation challenges from the previous studies. These challenges are taken for soil slope.

4.2.1. Case 1

In the first text, the efficiency and applicability of the recommended model in automatically predicting stability and factor of safety are observed by adopting the homogeneous earth slope from the publication study of Nouri *et al*. [39]. In the current test, the slope status and FS predicted by the ANN model matched with those acquired by prior

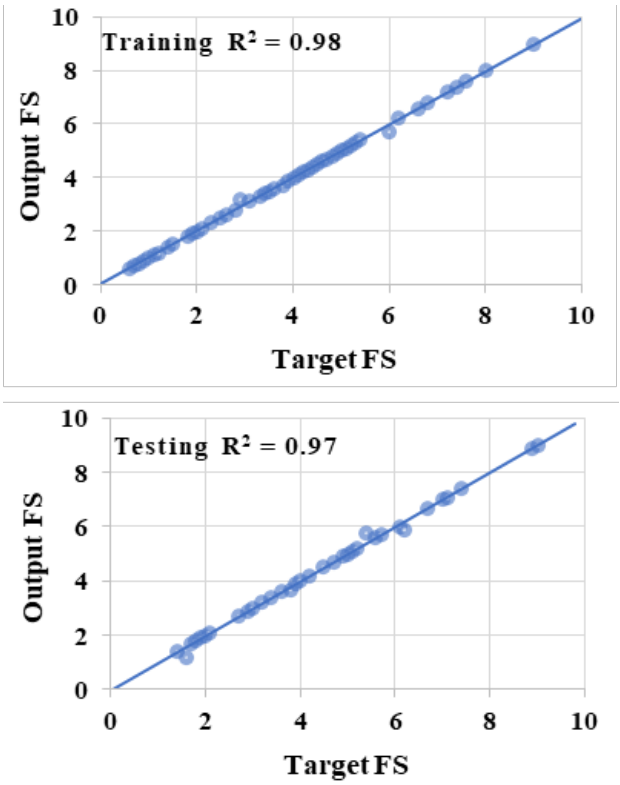

Fig. 2. Neutral model for FS prediction.

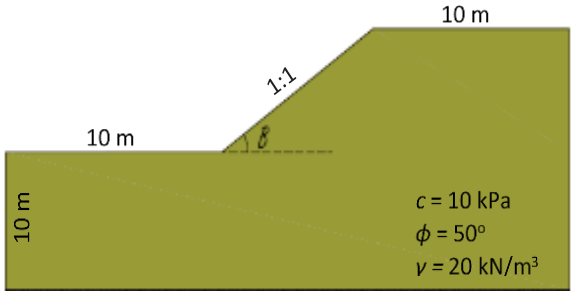

Fig. 3. Properties of soil slope, from Nouri *et al.* [39].

Table 3. Input parameters for case 2, from Sakellariou and Ferentinou [40].

Case No.	γ (kN/m³)	c (kPa)	ϕ (°)	θ (°)	H (m)
1	18.84	14.36	25	20	35.50
2	20.60	16.28	26.5	30	40.00
3	21.40	10.00	30.34	30	20.00
4	20.96	19.96	40.01	40.02	12.00

Table 4. Difference between the actual and forecasted FS.

Case No.	Slope/W	[40]	[25]	Current model
1	1.87	1.95	1.87	1.88
2	1.25	1.24	1.25	1.25
3	1.70	1.75	1.70	1.70
4	1.84	1.91	1.84	1.84

studies including those achieved by SLOPE/W. The strength and geometric input parameters of the soil slope are presented in Figure 3. Slope angle is 45° and the height is 20 m. The minimum value of FS was generated from SLOPE/W and proposed ANN model. The actual FS of soil slope as reported by Nouri *et al*. [39] is 0.288. The FS of 0.294 and 0.289 were estimated by using SLOPE/W and proposed ANN model, respectively. These findings show that the new ANN model is more effective in forecasting the stability factor of soil slope.

4.2.2. Case 2

Here, 4 slope cases studied by Sakellariou and Ferentinou [40] are reanalyzed as test studies. These cases are totally dry soil slopes. The input data set of these cases is presented in Table 3.

The simulated value of FS of these studies is given in Table 4. Furthermore, the factor of safety forecasted by Sakellariou and Ferentinou [40] and Khajehzadeh *et al*. [25] are given, respectively, in the third and fourth columns of Table 5. The predicted FS from the ANN model is presented in the last column of Table 5. As the findings reveal, matched with SLOPE/W and the previous surveys, the forecasted safety factors utilising the anticipated ANN model are greatly closer to the actual safety factors.

5. CONCLUSIONS

In this study, a new genetic algorithm-based ANN model is proposed to predict the soil slope status and corresponding stability factor. A potential homogenous soil slope with different values of slope angle (θ), height (H), soil internal friction (ϕ), density (γ) and cohesion force (c), are considered as input data sets to train and develop artificial models. The accuracy of the proposed model is checked by SLOPE/W software and previous case studies. Based on the findings, the following conclusions can be drawn:

a) The comparison of the anticipated GA shows that the artificial neural network model is betters than Slope/W and the other techniques. The new GA can be effectively used for the case studies of homogeneous dry soil slopes to estimate FS with a coefficient of correlation R^2 almost equal to 0.98.
b) According to the numerical experiment, the GA outperforms the other methods and could provide a lower value of FS.
c) The engineering examples showed that the forecasting accuracy of the proposed method is high; it is generally difficult to find the optimal network structure by this method.

6. ACKNOWLEDGEMENTS

This work was conducted with support from the Northeastern University, Shenyang, China, Bahauddin Zakariya University, Multan, Pakistan and Mir Chakar Khan Rind University of Technology, DG Khan, Pakistan.

7. CONFLICT OF INTEREST

The authors declare no conflict of interest.

8. REFERENCES

1. Y. Wang, J. Huang, and H. Tang. Automatic identification of the critical slip surface of slopes. *Engineering Geology* 273: 105672 (2020).
2. X. Zhou, X. Huang, and X. Zhao. Optimization of the critical slip surface of three-dimensional slope by using an improved genetic algorithm. *International Journal of Geomechanics* 20(8): 04020120 (2020).
3. Z. Ahmed, S. Wang, O.H. Jasim, Y. Xu, and P. Wang. Variability effect of strength and geometric parameters on the stability factor of failure surfaces of rock slope by numerical analysis. *Arabian Journal of Geosciences* 13: 1112 (2020).
4. Z. Ahmed, S. Wang, and D. Furui. Estimation of Repeated Slip Surface in Cut Slope Stability Analysis. In: Experimental Vibration Analysis for Civil Structures, J. Zhang, Z. Wu, M. Noori, and Y. Li (Eds.). *CRC Press, Boca Raton,* pp. 561-569 (2020).
5. A. Bishop, and N. Morgenstern. Stability coefficients for earth slopes. *Geotechnique* 10(4): 129-153 (1960).
6. Z. Ahmed, S. Wang, M.Z. Hashmi, Z. Zishan, and Z. Chengjin. Causes, characterization, damage models, and constitutive modes for rock damage analysis: a review. *Arabian Journal of Geosciences* 13: 806 (2020).
7. S. Wang, Z. Ahmed, M. Z. Hashmi, and W. Pengyu. Cliff face rock slope stability analysis based on unmanned arial vehicle (UAV) photogrammetry. *Geomechanics and Geophysics for Geo-Energy and Geo-Resources* 5: 333-344 (2019).
8. A.W. Bishop. The use of the slip circle in the stability analysis of slopes. *Geotechnique* 5(1): 7-17 (1955).
9. Y. Zhao, ZY. Tong, and Q. Lü. Slope stability analysis using slice-wise factor of safety. *Mathematical Problems in Engineering* 2014 (2014).

10. X. Qi, and D. Li. Effect of spatial variability of shear strength parameters on critical slip surfaces of slopes. *Engineering Geology* 239: 41-49 (2018).
11. R. Regmi, and K. Jung. Application of dynamic programming to locate the critical failure surface in a rainfall induced slope failure problem. *KSCE Journal of Civil Engineering* 20(1): 452-462 (2016).
12. H. Pham, and D. Fredlund. The application of dynamic programming to slope stability analysis. *Canadian Geotechnical Journal* 40(4): 830-847 (2003).
13. A. Malkawi, W. Hassan, and S. Sarma. Global search method for locating general slip surface using Monte Carlo techniques. *Journal of Geotechnical and Geoenvironmental Engineering* 127(8): 688-698 (2001).
14. H. Zheng, D. Liu, and C. Li. Slope stability analysis based on elasto-plastic finite element method. *International Journal for Numerical Methods in Engineering* 64(14): 1871-1888 (2005).
15. Y. Cheng, T. Lansivaara, and W. Wei. Two-dimensional slope stability analysis by limit equilibrium and strength reduction methods. *Computers and Geotechnics* 34(3): 137-150 (2007).
16. R. Baker. Determination of the critical slip surface in slope stability computations. *International Journal for Numerical and Analytical Methods in Geomechanics* 4(4): 333-359 (1980).
17. J. Jiang and T. Yamagami. Three-dimensional slope stability analysis using an extended Spencer method. *Soils and Foundations* 44(4): 127-135 (2004).
18. G. Sun, S. Cheng, W. Jiang, and H. Zheng. A global procedure for stability analysis of slopes based on the Morgenstern-Price assumption and its applications. *Computers and Geotechnics* 80: 97-106 (2016).
19. E. Boutrup, and C. Lovell. Searching techniques in slope stability analysis. *Engineering Geology* 16(1-2): 51-61 (1980).
20. M. Azarafza, E. Asghari-Kaljahi, and H. Akgün. Numerical modeling of discontinuous rock slopes utilizing the 3DDGM (three-dimensional discontinuity geometrical modeling) method. *Bulletin of Engineering Geology and the Environment* 76: 989-1007 (2017).
21. M. Azarafza, H. Akgün, A. Ghazifard, and E. Asghari-Kaljahi. Key-block based analytical stability method for discontinuous rock slope subjected to toppling failure. *Computers and Geotechnics* 124: 103620 (2020).
22. M. Azarafza, H. Akgün, M.R. Feizi-Derakhshi, M. Azarafza, J. Rahnamarad, and R. Derakhshani. Discontinuous rock slope stability analysis under blocky structural sliding by fuzzy key-block analysis method. *Heliyon* 6(5): e03907 (2020).
23. A. Zolfaghari, A. Heath, and P. McCombie. Simple genetic algorithm search for critical non-circular failure surface in slope stability analysis. *Computers and Geotechnics* 32(3): 139-152 (2005).
24. W. Gao. Determination of the noncircular critical slip surface in slope stability analysis by meeting ant colony optimization. *Journal of Computing in Civil Engineering* 30(2): 06015001 (2016).
25. M. Khajehzadeh, M. Taha, S. Keawsawasvong, H. Mirzaei, and M. Jebeli. An effective artificial intelligence approach for slope stability evaluation. *IEEE Access* 10: 5660-5671 (2022).
26. R. Y. Liang, J. Zhao, and S. Vitton. Determination of interslice force in slope stability analysis. *Soils and Foundations* 37(1): 65-72 (1997).
27. O. Hungr, F. M. Salgado, and P. Byrne. Evaluation of a three-dimensional method of slope stability analysis. *Canadian Geotechnical Journal* 26(4): 679-686 (1989).
28. H. Alateya, and A.A. Asr. Numerical investigation into the stability of earth dam slopes considering the effects of cavities. *Engineering Computations* 37(4): 1397-1421 (2020).
29. J. Ribas, J. Severo, L. Guimaraes, and K. Perpetuo. A fuzzy FMEA assessment of hydroelectric earth dam failure modes: A case study in Central Brazil. *Energy Reports* 7: 4412-4424 (2021).
30. H. Moayedi, A. Osouli, H. Nguyen, and A.S.A. Rashid. A novel Harris hawks' optimization and k-fold cross-validation predicting slope stability. *Engineering with Computers* 37: 369-379 (2021).
31. B. Gordan, D. Jahed Armaghani, M. Hajihassani, and M. Monjezi. Prediction of seismic slope stability through combination of particle swarm optimization and neural network. *Engineering with Computers*, 32: 85-97 (2016).
32. A. Verma, T. Singh, N. Chauhan, and K. Sarkar. A hybrid FEM–ANN approach for slope instability prediction. *Journal of The Institution of Engineers (India): Series A* 97: 171-180 (2016).
33. A. Ray, V. Kumar, A. Kumar, R. Rai, M. Khandelwal, and T. Singh. Stability prediction of Himalayan residual soil slope using artificial neural network. *Natural Hazards* 103(3): 3523-3540 (2020).
34. Z. Qian, A. Li, W. Chen, A. Lyamin, and J. Jiang. An artificial neural network approach to inhomogeneous soil slope stability predictions based on limit analysis methods. *Soils and Foundations* 59(2): 556-569 (2019).
35. C. Deng, H. Hu, T. Zhang, and J. Chen. Rock slope stability analysis and charts based on hybrid online sequential extreme learning machine model. *Earth Science Informatics* 13: 729-746 (2020).
36. J. Egbueri. Prediction modeling of potentially toxic elements' hydrogeopollution using an integrated Q-mode HCs and ANNs machine learning approach in SE Nigeria. *Environmental Science and Pollution Research* 28(30): 40938-40956 (2021).
37. J. Meng, H. Mattsson, and J. Laue. Three-dimensional slope stability predictions using artificial neural

networks. *International Journal for Numerical and Analytical Methods in Geomechanics* 45(13): 1988-2000 (2021).
38. A. Li, S. Khoo, A. Lyamin, and Y. Wang. Rock slope stability analyses using extreme learning neural network and terminal steepest descent algorithm. *Automation in Construction* 65: 42-50 (2016).
39. M. Nouri, P. Sihag, F. Salmasi, and J. Abraham. Prediction of homogeneous earthen slope safety factors using the forest and tree based modelling. *Geotechnical and Geological Engineering* 39: 2849-2862 (2021).
40. M. Sakellariou and M. Ferentinou. A study of slope stability prediction using neural networks. *Geotechnical & Geological Engineering* 23: 419-445 (2005).

Proceedings of the Pakistan Academy of Sciences: A Physical and Computational Sciences 61(1): 19-31 (2024)

ISSN (Print): 2518-4245; ISSN (Online): 2518-4253
https://doi.org/10.53560/PPASA(61-1)674

Pakistan Academy of Sciences

Research Article

Efficient Resource Scheduling in Fog: A Multi-Objective Optimization Approach

Tayyiba Hameed, Bushra Jamil, and Humaira Ijaz*

Department of Information Technology, University of Sargodha, Sargodha, Pakistan

Abstract: Fog computing is a novel idea that extends cloud computing by offering services like processing, storage, analysis, and networking on fog devices closer to IoT devices. Numerous fog devices are required to process the ever-growing amount of data generated by IoT applications. The heterogeneous tasks from various IoT applications compete for a limited number of resources of these devices. The process of assigning this set of tasks to different available fog nodes according to QoS requirements for processing is resource scheduling. Resource scheduling aims to optimize resource utilization and performance metrics however, the dynamic nature of the Fog environment, resource-constrained, and heterogeneity in fog devices make resource scheduling a complex issue. This research presents the design and implementation of a multi-objective optimization-based resource scheduling algorithm using Modified Particle Swarm Optimization (MPSO) that addresses the application module placement and task allocation issues. This two-step MPSO-based resource scheduling model finds the optimal fog node to place each application module and assigns appropriate tasks to the most optimal fog nodes for execution. The proposed model unlocks the full potential of fog resources along with maximization of overall system performance in terms of optimization of cost, latency, energy consumption, and network usage. The simulation results indicate that using MPSO energy consumption is reduced by 53.94% and 43.58% as compared to First Come First Serve (FCFS) and Particle Swarm Optimization (PSO), respectively. The loop delay, network usage and cost using MPSO are reduced by 40.3%, 67.69% and 90.01% respectively, as compared to PSO algorithm.

Keywords: Fog Computing, MPSO, Multi-Objective Optimization, Resource Scheduling, Task Allocation, Cloud Computing, Internet of Things (IoT).

1. INTRODUCTION

The Internet of Things (IoT) is a groundbreaking technology that has the potential to transform the manner we live and work [1]. It's a network of physical objects, machines, gadgets, automobiles, and other things, having sensors, software, and connectivity, that enables them to gather and share data to make intelligent decisions. IoT makes devices intelligent and responsive to their surroundings. This interconnected network of devices spans various industries, from smart homes, cars, and cities to healthcare and manufacturing, and has the potential to enhance automation, decision-making, and efficiency. This interconnectivity of devices has led to an accelerated growth in the amount of data produced by these devices. Currently, cloud-based IoT (CIoT) is providing a powerful solution for storing, processing and analyzing this sheer amount of data. As CIoT architecture is centralized and the cloud data centers are multi-hops away that increases latency bandwidth consumption and network bottlenecks while processing this sheer amount of IoT data [2].

Later on, Edge computing was used to handle the high latency problem in delay-sensitive applications by providing storage and processing resources near the end user IoT devices. Edge computing provides many advantages like high-speed processing, low latencies, and real-time availability of network resources. This paradigm can solve many issues like energy usage, security, and privacy by reducing the distance the data must travel [3]. However, although edge devices have short access latencies because of their proximity to end users, they are still resource-constrained and prone to availability issues.

Received: December 2023; Revised: February 2024; Accepted: March 2024
*Corresponding Author: Humaira Ijaz <humaira.bilalrasul@uos.edu.pk>

To address this problem fog computing has been introduced, which just evolved as a logical extension of cloud computing [4]. The term "Fog Computing" refers to moving services like computing, processing, storage, and networking services near the proximity of the end user [5]. This results in reduced latency, faster decision-making conservation of network bandwidth, and improved reliability. Fog computing has different characteristics like dense distribution of heterogeneous, resource-limited fog nodes, context awareness, mobility, real-time interaction, and executing diverse-natured IoT applications. The advancement in communication technologies and the development of pervasive computing caused a rapid surge in the number of IoT applications and IoT devices that generate a massive amount of data to be processed by these fog devices [6]. The heterogeneous, resource and energy-limited, dynamic nature of fog applications makes resource management challenging [7]. Among various resource management techniques, resource scheduling is crucial for taking full benefits of fog computing. Resource scheduling determines when and where different applications or services should use resources, such as CPU, memory, storage, and network bandwidth. Resource scheduling aims to identify the available resources and allocate them to specific applications to ensure their effective utilization and timely completion of latency-sensitive tasks. Efficient resource allocation thus leads to better resource utilization, reduced latency, energy consumption, and improved user experience. Resource scheduling becomes a challenging issue due to the diverse and highly dynamic nature of fog computing. We have reviewed the existing resource scheduling techniques for fog computing environments presented by researchers and highlighted different metrics optimized in these studies, such as latency, network bandwidth, energy consumption, cost, and quality of service, etc.

Benedetti *et al*. [8] developed the distributed job scheduler JarvSis for fog-based IoT applications. To optimize time and energy consumption, Movahdi *et al*. [9] employed Integer Linear Programming to formulate the task scheduling problem in fog computing environment.

Wu *et al*. [10] presented a multi-objective algorithm that learns and optimizes the fuzzy offloading technique from various IoT applications and allocate tasks in fog computing environment. Jamil *et al*. [11] proposed a heuristic-based task-scheduling algorithm that schedules the tasks on the fog nodes according to their processing needs. iFogSim is used for implementation with the objective to optimize delay and energy consumption. In another study, Josilo [12] considers a fog computing system to offload the computational tasks to nearby devices or an edge server.

The selection and distribution of resources are studied by Zhang *et al*. [13], who use the Stackelberg game for solving resource allocation problems. Zhang [14] describes a game-based resource management system consisting of three entities authorized users, fog nodes, and data service operators. This stable paradigm maximizes the usefulness of each entity.

The resource scheduling between fog devices in the same fog groups is presented by Sun *et al*. [15] and Bitam *et al*. [16] using meta-heuristic algorithms. Chen and Wang [17] developed two dynamic scheduling methods based on dynamics in the fog infrastructure response times and latency.

Bittencourt *et al*. [18] proposd a paradigm for scheduling that categorizes applications and client mobility as two key elements to provide effective resource management related to scheduling. Wadhwa and Aron [19] introduced OSCAR to optimize task scheduling in fog-based IoT environments. They use QoS-based scheduling and task clustering to enhance system throughput and increased bandwidth usage. Du *et al*. [20] proposed a computational offloading method to reduce device delay and energy usage. The method solves the nested resource allocation problem by taking offloading decisions.

Shahidani *et al*. [21] suggested a multi-objective task scheduling approach for fog-edge-cloud environment using reinforcement learning. They optimized network congestion, service delays, energy consumption and network usage. Subbaraj *et al*. [22] proposed a hybrid metaheuristic optimization technique called the Cow Search Algorithm (CSA) for solving resource allocation and scheduling issues in the fog environment. The proposed algorithm combines the pivoting

rule (local search) with the crow search algorithm (global search) to harness the advantages of both exploration and exploitation.

Liu *et al*. [23] introduced a resource-scheduling strategy to address the challenges of load balancing and task scheduling in a fog computing environment to decrease latency and energy consumption. The proposed technique uses a particle swarm optimization algorithm to search the optimal load balance on fog devices in a single cluster. They use a particle swarm algorithm for genetic joint optimization and an Artificial Bee Colony algorithm (PGABC) for optimizing the task scheduling among fog clusters.

After reviewing the existing literature, we found that most resource scheduling approaches are based on mono or bi-objective optimization that cannot balance these objectives effectively generating sub-optimal solutions. Therefore, we need a multi-objective optimization-based resource scheduling that generates a set of Pareto-optimal solutions to simultaneously trade off multiple and conflicting objectives of various heterogeneous tasks of different applications in a dynamic fog computing environment. There is a need to design an efficient multi-objective optimization-based resource scheduling approach that will perform optimal application module placement and allocate resources of fog nodes to tasks along with efficient utilization of resources and performance optimization. Therefore, we have designed and implemented a multi-objective optimization-based resource-scheduling algorithm based on MPSO to optimize different metrics. We have compared the results of MPSO with PSO and FCFS using the iFogsim simulator.

This research paper is concerned with the design, implementation, and evaluation of a multi-objective optimization-based resource scheduling algorithm that efficiently allocates resources to available suitable fog nodes according to the given requirements. The following are the main contributions of the suggested work.

1. To review current resource scheduling techniques for fog computing.
2. To investigate the limitations and shortcomings of the recently used task allocation (resource scheduling) methods.
3. An MPSO-based two-level model for resource scheduling is proposed that combines application module placement and task allocation with objectives to minimize latency, network usage, cost, and energy consumption to optimize resource utilization.
4. Moreover an effective task-scheduling algorithm based on the traditional Shortest Job First (SJF) is applied that prioritizes and executes the shortest tasks first on fog nodes, which minimizes the latency for critical tasks.
5. To compare the performance of the suggested resource scheduling algorithm to other algorithms and evaluate the execution results.

The remainder of the article is structured as follows. Fog computing architecture and proposed modified optimization-based (MPSO) resource scheduling are presented. Then the proposed simulation model and evaluation results of the MPSO-based resource scheduling algorithm are described. Finally, we explain the present research outcomes and provide recommendations for further study.

2. MATERIALS AND METHODS

The Fog-IoT model is comprised of three layers, each performing crucial functions: IoT, fog, and cloud layer. Figure 1 presents the architecture of Fog computing.

IoT Layer: The IoT layer is the bottommost layer in FIoT architecture. It includes devices such as sensors, actuators, and internet-connected IoT devices closer to the end-users [4]. This layer gathers and transfers data generated by IoT devices to upper layers for further processing.

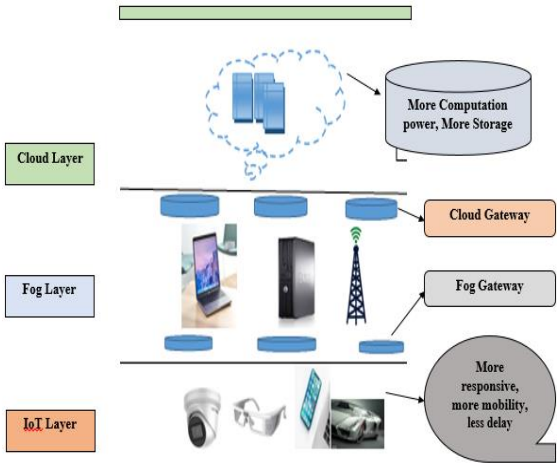

Fig. 1. Fog Computing Architecture.

Fog Layer: This intermediate layer is made up of heterogeneous fog nodes having different processing, storage, and networking capabilities; for example, routers, roadside units, proxy servers, cellular base stations, and mobiles [6]. These fog nodes collect data from the IoT layer, process it, perform necessary computations for intelligent decisions, and transfer it to the Cloud Layer for long-term decision-making.

Cloud Layer: The topmost layer servers as the central repository comprised of many powerful computers and data centers. Data centers give storage and processing services to IoT devices for storage and long-term analysis.

Fog devices are heterogeneous, dynamic, and resource-constrained, and the applications send requests/tasks for processing to these nodes [24]. Firstly, the resources of fog nodes are compared with the computational needs of these tasks, and if the resources are sufficient to process these tasks they should be allocated to that node and executed. The task will be shifted to the cloud for execution if no resources are available at the fog nodes. Figure 2 presents the block diagram of existing edge-ward resource scheduling in which modules are placed using FCFS on the nearest edge, fog nodes and cloud. Using FCFS, fog node manager places incoming module on fog nodes in order or arrival without prioritizing computing layers.

Effective task allocation or resource scheduling strategies are necessary to optimize resources, accelerate response times, and minimize cost and energy utilization. Therefore, we have developed

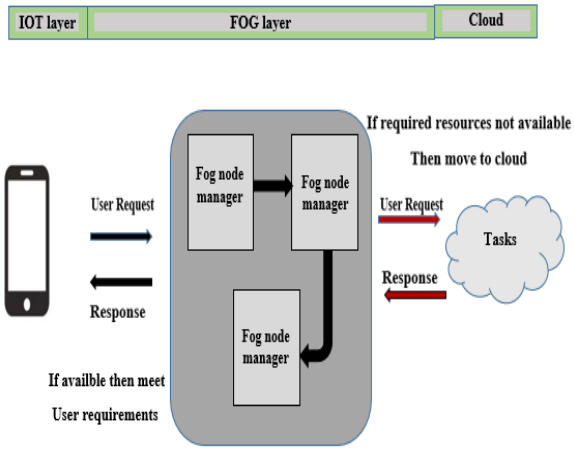

Fig. 2. Block Diagram of existing edge-ward resource scheduling.

a multi-objective optimization-based resource scheduling approach to allocate resources of fog nodes to user's jobs according to their needs while maximizing resource utilization, minimizing latency, cost, energy consumption, and network usage.

2.1. Case Study

We have selected a healthcare scenario as a fog computing use case that includes an Appointment Coordination System, Health Record Management System, and Urgent Notification System as healthcare applications [12].

Urgent Notification System: The Urgent Notification System monitors patient's critical data such as heart rate, sugar, blood pressure, oxygen saturation and generates instant response to this critical data.

Appointment Coordination System: This system manages appointments of different patients in different time slots with less critical data as compared to data of urgent notification systems.

Health Record Management System: The Healthcare Record Management System contains information such as names, addresses, and historical records of health that are recorded and stored on the cloud for future analysis and decision-making.

Challenges: Accurate results and quick responses are essential for real-time health data processing. However, various tasks compete in a heterogeneous environment for a limited number of resources of fog devices. Therefore, one of the main difficulties in fog and edge computing is resource management. For instance, a patient's status in a smart healthcare system requires quick notice to rescue the patient. It is difficult to allocate resources to requested tasks while maintaining low latency and efficient energy use. Therefore, we have applied a multi-objective optimization-based resource scheduling algorithm called MPSO to solve the resource management issues of latency, energy consumption, and resource utilization in smart healthcare.

2.1.1 MPSO algorithm for resource scheduling

Modified Particle Swarm Optimization (MPSO) [25] is an ideal solution for resource scheduling because it can handle multiple objectives and constraints

due to its meta-heuristic nature. It is adaptive to dynamic environments and easy to implement in a distributed and scalable environment. In short, MPSO-based resource scheduling can improve the efficiency, adaptability, and user satisfaction of the fog computing system, making it more suitable for a wide range of applications. MPSO algorithm follows the steps given below:

1. *Issue Propagation*
   i. Reduce Latency: The main objective is to reduce the time needed to process and analyze health data.
   ii. Reduce Energy Consumption: The second objective is to reduce energy use, while carrying out tasks through wearable technology and fog nodes.
2. *Population Initialization*
   Each possible solution in the population represents a method for task allocation (resource scheduling). Each solution specifies, taking into consideration processing power and energy resources, which tasks are assigned to which fog nodes. The population (swarm) is initialized randomly in the MPSO algorithm.
3. *MPSO Execution*
   To identify a collection of best-optimal solutions that balance minimizing delay, network usage, cost and energy usage, MPSO develops the population. To select the best work task allocation arrangements, MPSO refines solutions by adding a new variable named inertia weight $\boldsymbol{w}$ to the initial part of velocity updation.
4. *Fitness Evaluation*
   Based on task execution time, communication latency, and energy consumption, solutions are assessed. The properties of wearable technology, fog nodes, and the communication network are used to determine these measures.
5. *Inertia Weight*
   The best optimal solutions found by MPSO using additional concept inertia weight in PSO reflect various trade-offs between reducing latency and maximizing energy efficiency.
6. *MPSO Swarm Update*
   MPSO particles modify their locations to move in the direction by updating their local best and global best by changing velocity and position. The task allocation (resource scheduling) configurations are improved using the swarm exploration method.
7. *Resource Allocation Decision*
   The trade-offs between minimizing latency and energy usage are considered while making final resource allocation selections. To save energy, fewer time-sensitive processes might be assigned to the cloud and, critical jobs can be allocated to fog nodes for speedy analysis. To utilize resources, we arranged tasks into two categories: critical and non-critical.

Fog computing's resource allocation system enhances real-time health data analysis in healthcare settings by combining MPSO algorithms. In a hospital setting, this method assures prompt replies, resource efficiency, and energy effectiveness, all of which improve patient care and medical decision-making.

Therefore, we have proposed an MPSO-based two-level model for resource scheduling that combines application module placement and task allocation with the objectives of minimizing latency, network usage, cost, and energy consumption to optimize resource utilization and improve system performance. In the first step, the application module placement is used to find the optimal fog node to place each application module, considering different criteria such as the computing capacity, available bandwidth, and energy consumption of each node.

Afterward, task allocation deals with assigning the appropriate tasks to the most optimal fog nodes for execution by taking into account the available resources of fog nodes and the requirements of various heterogeneous tasks of different applications. This two-step MPSO-based resource scheduling model has paved the way to unlock the full potential of fog resources and optimize overall system performance.

The algorithm for MPSO-based resource scheduling is given as (Algorithm 1). We adopted MPSO for resource scheduling in our proposed algorithm. To choose the optimal tool for processing incoming jobs, MPSO is employed. In this algorithm, we've created a resource pool in which all resources are kept. In the first step, the decision maker will decide where to place the application modules. In the second step, when a task arrives, it will compare with the resources of each fog device using MPSO before sending it to fog devices; if the

device is found then it will be added to the hash map (queue). If the current device is not suitable, then the same steps will be performed for searching the next devices. If not, all available devices fulfill the task's needs, it will move to the cloud.

Algo. 1. MPSO-based resource scheduling.

```
Input: Tuples
Output: Task execution
    Fog devices created
    Application created
    Tuple generated by the sensor
    Reached at gateway
    Passed to the decision-maker
    The decision maker placed the modules on
    respective fog nodes
    The decision maker checks the available
    best fog node against the generated task by
    Algorithm 2
    Fog node process task
    Sent back to the respective gateway
    The result sent to the Actuator
For all unassigned tasks t1, t2, t3…tn do
    send to Cloud
End
```

Algorithm 2 will assign resources to tasks to the appropriate fog nodes.

Algo. 2. Steps of MPSO

```
Input: Tuple's Mips, Resources
Output: Best fog node
For received request t1, t2, t3…tn do
    For Bz = b1, b2, b3….bn do
        Bz <=  G (leastloaded)
            Allocatelbz  <=  Bz
    End
    Allocate gb = leastlbz
    Assign next task t <= G (gb)
    If nextassigned == last used GB then
        Goto step 3 (leastloadedF)
    Else
        Goto step 7
    End
End
Personalbest (lbz) <=  0
Globalbest (gb) <=  0
G <= g1.g2.g3……gj
Multiplenodes Bz  <= b1.b2.b3….bz
Multiplenodesize <= j/Bz
```

The steps of Algorithm 2 are given as follows:

1. Begin each particle with its position and speed.
2. Each particle's fitness value is assessed in comparison to its top performance, the personal best (pbest). If the current fitness value is higher, the pbest is upgraded to the new best.
3. Calculate the fitness value of each particle using the fitness function.
4. Assign the particle with the highest fitness value, determined in the previous phase to a new position; it was then randomly positioned with a radius of *r* around it, and the other particles' positions and velocities were adjusted following the fitness function. To determine whether a particle's new position is appropriate, compare it to the particle with the lowest (optimal) fitness value.
5. To find the optimal answer, verify the stated criteria (fitness function); if it is discovered, the algorithm has done iterating; otherwise, return to step 4.

Figure 3 presents the flowchart of the MPSO algorithm.

2.2. Simulation Setup

We have selected a healthcare scenario as a fog computing use case discussed in subsection 2.1 and simulated it using iFogSim. Our work can be considered as a combination of both theoretical and experimental work. In a theoretical sense, we

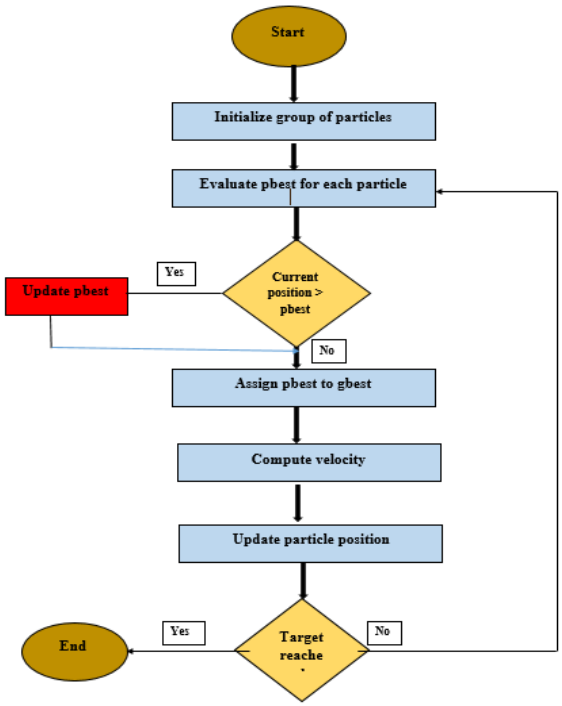

Fig. 3. Flowchart of MPSO.

have simulated a real-world healthcare scenario consisting of three healthcare applications: Appointment Coordination System, Health Record Management System, and Urgent Notification System. In fog computing, it is common practice to compare the resource scheduling based on modified-PSO to base-PSO and First-Come-First-Serve (FCFS) for many reasons. PSO is a nature-inspired optimisation algorithm that finds the optimal solution by moving a population of candidate solutions, known as particles, around the search space. Each particle adjusts its position based on its own and its neighbours' experiences, to arrive at the best solution. Whereas, the FCFS scheduling algorithm is a basic scheduling technique that arranges tasks according to arrival order and always executes the first task. These algorithms serve as baseline scheduling algorithms that help researchers to establish a baseline for performance evaluation that demonstrates the impact and effectiveness of introduced changes, ensuring a thorough evaluation and understanding of their contributions in the context of resource optimization. These comparisons also help to understand the trade-offs between conflicting objectives introduced by the modifications in PSO and whether they strike a better balance across multiple performance criteria such as latency, network usage, cost and energy in a dynamic fog computing environment.

In terms of experimentation, we used iFogsim to compare our proposed resource scheduling algorithm MPSO with traditional (FCFS) and recent meta-heuristic resource scheduling algorithm (PSO) under various conditions and policies. We used real-world data and different scenarios to test our model against real-world performance metrics, showcasing the practical benefits and limitations of modified PSO.

We have used iFogSim [26] to simulate our MPSO-based resource scheduling (task allocation) strategies to allocate the available resources to the task. IFogsim is a powerful toolset for simulating resource management strategies in IoT and fog computing scenarios. For this, we have extended iFogSim with the proposed case study of the healthcare scenario and added some more classes. These classes are used to implement our proposed MPSO-based scheduler. Below is a quick overview of the classes commonly used:

Sensors: The sensor class helps to simulate IoT sensors that generate data tuples with variable lengths and then send them to fog devices.

Fog Device: This class instance imitates different fog nodes with specified memory, computing power, storage space, and uplink and downstream bandwidth.

Tuples: All Fog's entities communicate with each other utilizing tuple class instances. Each tuple has source, destination, and processing demands expressed in MIPS.

Actuator: This class simulates an actuator by defining the outcome of actuation and its network connectivity properties. When a tuple from an application module is received, this classes executes a method that calculates useful metrics.
MPSO System: This class contains the details of fog devices involved in the modified proposed particle swarm algorithm that is in charge of assigning tasks to appropriate fog nodes.

PSO System: This class contains the implementation of the PSO algorithm that employs a group of potential solutions, i.e., particles (known as a swarm). We can use certain equations to shift these particles in the search space.

Scheduler: This class controls the sequence of execution of a list of upcoming tuples by using different algorithms (FCFS, PSO, MPSO).

Particles: The particle class is used for the swarm of particles and looks for the optimal position in the search space. Each element has a specific location $pi = (pi^1, pi^2 \ldots. pi^N)$ and the speed $si = (vi^1, vi^2, \ldots, vi^N)$ in the N-dimensional issue space, the i^{th} particle is represented by I, and N specifies the problem's dimension or the number of unknown variables.

Vector: Vector class is used to determine the specific position and coordinates. To find the location of the particle or node requires the axis and coordinates information. With the help of that, the system can find out the specific location. The vector class, location inside the search space, and best-known position of the entire swarm all serve as cues for the particle motions. These will eventually start

to direct the swarm's motions once better sites are found.

Swarm: The MPSO algorithm's fundamental version uses a swarm class, which employs a population of potential solutions (called particles). These particles are moved around in the search space using a few simple formulae.

Figure 4 displays the tuple emission, MPSO-based task allocation, and execution of tuples. In the first step, the sensor transmits a tuple using the transmit() function. The MPSO-based scheduler class calls the findbestFog() function to choose the best fog node for placement of appropriate application modules on optimal fog nodes. Afterward, the tasks are allocated to these modules for processing. In findbestFog() function the MPSO scheduler uses both the local best module placement and task allocation solution that it has found by using any task allocation strategy and a set of non-dominated module placement and task allocation strategies for multiple objectives to find the overall best fog node to process the task. The objective function was to minimize delay, energy consumption, and cost. When a tuple is received at any fog node, the fog node calls processTupleArrival() function to execute the tuple or forward it to a higher-level fog node. When a tuple is fully executed, the CloudletFinish() method notifies the scheduler to request the execution of the next tuple.

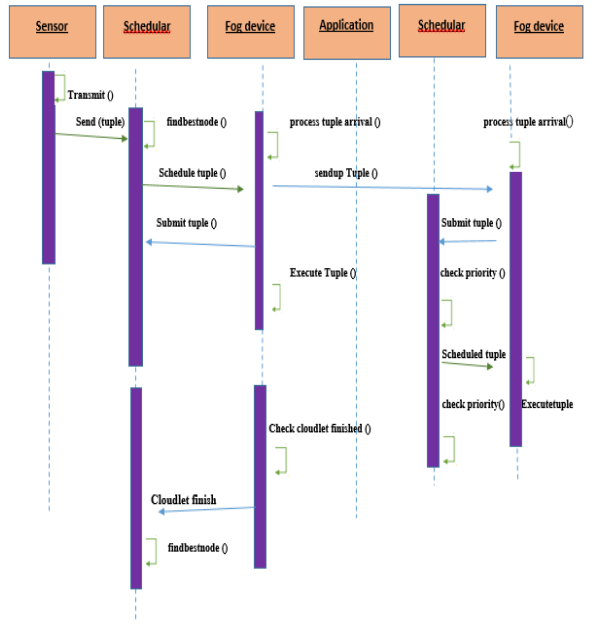

Fig. 4. Sequence diagram of resource scheduling on best node by using MPSO.

2.2.1 Configurations

We have conducted a thorough simulation-based investigation to examine the impact of the modified particle swarm optimization (MPSO) technique. In our simulation, we have used six topologies of 100, 150, 200, 250, 300, and 350 nodes that are arranged in four tiers: sensors and actuators at the bottom-most layer are connected with a set of low-level fog devices that serve as Data Collector and Processor (DCP). These lower-level fog nodes are connected with upper-level fog nodes (that serve as the Coordinator) at the third tier and these high-level fog devices are connected with the Cloud (serving as the patient record database) at the top. We fixed the number of cloud and high-level fog devices for each set of experiments to 1 and 4, respectively. The number of low-level fog generators we used ranged from 25, 50, 75, and 100, resulting in six topologies with 100, 150, 200, 250, 300, and 350 nodes, respectively. Each fog device receives information from sensors that are attached to it and takes appropriate action. For each arrangement, the simulation takes 400 units of time. The configuration of fog devices containing MIPS, Ram, upper-level bandwidth, and down-level bandwidth are given in Table 1.

The details of tuples that are generated by modules and their respective CPU length requirements are mentioned in Table 2.

3. RESULTS AND DISCUSSION

We have compared the performance of MPSO with both traditional and recent meta-heuristic resource scheduling algorithms. We have chosen FCFS from traditional algorithms and PSO from recent meta-

Table 1. Fog nodes configuration.

Device Name	MIPS	Memory	UBW	DBW
Cloud	44800	40000	100	10000
Base station	5600	4000	10000	10000
Upper-level Fog Nodes	5600	4000	10000	10000
Lower-level Fog Node	800	1000	10000	270

Table 2. Tuples with their CPU length (in MIPS).

Tuple type	CPU length
ECG	3000
SENSOR	3500
DATA_REC	1000
DATA_Type	14
RECV_REQ	28
CRITICAL	1000
NON_CRITICAL	1000
DISPLAY	500

heuristic algorithms as used in many recent studies [26-34]. The performance of MPSO algorithms is evaluated by minimizing latency, network usage, cost, and energy consumption.

3.1 Performance Metrics

We have chosen four metrics, latency is calculated using the overall system whole loop as well as for each loop, energy consumption, network utilization, and cost of execution.

i) Average Loop Delay

We have used the term "loop delay" to calculate the end-to-end latency. Loop delay refers to the time required to shift data in multiple modules that are placed on different nodes. The end-to-end latency of each module in the loop is calculated by using a control loop. We have calculated the control loops for different types of tuples transferring data among different modules of the healthcare case study that are explained in subsection 2.1, namely, the Appointment Coordination System, Health Record Management System, and Urgent Notification System.

i. Urgent Notification Loop: DCP->Coordinator->display
ii. Appointment Coordination Loop: DCP-> Coordinator ->DCP->display
iii. Healthcare Record Management Loop: DCP-> Coordinator ->Medical Record Database
iv. History: Coordinator -> Medical Record Database-> Coordinator ->DCP
v. ECG -> MedicalRecordDB-> Coordinator-> MedicalRecordDB -> display

To determine the loop latency, we computed the average processor time T_{cpu}, consumed by tuples of the same type. This average is then calculated using Equation (1).

$$T_{cpu} = \begin{cases} \frac{IT_c \times N + LT_i - IT_i}{N+1}, & \text{if the average CPU time is already computed} \\ LT_i - IT_i, & \text{otherwise} \end{cases} \quad (1)$$

Where IT_i is the initial execution time by all tuples of a specific type of tuple, LT_i is the end execution time of i^{th} tuple, and N is the total number of executed tuples of a certain type. By using Equation (2) we can calculate the execution delay of each tuple.

$$Delay_i = LT_i - IT_i \qquad \forall i \in T \qquad (2)$$

Where T represents the current tuple set.

We have shown along the x-axis number of nodes and y-axis loop delay in Figures 5, 6, 7, 8, 9, and 10 with blue, red, and green bars for FCFS, PSO, and MPSO, respectively. Figure 5 shows the average loop delay for an emergency alert system computed using FCFS, PSO, and MPSO. The loop delay of MPSO and PSO remains almost the same even with an increasing number of nodes but for FCFS it fluctuates.

The urgent notification system needs minimal latency to be efficient, therefore, both PSO and MPSO have placed the urgent notification system at edge devices ingrained in low latency, high priority and local data processing that leads to similar performance.

In Figure 6 the loop delay of the Appointment Coordination System is shown. The results of

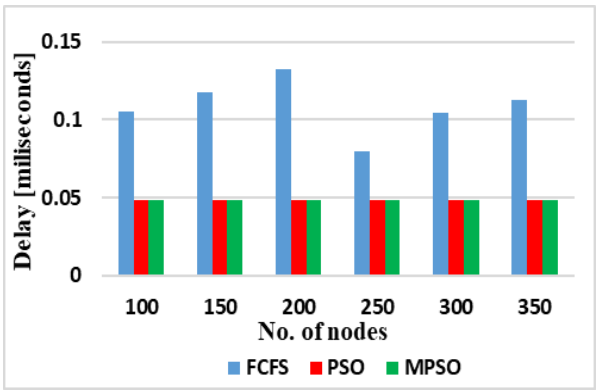

Fig. 5. Loop delay for Urgent Alert.

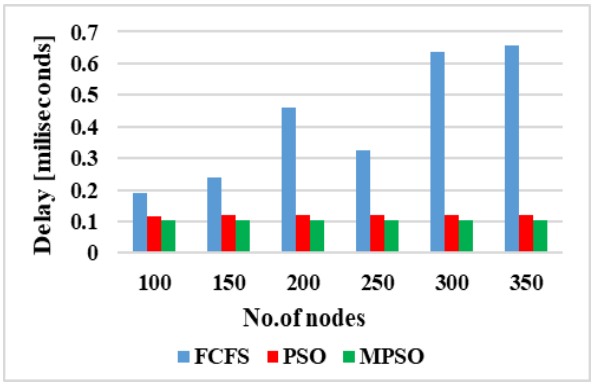

Fig. 6. Loop delay for appointment coordination.

MPSO are better than PSO and FCSF. FCFS has a greater amount of delay starting from a small size and grows as the no. of nodes rises, whereas the PSO and MPSO are the same denoted by bars.

Figure 7 shows the loop delay for medical record management where FCFS performs better than PSO and MPSO but with an increase in the number of nodes from 250 to 350 MPSO shows better results than FCFS and PSO.

In Figure 8 the loop delay of the medical history of patients is plotted, which shows that MPSO causes less delay in processing this record

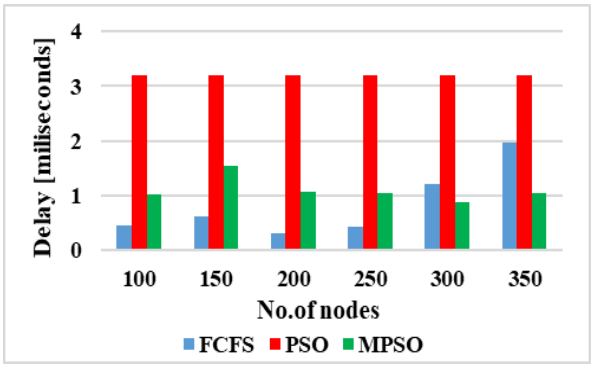

Fig. 7. Loop delay for healthcare record management.

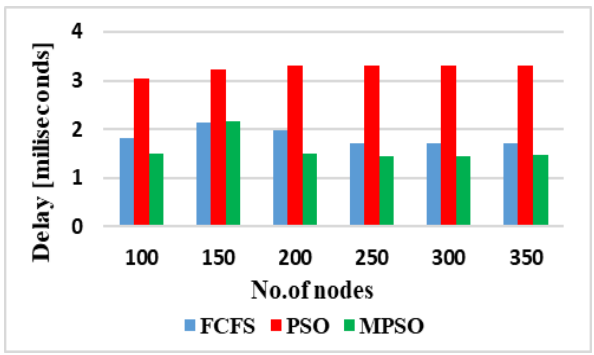

Fig. 8. Loop delay for history.

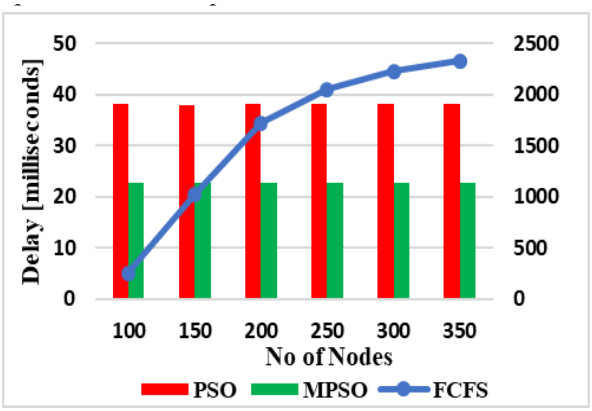

Fig. 9. System whole loop delay.

as compared to PSO and MPSO even with an increasing number of nodes.

ii) System whole loop delay

System whole loop latency is the time delay between the start of the application in a system to the end of the results of the application in a system. Equation (3) shows the formalization of System Latency L_{sys}.

$$L_{sys} = E_T \times N_{tp} (T_f - T_i)/N_{ttp} \quad (3)$$

Where E_T is the total execution time of N^{th} tuples N_{tp}, T_f is the final time of tuple N, N_{ttp} is the total number of tuples, and T_i is a tuple's initial time.

Figure 9 presents the combo plot of the system whole loop delay of FCFS, PSO, and MPSO. MPSO shows less delay as compared to PSO. The blue line represents the loop delay of FCFS which is quite large as compared to the MPSO and PSO.

iii) Energy Consumption

Energy loss is defined as energy supplied to a system that is not immediately consumed by computing processes such as power delivery and conversion, cooling, and lighting. Equation (4) is used to calculate the devices in the system's energy consumption; we can calculate how much energy a Fog device E_{FN} uses.

$$E_{FN} = E_i + (T_{pf} - T_{pi}) \times P_H \quad (4)$$

The energy consumption of any fog node is calculated by the power of all the host nodes in a specific period required for execution. E_i denotes the current consumed energy, T_{pf} is the recent time,

T_{pi} is the update time of last utilization, and P_H is the host power in last utilization.

Figure 10 shows the energy utilized by various fog nodes of the system. Along the x-axis we have plotted the number of fog nodes for all six sets of experiments starting from 100 and ending at 350. Along the y-axis we have plotted the energy consumed by these fog devices.

iv) Network Usage

Network utilization, N_{use}, is the third assessment factor. As the quantity of units expands, so does network consumption, which causes congestion. We compute network usage using Equation (5).

$$N_{use} = \sum_{i=1}^{N} D_i * N_i \quad (5)$$

N signifies the total number of tuples, D_i denotes the delay, and N_i is the size of the i^{th} tuple.

To illustrate how fog devices use the network, this section compares the FCFS algorithm to the MPSO and PSO. The network use of PSO, MPSO, and FCFS is compared using a combo plot in Figure 11. The x-axis represents the number of nodes, and the y-axis represents the average network utilization. The outcome demonstrates that network usage of MPSO is less than PSO and FCFS for all sets of nodes in all experiments.

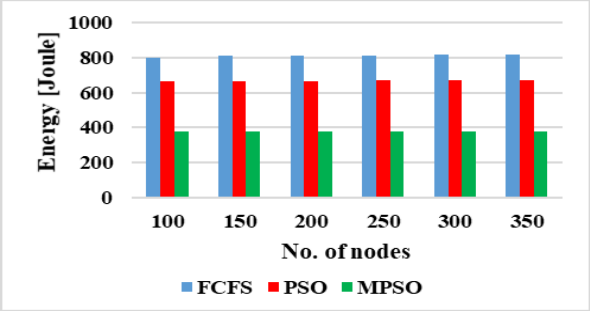

Fig. 10. Energy Consumption.

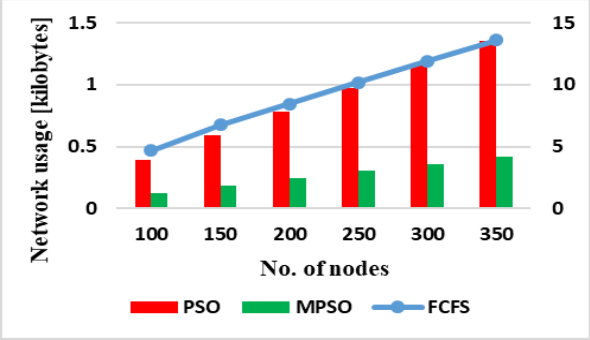

Fig. 11. Network Usage.

v) Cost of Execution

To check the availability and reliability of the proposed module, one of the parameters is the cost of execution. Execution cost can be computed by using Equation (6).

$$C_E = F_C + V_C/NUP \quad (6)$$

C_E is the total cost of execution F_C is for the fixed cost V_C is used instead of variable cost and NUP is for the number of units produced.

Figure 12 shows the execution cost of all six sets of nodes for all experiments. Along x-axis we have taken several nodes and along the y-axis, the cost consumed by various fog nodes in all experiments. The combo graph shows that MPSO has less cost as compared to PSO. The execution cost using FCFS is represented by a blue line that indicates its worst performance.

The outcomes demonstrate that the suggested MPSO outperforms FCFS and PSO in all performance metrics including latency, energy consumption, network usage, and cost of execution. These results reveal the effectiveness and superiority of the proposed MPSO-based resource scheduling as compared to the traditional FCFS and recent meta-heuristic PSO.

4. CONCLUSIONS

Resource scheduling in fog computing aims to maximize resource utilization along different performance metrics, but the heterogeneity of resource-limited fog devices, and the dynamic nature of the fog environment, make resource scheduling a challenging problem. To address this issue, we have proposed a Modified Particle Swarm Optimization (MPSO) based resource scheduling algorithm that

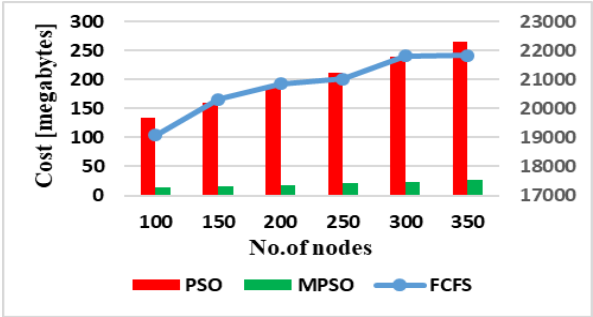

Fig. 12. Cost of Execution.

combines application module placement and task allocation by finding the optimal fog node to place each application module and assign appropriate tasks to the most suitable fog nodes for execution. The MPSO-based resource scheduling aims to maximize the utilization of resources by doing a trade-off of multiple objectives simultaneously, such as minimization of latency, network usage, energy consumption, and execution cost. We have applied our MPSO-based resource scheduling on a healthcare scenario with three healthcare applications namely the Urgent Notification System, Appointment Coordination System, and Health Record Management System as part of our fog computing use case. We then used iFogSim to design, model, and evaluate the performance of these systems under various conditions and scenarios. MPSO outperforms FCFS and PSO in minimizing latency for all healthcare applications including, the Urgent Notification System, Appointment Coordination System, and Health Record Management System. The comparison of results show that MPSO is better suited for all three applications of healthcare scenarios. At the start, the FCFS shows less loop delay than PSO and MPSO, but as the number of nodes increases MPSO shows better results as compared to FCFS and PSO. Furthermore, the analysis of results reveals that MPSO optimizes resource utilization by consuming less energy, low network usage, and reduced cost when compared with FCFS and PSO.

Although the modified PSO improved the performance in dynamic and distributed fog computing environment, but it also results in additional computational complexity and slow convergence. In future, we will address these challenges by applying machine learning algorithm with MPSO to improve its performance.

5. CONFLICT OF INTEREST

The authors declare no conflict of interest.

6. REFERENCES

1. A. Alabdulatif, N.N. Thilakarathne, Z.K. Lawal, K.E. Fahim, and R.Y. Zakari. Internet of nano-things (iont): A comprehensive review from architecture to security and privacy challenges. *Sensors* 23(5): 1–26 (2023).
2. F. Alhaidari, A. Rahman, and R. Zagrouba. Cloud of Things: architecture, applications and challenges. *Journal of Ambient Intelligence and Humanized Computing* 14(5): 5957-5975 (2023).
3. K. Cao, Y. Liu, G. Meng, and Q. Sun. An overview on edge computing research. *IEEE access* 8: 85714–85728 (2020).
4. S.N. Srirama. A decade of research in fog computing: relevance, challenges, and future directions. *Software: Practice and Experience* 54(1): 3-23 (2024).
5. M. Aazam, S. Zeadally, and K.A. Harras. Fog computing architecture, evaluation, and future research directions. *IEEE Communications Magazine* 56(5): 46–52 (2018).
6. B. Jamil, H. Ijaz, M. Shojafar, K. Munir, and R. Buyya. Resource allocation and task scheduling in fog computing and internet of everything environments: A taxonomy, review, and future directions. *ACM Computing Surveys* 54(11s): 233 (2022).
7. M. Ghobaei-Arani, A. Souri, and A.A. Rahmanian. Resource management approaches in fog computing: a comprehensive review. *Journal of Grid Computing* 18(1): 1–42 (2020).
8. M.D. Benedetti, F. Messina, G. Pappalardo, and C. Santoro. JarvSis: a distributed scheduler for IoT applications. *Cluster Computing* 20(2): 1775–1790 (2017).
9. Z. Movahedi, B. Defude, and A.M. Hosseininia. An efficient population-based multi-objective task scheduling approach in fog computing systems. *Journal of Cloud Computing: Advances, Systems and Applications* 10(1): 53 (2021).
10. C.G. Wu, W. Li, L. Wang, and A.Y. Zomaya. An evolutionary fuzzy scheduler for multi-objective resource allocation in fog computing. *Future Generation Computer Systems* 117: 498-509 (2021).
11. B. Jamil, M. Shojafar, I. Ahmed, A. Ullah, K. Munir, and H. Ijaz. A job scheduling algorithm for delay and performance optimization in fog computing. *Concurrency and Computation: Practice and Experience* 32(7): e5581 (2019).
12. S. Jošilo, and G. Dán. Decentralized algorithm for randomized task allocation in fog computing systems. I*EEE/ACM Transactions on Networking* 27(1): 85–97 (2019).
13. H. Zhang, Y. Xiao, S. Bu, D. Niyato, R. Yu, and Z. Han. Computing resource allocation in three-tier IoT fog networks: A joint optimization approach combining Stackelberg game and matching. *IEEE Internet of Things Journal* 4(5): 1204–1215 (2017).
14. H. Zhang, Y. Zhang, Y. Gu, D. Niyato, and Z. Han. A hierarchical game framework for resource management in fog computing. *IEEE Communications Magazine* 55(8): 52–57 (2017).
15. Y. Sun, F. Lin, and H. Xu. Multi-objective optimization of resource scheduling in fog computing using an improved NSGA-II. *Wireless*

Personal Communications 102(2): 1369–1385 (2018).
16. S. Bitam, S. Zeadally, and A. Mellouk. Fog computing job scheduling optimization based on bees swarm. *Enterprise Information Systems* 12(4): 373–397 (2018).
17. X. Chen, and L. Wang. Exploring fog computing-based adaptive vehicular data scheduling policies through a compositional formal method - PEPA. *IEEE Communications Letters* 21(4): 745–748 (2017).
18. L.F. Bittencourt, J. Diaz-Montes, R. Buyya, O.F. Rana, and M. Parashar. Mobility-aware application scheduling in fog computing. *IEEE Cloud Computing* 4(2): 26–35 (2017).
19. H. Wadhwa, and R. Aron. Optimized task scheduling and preemption for distributed resource management in fog-assisted IoT environment. *The Journal of Supercomputing* 79(2): 2212-2250 (2023).
20. J. Du, L. Zhao, J. Feng, and X. Chu. Computation offloading and resource allocation in mixed fog/cloud computing systems with min-max fairness guarantee. *IEEE Transactions on Communications* 66(4): 1594–1608 (2018).
21. F.R. Shahidani, A. Ghasemi, A.T. Haghighat, and A. Keshavarzi. Task scheduling in edge-fog-cloud architecture: a multi-objective load balancing approach using reinforcement learning algorithm. *Computing* 105(6): 1337-1359 (2023).
22. S. Subbaraj, R. Thiyagarajan, and M. Rengaraj. A smart fog computing based real-time secure resource allocation and scheduling strategy using multi-objective crow search algorithm. *Journal of Ambient Intelligence and Humanized Computing* 14: 1003–1015 (2023).
23. W. Liu, C. Li, A. Zheng, Z. Zheng, Z. Zhang, and Y. Xiao. Fog Computing Resource-Scheduling Strategy in IoT Based on Artificial Bee Colony Algorithm. *Electronics* 12(7): 1511 (2023).
24. M. Aldossary. Multi-layer fog-cloud architecture for optimizing the placement of IoT applications in smart cities. *Computers, Materials & Continua* 75(1): 633-649 (2023).
25. D. Tian, and Z. Shi. MPSO: Modified particle swarm optimization and its applications. *Swarm and Evolutionary Computation* 41: 49-68 (2018).
26. H. Gupta, V.D. Amir, K.G. Soumya, and R. Buyya. iFogSim: A toolkit for modeling and simulation of resource management techniques in the Internet of Things, Edge and Fog computing environments. *Software: Practice and Experience* 47(9): 1275-1296 (2017).
27. R. Poli, J. Kennedy, and T. Blackwell. Particle swarm optimization: An overview. *Swarm Intelligence* 1: 33-57 (2007).
28. S.S. Hajam, and S.A. Sofi. Resource management in fog computing using greedy and semi-greedy spider monkey optimization. *Soft Computing* 27(24): 18697-18707 (2023).
29. N. Potu, C. Jatoth, and P. Parvataneni. Optimizing resource scheduling based on extended particle swarm optimization in fog computing environments. *Concurrency and Computation: Practice and Experience* 33(23): e6163 (2021).
30. C. Huang, H. Wang, L. Zeng, and T. Liu. Resource scheduling and energy consumption optimization based on Lyapunov optimization in fog computing. *Sensors* 22(9): 3572 (2022).
31. M. Fahad, M. Shojafar, M. Abbas, I. Ahmed, and H. Ijaz. A multi-queue priority-based task scheduling algorithm in fog computing environment. *Concurrency and Computation: Practice and Experience* 34(28): e7376 (2022).
32. S. Javanmardi, M. Shojafar, V. Persico, and A. Pescapè. FPFTS: A joint fuzzy particle swarm optimization mobility-aware approach to fog task scheduling algorithm for Internet of Things devices. *Software: Practice and Experience* 51(12): 2519-2539 (2021).
33. U.K. Saba, S.ul. Islam, H. Ijaz, J.J. Rodrigues, A. Gani, and K. Munir. Planning Fog networks for time-critical IoT requests. *Computer Communications* 172(C): 75-83 (2021).
34. H. Rafique, M.A. Shah, S.U. Islam, T. Maqsood, S. Khan, and C. Maple. A novel bio-inspired hybrid algorithm (NBIHA) for efficient resource management in fog computing. *IEEE Access* 7: 115760-115773 (2019).

Proceedings of the Pakistan Academy of Sciences: A Physical and Computational Sciences 61(1): 33-39 (2024)

ISSN (Print): 2518-4245; ISSN (Online): 2518-4253
https://doi.org/10.53560/PPASA(61-1)675

Pakistan Academy of Sciences

Research Article

Green Synthesis of Aluminum Silicate and Aluminum Iron Oxide Nanocomposites for Industrial Applications

Muhammed Saad Shabir[1], Hina Zain[1*], Moin Maqsood[1], Aysha Bukhari[2], and Ammara Nazir[2]

[1]Department of Chemistry, Superior University, Lahore, Pakistan
[2]Department of Chemistry, Minhaj University, Lahore, Pakistan

Abstract: Nano chemistry is revolutionizing the chemical industry. This research targets the green synthesis of Al-Si and Al-Fe nanocomposites and their application in the cement industry to produce durable cement coating. The nanocomposites were prepared by incorporating the green ingredients as reducing and stabilizing agents followed by the direct heating and calcination of the samples. The X-ray diffraction analysis and SEM were performed to confirm crystallinity and the nano-dimensional structure of the prepared nanocomposites. The SEM micrographs of Al-Si and Al-Fe nanocomposites provided the sizes as 15-37 nm and 17-61 nm, respectively. BET analysis revealed the surface area as 1.084 m^2/g and 0.884 m^2/g, respectively, for Al-Si and Al-Fe nanocomposites. These were applied in cement mortar and stability was checked for 07 and 28 days. The samples with 07 days of stability time showed an increase while the samples with 28 days showed a decrease in compressive strength.

Keywords: Nanocomposites, Cement Industry, Compressive Strength, Green Synthesis.

1. INTRODUCTION

Nanoscience has emerged as an outstanding field in the recent past and has been producing advancement in different departments of science, engineering, and technology. Nanomaterials have at least one dimension in the nanoscale, i.e., length or width, size, morphology, etc. There are several methods to prepare efficient and functional nano-surfaces that can help to reduce reaction times, do better yields, and produce durable materials. Sol-gel, chemical vapor deposition, hydrothermal procedures, green techniques, and Laser methods are some popular methods to produce nano-engineered substance [1]. Nanoparticles and nanocomposites are two important classes of nanomaterial that have been utilized in different industries to enhance the efficiency and capability of materials, i.e., cement, paints, coating, and many other industries. Nanoparticles like nano-silica, alumina, and titanium nanoparticles have improved the structure and function of numerous materials and surfaces. When two elements are combined, a composite is obtained which has more efficiency and functionality than the individual particles. Recently, a widespread use of nanocomposites has been observed in the infrastructure department where they have contributed to producing comprehensive and functional surfaces with improved durability and versatile properties. The incorporation of silica and iron-based nanocomposites into cement has generated substantial interest due to their ability to enhance the mechanical, thermal, and durability characteristics of cementitious materials. Silica and iron-based nanocomposites have impacted very much on the properties of cement mortar like CO_2-impregnated silica [2], titanium-coated silica [3], alumino-silicates, barium silicate [4], Fe/Al [5] and Fe/Cu [6] have enhanced the durability, compressive and mechanical strength. The modern surfaces containing nanocomposites have resolved the issues of cracks, fouling of surface, less durability, and unwanted photo-catalytic processes to some extent [7-9].

As demand is continues rising for sustainable, high-performance construction materials, exploring nanocomposites in cement manufacturing has

Received: December 2023; Revised: February 2024; Accepted: March 2024
*Corresponding Author: Hina Zain <hina.zain@superior.edu.pk>

grown increasingly crucial. This research paper seeks to examine the importance of the inculcation of silica and iron-based nanocomposites in cement, emphasizing their capacity to boost the strength, durability, and environmental sustainability of concrete structures. Research is underway to improve the quality of the cement mortar and provide the best product for infrastructure strength [10, 11]. However, there is still a need for a more durable and functional surface, i.e., cement mortar which can enhance the lifetime of the material and avoid said issues to a maximum extent. Therefore, this topic has great potential for research and development of sustainable construction materials and practices.

2. MATERIALS AND METHODS

2.1. Preparation of *Azadirachta indica* Leaves Extract

Fresh and green leaves of *Azadirachta indica* were collected from the Lahore region and were washed with distilled water. 40 g of leaves were boiled in 350 ml distilled water for 30 minutes. The extract was cooled and filtered. The prepared extract was stored for further processing [12].

2.2. Preparation of Al-Si Nanocomposite

0.001 M SiO_2 solution was added dropwise in 0.001 M $Al(OH)_3$ with constant stirring at room temperature. When the solution was homogenized the *Azadirachta indica* leaves extract was added in a ratio of 1:2 with constant stirring. A clear yellow solution was formed. It was kept in the oven for overnight at 90 °C, hard dry mass was obtained which was ground and calcination was done at 600 °C for 2 hours [13].

2.3. Preparation of Al-Fe Nanocomposite

0.001 M $FeCl_3$ solution was mixed with 0.001 M $Al(OH)_3$ with constant stirring for 30 minutes at room temperature. When the solution was homogenized the *Azadirachta indica* leaves extract was added in a ratio of 1:2. The solution was turned black. It was then dried in an oven overnight at 100 °C. The dried mass was calcinated in an oven at 650 °C for three hours [12].

2.4. Characterization of Nanocomposites

Scanning electron microscopy (SEM) analysis was performed through Nova Nano SEM to evaluate the size and morphology of Al-Si and Al-Fe nanocomposites. X-ray diffractometer was also used to identify the synthesized nanocomposites. In addition to it, the EDX analysis was also performed to check the elemental composition of the nanocomposites.

Surface area analysis and adsorption capacity of nanocomposites were studied from BET analysis. It is the physical adsorption of gas molecules on a solid surface. The surface area can be calculated from the BET equation stated below.

$$1/W[(P0/P) - 1] = 1/W_mC + C - 1/W_mC(P/P0) \quad (1)$$

Samples were prepared for BET analysis. Nitrogen gas was used to check the adsorption level of the nanomaterial and to assess the possible sites available for adsorption purposes. The temperature was kept at 77 K which is the standard temperature for performing the analysis. Powdered samples were used for the analysis. The experiment was performed at the Comsats University Islamabad, Lahore Campus.

2.5. Compressive Strength of Cement Mortar

To study the effect of nanocomposites on the compressive strength of cement mortar was studied. Four samples of cement mortar cubes were prepared by mixing sand and cement in a 2:1 ratio. Each nanocomposite in the concentration of 0.1% and 0.15% of the total weight of mortar was added. Samples were mixed thoroughly in water and poured into the 4 cm × 4 cm wooden molds for setting prepared. A control sample was also prepared without adding nanocomposites. Compressive strength testing was done on cubes after 7 and 28 days of setting [7, 8]. The instrument used for the testing of the cubes was Compression Testing Machine from Islamia University of Bahawalpur. The cubes were kept in the machine one by one and a pressure was released by the presser within the machine. The reading on the digital meter was the compressive strength of the cube which it was bearing inside the machine.

3. RESULTS AND DISCUSSION

3.1. SEM and EDX of Al-Si and Al-Fe Nanocomposites

The SEM images obtained revealed the size of the nanoparticles. Figure 1(a) shows that the silica nanoparticles were 15-37 nm in size with the morphology of rod shape embedded in the aluminum matrix [14]. The shape looks more like a core-shell nanoparticle in which silica nanoparticles behave like the core and aluminum matrix as a shell. The per unit percentage of silica nanoparticles was high in the aluminum matrix. SEM micrograph shows a strong interfacial interaction between the aluminum and silicon nanocomposites. There also exists a pore formation and it has a direct relation with the size of silica nanoparticles. In Figure 1(b), iron nanoparticles can be seen evenly distributed at different interfacial angles with the aluminum nanoparticles. The morphology of the iron nanoparticles can be seen as cubic and spherical

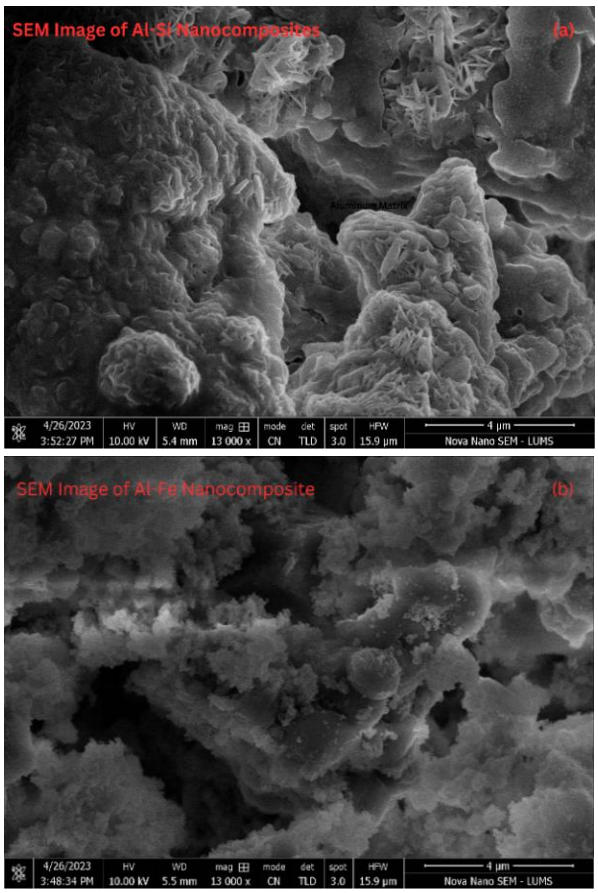

Fig. 1. (a) SEM image of Al-Si Nanocomposite, (b) SEM image of Al-Fe Nanocomposite.

Table 1. Energy-Dispersive X-Ray Spectroscopy results of Al-Si Nanocomposites.

Sr. No.	Element	Percentage (%)
1	Carbon (C)	22.08
2	Oxygen (O)	41.33
3	Magnesium (Mg)	2.62
4	Aluminum (Al)	0.11
5	Silicon	2.92

Table 2. Energy-Dispersive X-Ray Spectroscopy results of Al-Fe Nanocomposites.

Sr. No.	Element	Percentage (%)
1	Carbon (C)	23.24
2	Oxygen (O)	28.32
3	Magnesium (Mg)	4.62
4	Aluminum (Al)	0.12
5	Silicon (Si)	1.36
6	Iron (Fe)	4.29
7	Calcium (Ca)	9.51
8	Potassium (K)	15.4

particles in contact with the aluminum surface and dispersed in a good manner. The bonding between the aluminum and iron nanoparticles as well as dispersion can be seen across the micrograph. Particle sizes ranging from 17-61 nm are present [15]. The pore density is very low in between the iron and aluminum nanoparticles. This in turn happens good for the mechanical and functional properties of the material.

The elemental breakup of the nanocomposites obtained from the SEM-EDX analysis is presented in Table 1 for Al-Si nanocomposites and in Table 2 for Al-Fe nanocomposites.

3.2. XRD Analysis of Al-Si and Al-Fe Nanocomposites

X-ray diffraction spectrum of Al-Si nanocomposites is shown in Figure 2(a), the peaks observed at 28.3˚, 34.1˚, 40.6˚, 50.2˚, and 66.4˚ correspond to the plane of quartz (001), kaolinite (001), muscovite (001), kaolinite (110) and (102), respectively, and agree with the JCPDS file (46-1045), (29-1488), (39-1484) and (29-1488) for both the phases of kaolinite. These planes or diffraction angles correspond to different mineral compositions of the Alumino-

silicate nanocomposites. These results show the presence of different crystallographic planes of aluminum oxide and iron oxide nanoparticles. The major phases include kaolinite, feldspar, andalusite, and quartz. These different phases exist due to the difference in the ratio of Al_2O_3 and SiO_2. While in Figure 2(b), the XRD peaks observed at 28.36° (001 planes of Boehmite, JCPDS file number, 21-1307); the peaks at 40.56°, 50.44°, 66.8° and 73.96° correspond to hematite (024, 001, 014 planes) and maghemite (001, 110, 113) with JCPDS file numbers as 33-0664 and 39-1346, respectively.

3.3 BET Analysis of Al-Si and Al-Fe Nanocomposites

Two Different types of adsorption isotherms were obtained showing adsorption of the materials against the relative pressure (Figure 3). As the amount of the material is enhanced, the adsorption also becomes greater.

3.3.1. Adsorption analysis of Al-Si and Al-Fe nanocomposites through BET

In order to calculate the surface area of the nanocomposites Equation (1) is employed. To find the surface area, a graph is plotted between 1/[W((P0/P) - 1)] on the y-axis and relative pressure p/p◦ on the x-axis. Surface area can also be found through putting the available information. The total surface area of the Al-Si and Al-Fe nanocomposites was calculated as 1.084 m^2/g and 0.884 m^2/g, respectively. Another important factor is the total pore volume which is less than 2.6 nm of size in both cases and recorded as 4.528×10^{-4} and 3.37×10^{-4}. The micropore area and volume were recorded as 0.00 cc/g. The surface area calculated through multi-point BET is 1.084 m^2/g and 0.884m^2/g, for Al-Si and Al-Fe nanocomposite, respectively [16, 17].

In Figure 4(a), the isotherm represents the type II isotherm as given by IUPAC. There are a total of 06 types of isotherms which denote different

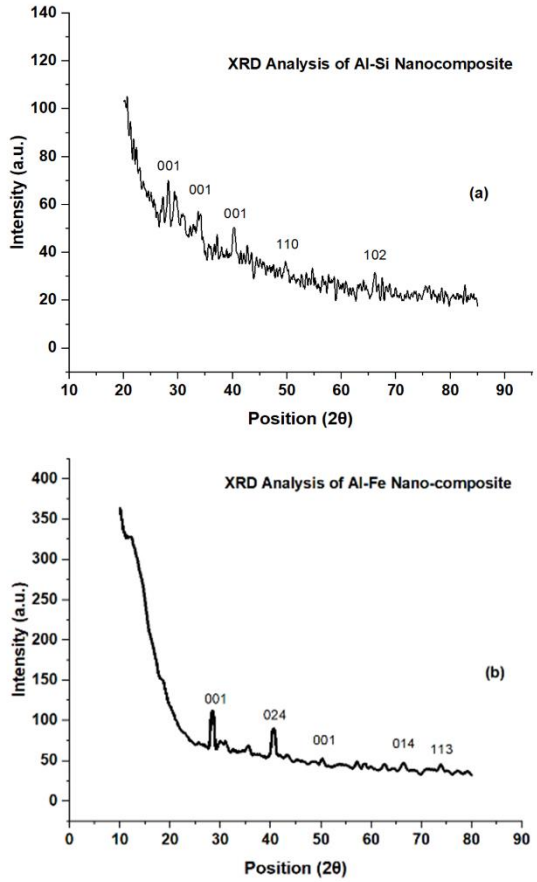

Fig. 2. (a) XRD Pattern of Al-Si nanocomposite, (b) XRD Pattern of Al-Fe nanocomposite.

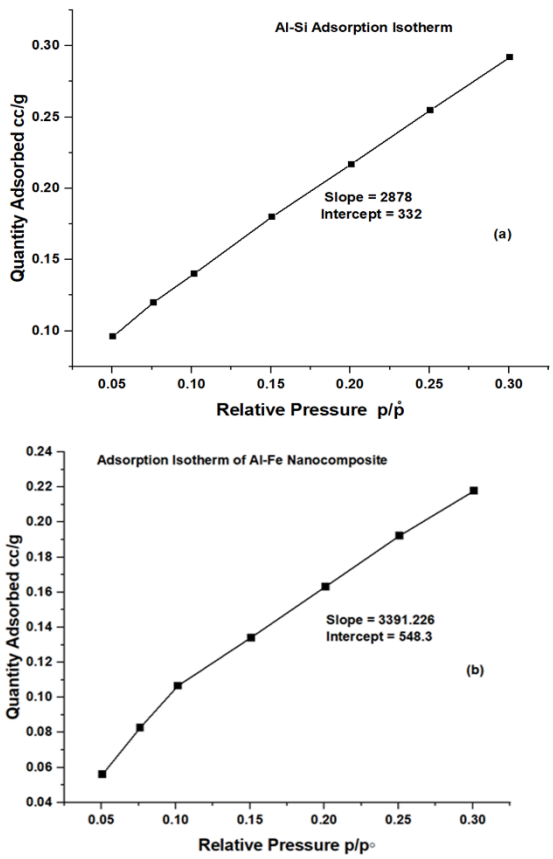

Fig. 3. (a) Adsorption Capacity of Nanocomposites Al-Si, (b) Adsorption Capacity of Al-Fe Nano-composite.

characteristics of adsorption of different materials [18]. The type II isotherm successfully explains the adsorption on porous monolayer materials at low pressure and on mesoporous multilayer materials at high pressure with no hysteresis**.** The process is termed Multiple Site Adsorption in which adsorbing sites are the unit sites of total adsorbing area. In Figure 4(b), the isotherm is more likely the type III isotherm which explains the more adsorbate-adsorbate reaction than the adsorbent and adsorbate reaction.

3.3.2. Compressive strength analysis of nanocomposite added cement mortar samples

After 07 days and 28 days of setting time, the cement mortar samples were tested. The mortar sample with both nanocomposites after 07 days of setting time showed high compressive strength as compared to the 28-day setting time.

The results mentioned in Table 3 show the compressive strength after 07 days of stability time, it is suggested that ratios for both the nanocomposites helped in accelerating the binding capacity of mortar. of the cement mortar as compared to the control sample. The application of alumino-silicate and aluminum iron oxide nanocomposite was done in the cement mortar to check the change in the compressive strength of the cement mortar. Alumino-silicate and aluminum iron oxide incorporated cement mortar showed an increase in the compressive strength of the cement mortar in comparison with the control group with no addition of nanocomposites. It can also be inferred that increasing the percentage of the nanocomposites caused the increase in strength. Control sample showed strength of 26.3 MPa while that of both nanocomposites showed more strength at 0.1% and 0.15%. This is due to an increase in the formation of calcium silicate hydrate gel through which the voids and spaces are filled, and the structure densifies [19, 20].

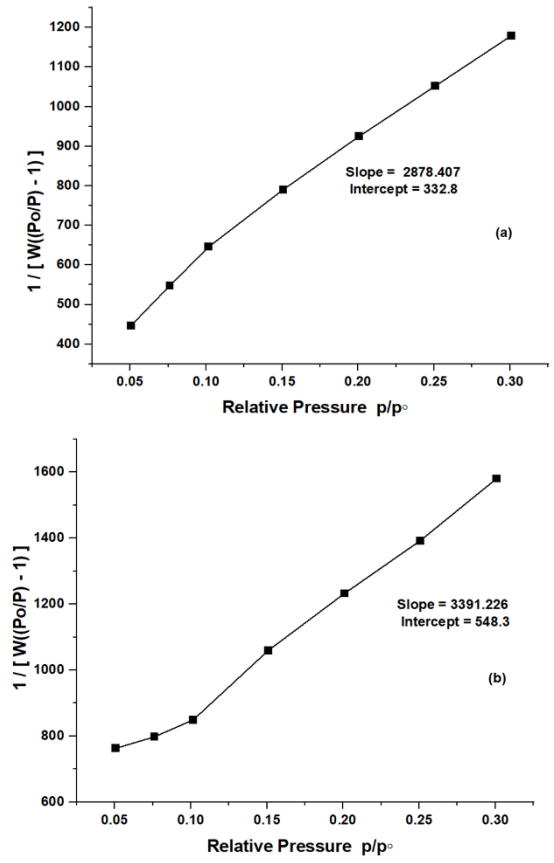

Fig. 4. (a) Plot of Al-Si Nano-Composites to determine surface area, (b) Plot of Al-Fe Nanocomposites to determine surface area.

Table 4 shows that after the curing time of 28 days, there was a decrease in the compressive strength which occurred due to weak bonding attraction developed between the particles of the cement and nanocomposite. It has been observed

Table 3. Compressive strength increases after 07 days of stability time.

Sr. No	Nanocomposite	Percentage of nano-composite Added	07 Days Strength Comparison (MPa)	Load (KN)
1	Control	0%	26.3	263
2	Al-Si	0.1%	35.2	352
3	Al-Si	0.15%	36.3	363
4	Al-Fe	0.1%	33.4	334
5	Al-Fe	0.15%	41.3	413

Table 4. Compressive strength increases after 28 days of stability time.

Sr. No	Nanocomposite	Percentage of nano-composite Added	28 Days Strength Comparison (MPa)	Load (KN)
1	Control	0%	28.7	287
2	Al-Si	0.1%	16.43	164.3
3	Al-Si	0.15%	21.22	212.2
4	Al-Fe	0.1%	21.48	214.8
5	Al-Fe	0.15%	14.65	146.5

in the previously published research, that 07 days cured cement mortar samples had more compressive strength than the 28 days cured cement [21, 22]. The composition of both the nanocomposites with 0.1% and 0.15% showed a decrease in the strength and on both cases the strength with all composition of Al-Si and Al-Fe was less than the strength of control. At early stages, the pozzolanic reaction caused the formation of calcium-silicate-nanocomposite - cement gel causing denser structure. Later continuous hydration may have caused the breakage of the gel structure causing more cracks in the cement mortar thereby causing reduction in the denser structure.

4. CONCLUSIONS

This research paper aimed at the preparation of Aluminum Silicate and Aluminum Iron Oxide nanocomposite through the green route followed by SEM, EDX, XRD, and BET characterization with their industrial application in the cement industry. The results obtained through characterization confirmed the nano dimensions of the materials. Furthermore, the prepared nanocomposites were applied in the cement mortar, and after 07 and 28 days of stability time, the compressive strength increase was observed in the samples cured for 07 days. Reduction in 28 days of cured samples' compressive strength was observed due to weak bonding attraction between the nanocomposites and cement mortar. The more strength at 07 days may be due to the filling up of the spaces and interaction sites of the cement mortar by the nanocomposites and later on agglomeration or leeching out of the nanocomposite caused lowering of strength.

5. ACKNOWLEDGEMENTS

GC University Lahore and Minhaj University Lahore provided instruments, chemicals and labs for research purposes.

6. CONFLICT OF INTEREST

The authors declare no conflict of interest.

7. REFERENCES

1. N. Baig, I. Kammakakam, and W. Falath. Nanomaterials: A review of synthesis methods, properties, recent progress, and challenges. *Materials Advances* 2(6): 1821-71 (2021).
2. T.M. Jassam, K. Kien-Woh, B. Lau, and M. Yaseer. Novel cement curing technique by using controlled release of carbon dioxide coupled with nanosilica. *Construction and Building Materials* 223: 692-704 (2019).
3. P. Sikora, K. Cendrowski, A. Markowska-Szczupak, E. Horszczaruk, and E. Mijowska. The effects of silica/titania nanocomposite on the mechanical and bactericidal properties of cement mortars. *Construction and Building Materials* 150: 738-46 (2017).
4. H.A. Abdel-Gawwad, K.A. Metwally, and T.A. Tawfik. Role of barium carbonate and barium silicate nanoparticles in the performance of cement mortar. *Journal of Building Engineering* 44: 102721 (2021).
5. F. Gulshan, and K. Okada. Preparation of alumina-iron oxide compounds by coprecipitation and gel evaporation methods and their characterization. *Journal of Engineering Research* 3: 1-8 (2015).
6. S.R. Dhruval, N. Pai, S.S. Dhanwant, B. Hussein, S. Nayak, C.V. Rao, A. Kumar, and M. Janakaraj. Rapid synthesis of antimicrobial Fe/Cu alloy nanoparticles using Waste Silkworm Cocoon extract for cement mortar applications. *Advances in Natural Sciences: Nanoscience and Nanotechnology* 11(2): 025006 (2020).
7. S. Kawashima, P. Hou, D.J. Corr, and S.P. Shah. Modification of cement-based materials with nanoparticles. *Cement and Concrete Composites* 36: 8-15 (2013).
8. A.S. Kadhim, A.A. Atiyah, and S.A. Salih. Properties of self-compacting mortar containing nano cement kiln dust. *Materials Today: Proceedings* 20: 499-504 (2020).
9. K.H. Younis, and S.M. Mustafa. Feasibility of using nanoparticles of SiO_2 to improve the performance of recycled aggregate concrete. *Advances in Materials Science and Engineering* 2018: 1512830 (2018).
10. N.H.A.S. Lim, H.M. Hosseini, M.M. Tahir, M. Samadi, and A.R.M. Sam. Microstructure and strength properties of mortar containing waste ceramic nanoparticles. *Arabian Journal for Science and Engineering* 43: 5305-13 (2018).
11. M. Kumar, M. Bansal, and R. Garg. An overview of beneficiary aspects of zinc oxide nanoparticles on performance of cement composites. *Materials Today: Proceedings* 43: 892-898 (2021).
12. M. Pattanayak, and P. Nayak. Green synthesis and

characterization of zero valent iron nanoparticles from the leaf extract of Azadirachta indica (Neem). *World Journal of Nano Science and Technology* 2(1): 6-9 (2013).

13. Y. Li, X. Zhang, C. Shang, X. Wei, L. Wu, X. Wang, W.D. Wu, X.D. Chen, C. Selomulya, D. Zhao, and Z. Wu. Scalable synthesis of uniform mesoporous aluminosilicate microspheres with controllable size and morphology and high hydrothermal stability for efficient acid catalysis. *ACS Applied Materials and Interfaces* 12(19): 21922-35 (2020).
14. V.T. Cong, K. Gaus, R.D. Tilley, and J.J. Gooding. Rod-shaped mesoporous silica nanoparticles for nanomedicine: recent progress and perspectives. *Expert Opinion on Drug Delivery* 15(9): 881-92 (2018).
15. A. Mahapatra, B. Mishra, and G. Hota. Adsorptive removal of Congo red dye from wastewater by mixed iron oxide–alumina nanocomposites. *Ceramics International* 39(5): 5443-51 (2013).
16. A. Chatterjee, J.K. Basu, and A.K. Jana. Alumina-silica nano-sorbent from plant fly ash and scrap aluminium foil in removing nickel through adsorption. *Powder Technology* 354: 792-803 (2019).
17. F. Gulshan, and K. Okada. Preparation of alumina-iron oxide compounds by coprecipitation and gel evaporation methods and their characterization. *Journal of Engineering Research* 3: 1-8 (2015).
18. M.A. Al-Ghouti, and D.A. Da'ana. Guidelines for the use and interpretation of adsorption isotherm models: A review. *Journal of Hazardous Materials* 393: 122383 (2020).
19. D.E. Ramírez-Arreola, C.S. Rosa, N.B. Haro-Mares, J. A. Ramírez-Morán, A.A. Pérez-Fonseca, and J.R. Robledo-Ortíz. Compressive strength study of cement mortars lightened with foamed HDPE nanocomposites. *Materials and Design* 74: 119-24 (2015).
20. W.N. Al-Rifaie, and W.K. Ahmed. Effect of nanomaterials in cement mortar characteristics. *Journal of Engineering Science and Technology* 11(9): 1321-32 (2016).
21. S.A. Zareei, F. Ameri, F. Dorostkar, and M. Ahmadi. Rice husk ash as a partial replacement of cement in high strength concrete containing micro silica: Evaluating durability and mechanical properties. *Case Studies in Construction Materials* 7: 73-81 (2017).
22. Y. Fang, Y. Sun, M. Lu, F. Xing, and W. Li. Mechanical and Pressure-sensitive Properties of Cement Mortar Containing Nano-Fe_2O_3. *Proceedings of the 4th Annual International Conference on Material Engineering and Application* (ICMEA 2017): 206-210 (2018).

Proceedings of the Pakistan Academy of Sciences: A Physical and Computational Sciences 61(1): 41-49 (2024)

ISSN (Print): 2518-4245; ISSN (Online): 2518-4253
https://doi.org/10.53560/PPASA(61-1)795

Pakistan Academy of Sciences

Research Article

Geographic Object-based Image Analysis for Small Farmlands using Machine Learning Techniques on Multispectral Sentinel-2 Data

Najam Aziz[1,2], Nasru Minallah[1,2*], Muhammad Hasanat[1,2], and Muhammad Ajmal[3]

[1]Department of Computer Systems Engineering, University of Engineering and Technology, Peshawar, 25120 Pakistan
[2]National Center for Big Data & Cloud Computing (NCBC), University of Engineering and Technology Peshawar, 25120 Pakistan
[3]Department of Agricultural Engineering, University of Engineering and Technology Peshawar, 25120 Pakistan

Abstract: This study intends to classify the land cover of an area especially small farmlands using object-based image analysis (OBIA) method and evaluates the performance of a supervised classifier. Multi-spectral Sentinel-2 imagery which is freely available is used and four supervised classifiers are applied to it. The study area was divided into four major classes namely Urban, Wheat, Tobacco, and other vegetation with varying accuracy values. The imagery was first resampled to 10 m spatial resolution and then NDI45 is layer stacked to it. A widely used MRS technique is used for delineating the objects in the imagery. Finally, classification is done through four supervised classifiers *k*-Nearest Neighbour (*k*NN), Bayes classifier, Decision Tree (DT), and Random Forest (RF). The accuracy was evaluated through a confusion matrix. The results show that Sentinel-2 imagery is capable of producing thematically detailed land cover maps via the Geographic Object-Based Image Analysis (GEOBIA) approach with accuracies of *k*-NN 95%, Bayes classifier 88%, DT 81% and RF 79%.

Keywords: Classification, Geospatial Analysis, GEOBIA, Landcover, Segmentation, Sentinel-2.

1. INTRODUCTION

During the past decade, Land cover classification using remote sensing satellite imagery was a well debated topic in developed countries. Now it is also getting attention in developing countries. With the advancement in satellite technology and high-resolution imagery, the need of real-time and accurate land cover maps for the monitoring and management of natural resources, resource planning, crop yield estimation and global climate change studies, etc. has increased [1]. Remote sensing has experienced enormous advancement in recent years. With the advent of high-resolution imagery, the need for computationally efficient algorithms and object-oriented image processing is increasing. One such technique is the GEOBIA [2]. Traditionally remote sensing imagery is classified based on the pixels, a basic unit of an image. With high-resolution imagery, within pixel variability changed the concept of classification and results in OBIA [3]. Objects are a group of pixels in representative shapes and sizes having similar spectral characteristics. Unlike developed countries, where average farmland sizes are relatively high, developing countries have small structured farmland, usually less than 1 hectare [4]. With such a small size, the accurate delineation of the underlying land is an issue that is highly important for the classification of land cover [5].

Chabot *et al*. [6] utilized RF technique for tracking shallow-water aquatic plants in multi-spectral data using OBIA. They have carried out operations to monitor aquatic vegetation using the graphical software tool GIS, which may be used

Received: February 2023; Revised: December 2023; Accepted: March 2024
*Corresponding Author: Nasru Minallah <n.minallah@uetpeshawar.edu.pk>

for a very wide range of tasks. GEOBIA is utilized by Georganos *et al.* [7] for urban application. They proposed a new metric classification optimization score and concluded that it works best with rigorous feature selection and significantly reduces the processing time and storage space while producing higher classification accuracy. Rizeei *et al.* [8] also utilized this approach for Urban object extraction while using worldview-3 satellite imagery. They divided machine learning techniques in various groups of features based, object based and pixel based and concluded that feature based techniques performed better in their use case than other applied techniques. Object oriented and pixel-based approaches were also utilized in the study of Tassi and Vizzari [9]. The object-oriented method outperformed the pixel-based technique in their investigation. but with a demand of high-resolution data. This was also concluded by Blaschke *et al.* [10] and Pu *et al.* [11], that in the analysis of high-resolution images, pixel-based algorithms are unable to deliver greater accuracy.

Using GEOBIA with a digital elevation model, the study in Arctic Sweden by Stammler *et al.* [12] identified and mapped aeolian sand dunes, revealing insights into their types, orientations, and historical sediment sources. The research contributes to understanding post-glacial landscape evolution and wind patterns in this environmentally sensitive area. Another study by Islam *et al.* [13] delves into the use of machine learning algorithms, particularly random forest (RF), support vector machine (SVM), and k-nearest neighbours (*k*NN), for object-based weed and crop classification in UAV images. With a focus on a chilli crop field in Australia, the research highlights the efficiency of RF and SVM, achieving weed detection accuracies of 96% and 94%, respectively. An object-oriented image analysis work, integrating slope unit division and multi-scale segmentation, to accurately map early landslides using various features done by Gao *et al.* [14]. They tested their method in the Xianshui River basin, and their results show improved accuracy in boundary extraction. Whereas, Li *et al.* [15] integrates deep learning and object-based image analysis to accurately extract check dams, demonstrating superior performance in the Loess Plateau for effective soil conservation and management. Advancing into deep learning further, a study conducted by Ye *et al.* [16] compares Mask R-CNN deep learning with OBIA-MDTWS for cabbage plant detection in UAV images, revealing superior performance in accuracy and computing efficiency for field nursery management.

The objective of this study was to effectively identify the small farmlands cover using the geographic object-based technique from multi-spectral Sentinel-2 imagery. Similarly, another objective was to propose an efficient machine learning technique for the classification of small farmlands.

2. AREA OF INTEREST AND DATA

2.1. Area of Interest

The area of interest for this study is Yar Hussain, located in Swabi district of Khyber Pakhtunkhwa, Pakistan. It is mainly a wide arable land contributing highly to the agriculture of the province. The land cover characteristics were acquired through Sentinel-2 imagery from the Copernicus open data source and is shown in Figure 1.

2.2. Data Used

Sentinel-2 multi-spectral imagery of level-2A was acquired from the scientific data hub portal of the European Space Agency (ESA) on 26th May, 2019 [Copernicus]. One multi-spectral sensor (MSI) with 13 spectral channels is carried by the Sentinel satellite for a variety of uses [17]. The resolution

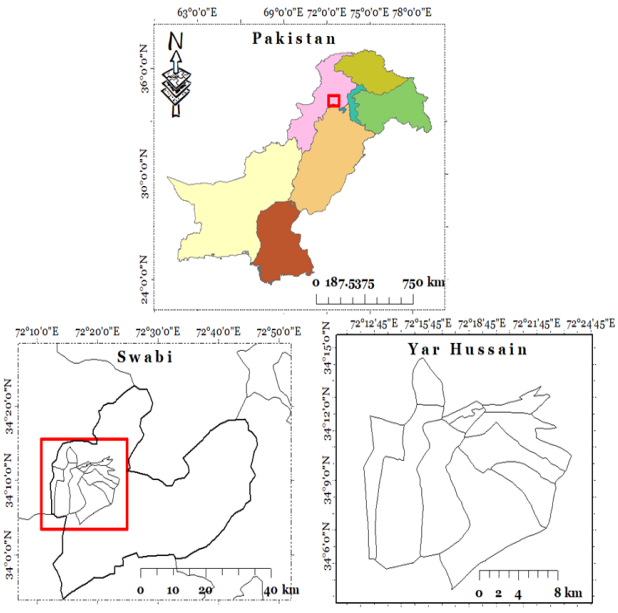

Fig. 1. Sentinel-2 imagery of the area of interest.

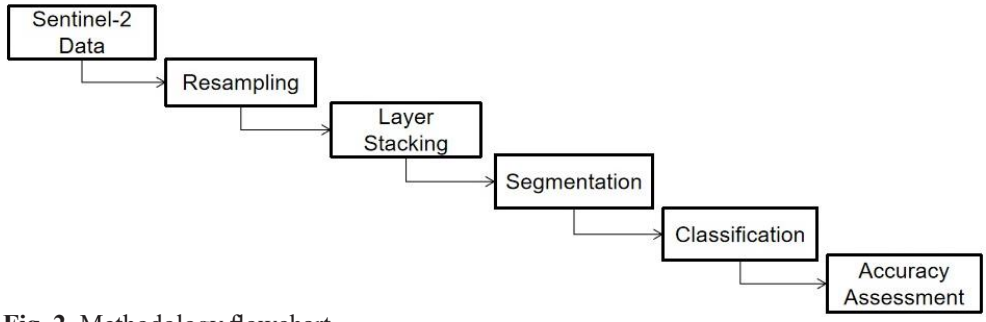

Fig. 2. Methodology flowchart.

of the channel varies between 10 and 60 m [18]. The visible (R, G, B) and near-infrared (NIR) bands are having 10 m resolution, the vegetation red edge bands (5, 6, and 7) and the short wave infrared bands (SWIR) at 20 m resolution and the rest of the bands have a resolution of 60 m [19]. Different bands of the Sentinel-2 imagery, their associated wavelengths and resolutions are shown in Table 1.

3. METHODOLOGY

A ground survey was conducted and land-cover data was collected in the study area using indigenously developed android application 'GEOsurvey'. A total of 4 classes were distinguished based on vegetated and non-vegetated areas. Further, the vegetation was divided into Wheat, Tobacco and Other vegetation classes (sugarcane, watermelon, shrubs, trees, etc.). Following that, the samples were split into training and testing samples. The classification was carried out based on training the classifier through these samples. Finally, accuracy was found through the test samples. For object-based image segmentation and classification, Definiens eCognition software was used [20]. This is the most widely used software due to its high capabilities of OBIA. The Figure 2 represent the methodology flowchart for this research work.

Table 1. Bands, their Resolution & Wavelengths of Sentinel-2.

Sentinel-2 Bands	Resolution (m)	Central Wavelength (um)
Coastal aerosol - Band 1	60	0.443
Blue - Band 2	10	0.49
Green - Band 3	10	0.56
Red - Band 4	10	0.665
Vegetation Red Edge - Band 5	20	0.705
Vegetation Red Edge - Band 6	20	0.74
Vegetation Red Edge - Band 7	20	0.783
NIR - Band 8	10	0.842
Vegetation Red Edge - Band 8A	20	0.865
Water vapor - Band 9	60	0.945
SWIR – Cirrus - Band 10	60	1.375
SWIR1 - Band 11	20	0.61
SWIR2 - Band 12	20	0.19

3.1 Pre-processing

In order to provide all the bands the same spatial resolution of 10 m, the imagery was first resampled [21]. Then NDI45 was calculated and added as an extra layer to the image [22]. The purpose of resampling was to layer stack NDI45 as an extra layer that helps in classifying vegetation. Both these tasks are carried out in the SNAP (Sentinel Application Platform). The layer stacked imagery was exported to eCognition for further processing. Training and testing samples were imported to eCognition as thematic layer. A rule-set is developed whereby all the processes take place according to that rule set.

3.2 Segmentation

In OBIA, image was converted to segments/objects and then these objects were used as the basic unit of imagery for classification [23]. Meaningful segmentation is the most important issue in the OBIA. There are many segmentation algorithms provided in Definiens eCognition that deals with object creation [24]. In this research, multi-resolution segmentation (MRS) which is the most widely used segmentation algorithm has been applied.

Through an iterative algorithm, the MRS assembles objects by grouping them, starting from individual pixels and continuing until a specified threshold, indicating the upper limit of object variance, is reached. The MRS is

controlled by three main factors including Scale, Shape and Compactness. These factors affect the overall segmentation process. Scale parameter or homogeneity criteria is user-defined threshold that establishes the highest permissible heterogeneity for the resulting segments. It controls the amount of spectral variation within objects. The process of segmentation terminates when a small increase in homogeneity exceeds the user-defined scale parameter as a threshold. Hence higher Scale Parameter (SP) value will result in bigger objects and vice versa. The SP considers the shape and colour of the objects while segmenting the image. If Shape is 0, this means that only colour is considered during segmentation, else if shape > 0, the colour as well as shape affects the segmentation process. The higher the value of the shape, the higher the weight shape is having in the resulting segments while producing fewer fractal boundaries between objects.

In this study, different levels of segmentation were carried out to achieve the best possible segments that describe the actual surface conditions of the image. The classification has been applied to the segmented imagery with a SP of 20, as it achieved the formation of fine objects. Figure 3 shows the segmented image with a SP value of 20, shape and compactness value of 0.9 and 0.5, respectively. The MRS also allows to assign different weights to spectral bands based on their importance in the underlying scenario. The weight of 5 is used for NDI45, NIR, and green bands. While RE1, RE2, RE3, and RE4 were given a weight of 2. Band 1 and band 10 were set to zero as these don't have significant contributions to this study.

3.3 Assigning Training Samples

Training samples collected during the ground survey were divided into training and testing sets and imported as a thematic layer into eCognition. The classes were assigned through these thematic layers. Eventually, the assigned objects were converted to sample objects and used for classification.

3.4 Classification

3.4.1. k – Nearest Neighbor (kNN)

The *k*-NN technique is the most straightforward machine learning algorithm. It is utilized for the classification of objects using nearby training examples in the feature space [25]. Based on the class properties of its *k* closest neighbours, an object is categorized using this approach. The ideal value of *k* for the training sample set was determined by examining various values of *k* [26]. After examination, it was found that for $k = 3$, it gives optimal results. K-NN uses the Euclidean distance between two points. When the feature space has m dimensions, two locations A and B are represented by feature vectors A = (x1, x2,..., xm) and B = (y1, y2,..., ym). Then the following formula is used to determine the separation between A and B:

$$d(A, B) = \sqrt{\sum_{i=1}^{m}(x_i - y_i)^2} \quad (1)$$

3.4.2. Bayes classifier

The Bayes classifier is based on the Bayes theorem of Bayesian statistics, which is a straightforward probabilistic classifier with solid independent

Fig. 3. MRS Segmented imagery with a magnified view.

assumptions. The presence (or absence) of one feature of a class is assumed to be independent of the presence (or absence) of any other feature(s). It is presumptive that the existence (or absence) of one feature of a class is unrelated to the presence (or absence) of any other feature [27]. It assumes that each feature works on its own to increase the likelihood that an unknown object belongs to a certain class. The Bayes classifier has the advantage of using less training data to determine the classification-related parameters (variable means and variances). Assuming independent variables, only the variances of the variables for each class need to be calculated, not the entire covariance matrix.

3.4.3. Decision tree

The DT is a machine learning algorithm that predicts the value of the target variable based on a number of input features. In OBIA, it predicts an unknown object based on training samples which have known classes [28]. As the MRS has various parameters for thresholding, the Decision Tree is a potential approach for modelling the problem.

3.4.4. Random forest

The RF is an ensemble learning technique that creates numerous DTs that are randomly produced and then aggregated to compute a classification [29]. It combines weaker, decorrelated classification trees and aggregate them for computing classification. When classifying land cover classes, the RF is proven to be reliable and effective algorithm [30]. Figure. 4. Shows the land cover of the study area classified by the KNN, Bayes, DT and RF classifier.

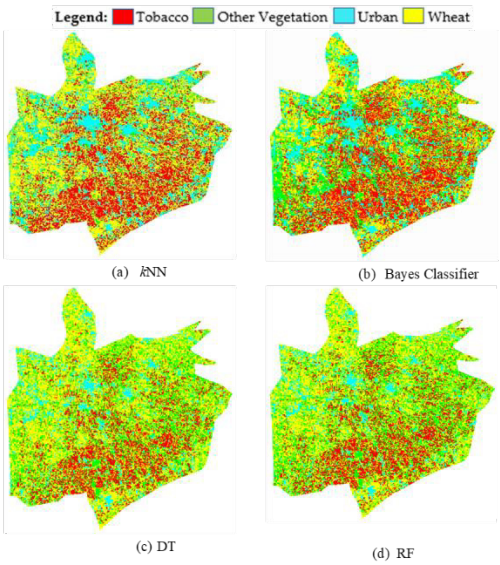

Fig. 4. Classified land cover of the study area using (a) kNN (b) Bayes (c) Decision Tree, and (d) RF Classifier.

4. RESULTS AND DISCUSSION

This study's goal was to assess how well the OBIA technique performed when used with Sentinel-2 data in areas having small farmland and sparse agriculture. The image objects delineated by the MRS were further classified by supervised classifier *k*-NN, Bayes classifier, DT and RF. The accuracy of these classifiers was assessed using a confusion matrix and is shown in Table 2, Table 3, Table 4, and Table 5, respectively. It was found that the *k*NN performed the best with overall accuracy (OA) of 95% and kappa Coefficient (KIA) of 0.91, followed by the Bayesian classifier with OA of 88% and KIA value of 0.82. The DT and RF have the OA of 81% and 79%, with KIA values of 0.72 and 0.70, respectively. The overall accuracy for various classifiers is calculated from the confusion matrix using the following mathematical formulation:

$$\text{Overall Accuracy} = \text{Correctly classified pixel/ Total number of classified pixels} \quad (2)$$

Below is a detailed discussion of the individual tables that represent the performance of the models. The k-Nearest Neighbors (kNN) classifier demonstrates strong performance across all land cover classes (Table 2). Notably, it achieves high user accuracies for Urban (97%), Wheat (92%), Other Vegetation (91%), and Tobacco (96%). The overall accuracy stands at an impressive 95%, indicating the model's effectiveness in classifying the samples. The Kappa Index of Agreement (KIA) further supports the robustness of the classifier, registering at 0.917, signifying substantial agreement beyond chance. The Bayes classifier exhibits commendable accuracy in classifying Urban (93%), Wheat (92%), and Tobacco (95%) land cover types (Table 3). However, it faces challenges in accurately categorizing Other Vegetation, with a notably lower accuracy of 42%. The overall accuracy is 88%, and the Kappa Index of Agreement (KIA) is 0.825, suggesting a substantial level of agreement. Despite the lower accuracy in one category, the Bayes classifier demonstrates competitive performance across the majority of land cover classes.

The Decision Tree classifier excels in accurately classifying Urban (93%) and Tobacco (98%) land cover types (Table 4). However, it struggles with Wheat (82%) and Other Vegetation (27%), indicating limitations in these specific classifications. The overall accuracy is 81%, with a Kappa Index of Agreement (KIA) of 0.725, signifying substantial agreement. While the model performs well in certain categories, improvements are needed for more balanced accuracy across all land cover types. Similar to the Decision Tree, the Random Forest classifier demonstrates high accuracy for Urban (93%) and Tobacco (98%) land cover types (Table 5). However, it faces challenges in accurately classifying Wheat (82%) and Other Vegetation (25%). The overall accuracy is 79%, with a Kappa Index of Agreement (KIA) of 0.705, indicating substantial agreement. While the model excels in specific categories, efforts should be directed towards improving accuracy for the challenging classes, such as Other Vegetation.

While comparing the results, all the classifiers were observed to perform more effectively. for urban, wheat and tobacco classes and is evident from the producer and user accuracies of these classes for all the applied classifiers. But the 'other vegetation' class is usually confused and misclassified with other classes in all the classifiers. For example, in KNN classification, the 'Other vegetation' class has a producer accuracy of 65% while user accuracy is 91%. This means that although 65% of the reference 'other vegetation' areas have been correctly classified as other vegetation, but 91% of the areas identified as "other vegetation" in the classification are actually other vegetation. The producer and user accuracies of other vegetation in Bayesian are 73% and 42%, in DT 80% and 27%, and in RF are 81% and 25%, respectively. This misclassification of other vegetation class in all the classifiers may be because of the overlap of some of the other vegetation areas with tobacco class due to its similarity, while the vegetation areas which are not fully grown and have more exposed barren land are confused with the wheat class as the wheat was in reaped stages.

Finally, the classification results also show that for some areas in the imagery, especially around borders, the pixels are not correctly categorized. The reason might be the extracted objects which are having different scale parameters. The similarity

Table 2. Confusion Matrix for classification using *k*NN.

User Class\Sample	Urban	Wheat	Other Vegetation	Tobacco	Sum	User Accuracy
Urban	315	4	4	2	325	97%
Wheat	8	488	17	17	530	92%
Other Vegetation	1	5	71	1	78	91%
Tobacco	2	22	17	886	927	96%
Sum	326	519	109	906		
Producer Accuracy	97%	94%	65%	98%		
Overall Accuracy	95%					
KIA	0.917					

Table 3. Confusion Matrix for classification using Bayes Classifier.

User Class\Sample	Urban	Wheat	Other vegetation	Tobacco	Sum	User Accuracy
Urban	306	13	3	7	329	93%
Wheat	7	409	18	14	448	92%
Other Vegetation	10	64	79	34	187	42%
Tobacco	3	33	9	851	896	95%
Sum	326	519	109	906		
Producer Accuracy	94%	79%	73%	94%		
Overall Accuracy	88%					
KIA	0.825					

Table 4. Confusion Matrix for classification using DT.

User Class\Sample	Urban	Wheat	Other vegetation	Tobacco	Sum	User Accuracy
Urban	273	18	1	1	293	93%
Wheat	44	400	18	29	491	82%
Other vegetation	9	93	87	129	318	27%
Tobacco	0	8	3	747	758	98%
Sum	326	519	109	906		
Producer	84%	77%	80%	83%		
Overall Accuracy	81%					
KIA	0.725					

Table 5. Confusion Matrix for classification using RF.

User Class\Sample	Urban	Wheat	Other vegetation	Tobacco	Sum	User Accuracy
Urban	270	17	1	1	289	93%
Wheat	46	371	17	21	455	82%
Other vegetation	10	120	88	134	352	25%
Tobacco	0	11	3	750	764	98%
Sum	326	519	109	906		
Producer	83%	72%	81%	83%		
Overall Accuracy	79%					
KIA	0.705					

between the spectral signature of some of the classes, such as wheat, immature other vegetation and urban structures makes them highly difficult to distinguish while working with the supervised classification method. It is expected that the introduction of more features like textural or spectral to the classifying algorithm may improve its quality.

5. CONCLUSIONS

This study significantly contributes to land cover mapping in small farmlands by utilizing Sentinel-2 imagery and GEOBIA, achieving a remarkable 95% accuracy with the *k*-NN classifier. Emphasizing the importance of finer object segmentation and accurate ground truth data, the research provides valuable insights into the successful application of these techniques in small agricultural landscapes. The study's findings offer a practical and effective approach for creating comprehensive thematic maps, showcasing the potential of GEOBIA on open-source satellite imagery for detailed land cover assessment.

6. CONFLICT OF INTEREST

The authors declare no conflict of interest.

7. REFERENCES

1. P.T. Noi, and M. Kappas. Comparison of random forest, k-nearest neighbor, and support vector machine classifiers for land cover classification using Sentinel-2 imagery. *Sensors* 18(1): 18 (2018).
2. X. Zhang, G. Chen, W. Wang, Q. Wang, and F. Dai. Object-based land-cover supervised classification for very-high-resolution UAV images using stacked denoising autoencoders. *IEEE Journal of Selected Topics in Applied Earth Observations and Remote Sensing* 10(7): 3373-3385 (2017).
3. X. Zhang, Q. Wang, G. Chen, F. Dai, K. Zhu, Y. Gong, and Y. Xie. An object-based supervised classification framework for very-high-resolution remote sensing images using convolutional neural networks. *Remote Sensing Letters* 9(4): 373-382 (2018).
4. J. Böhler, M. Schaepman, and M. Kneubühler. Crop classification in a heterogeneous arable landscape using uncalibrated UAV data. *Remote Sensing* 10(8): 1282 (2018).
5. B. Watkins, and A. Van Niekerk. A comparison of object-based image analysis approaches for field boundary delineation using multi-temporal Sentinel-2 imagery. *Computers and Electronics in Agriculture* 158: 294-302 (2019).
6. D. Chabot, C. Dillon, A. Shemrock, N. Weissflog, and E. P. Sager. An object-based image analysis workflow for monitoring shallow-water aquatic

vegetation in multispectral drone imagery. *ISPRS International Journal of Geo-Information* 7(8): 294 (2018).
7. S. Georganos, T. Grippa, S. Vanhuysse, M. Lennert, M. Shimoni, S. Kalogirou, and E. Wolff. Less is more: Optimizing classification performance through feature selection in a very-high-resolution remote sensing object-based urban application. *GIScience & Remote Sensing* 55(2): 221-242 (2018).
8. H.M. Rizeei, B. Pradhan, and M.A. Saharkhiz. Urban object extraction using Dempster Shafer feature-based image analysis from worldview-3 satellite imagery. *International Journal of Remote Sensing* 40(3): 1092-1119 (2019).
9. A. Tassi, and M. Vizzari. Object-oriented lulc classification in google earth engine combining snic, glcm, and machine learning algorithms. *Remote Sensing* 12(22): 3776 (2020).
10. T. Blaschke, C. Burnett, and A. Pekkarinen. Image segmentation methods for object-based analysis and classification. In: *Remote sensing image analysis: Including the spatial domain*, F.D. Meer and S. de Jong (Eds*.) Springer, Dordrecht* pp. 211-236 (2004).
11. R. Pu, S. Landry, and Q. Yu. Object-based urban detailed land cover classification with high spatial resolution IKONOS imagery. *International Journal of Remote Sensing* 32(12): 3285-3308 (2011).
12. M. Stammler, T. Stevens, and D. Hölbling. Geographic object-based image analysis (GEOBIA) of the distribution and characteristics of aeolian sand dunes in Arctic Sweden. *Permafrost and Periglacial Processes* 34(1): 22-36 (2023).
13. N. Islam, M.M. Rashid, S. Wibowo, C.Y. Xu, A. Morshed, S.A. Wasimi, and S.M. Rahman. Early weed detection using image processing and machine learning techniques in an Australian chilli farm. *Agriculture* 11(5): 387 (2021).
14. H. Gao, L. He, Z.W. He, and W.Q. Bai. Early landslide mapping with slope units division and multi-scale object-based image analysis-A case study in the Xianshui river basin of Sichuan, China. *Journal of Mountain Science* 19(6): 1618-1632 (2022).
15. S. Li, L. Xiong, G. Hu, W. Dang, G. Tang, and J. Strobl. Extracting check dam areas from high-resolution imagery based on the integration of object-based image analysis and deep learning. *Land Degradation & Development* 32(7): 2303-2317 (2021).
16. Z. Ye, K. Yang, Y. Lin, S. Guo, Y. Sun, X. Chen, and H. Zhang. A comparison between Pixel-based deep learning and Object-based image analysis (OBIA) for individual detection of cabbage plants based on UAV Visible-light images. *Computers and Electronics in Agriculture* 209: 107822 (2023).
17. G. Kaplan, and U. Avdan. Object-based water body extraction model using Sentinel-2 satellite imagery. *European Journal of Remote Sensing* 50(1): 137-143 (2017).
18. F.B. Balcik, G. Senel, and C. Goksel. Greenhouse Mapping using Object Based Classification and Sentinel-2 Satellite Imagery. *8th International Conference on Agro-Geoinformatics (Agro-Geoinformatics)* IEEE, pp. 1-5 (2019).
19. A. Novelli, M.A. Aguilar, A. Nemmaoui, F.J. Aguilar, and E. Tarantino. Performance evaluation of object based greenhouse detection from Sentinel-2 MSI and Landsat 8 OLI data: A case study from Almería (Spain). *International Journal of Applied Earth Observation and Geoinformation* 52: 403-411 (2016).
20. T. Blaschke. Object based image analysis for remote sensing. *ISPRS journal of photogrammetry and remote sensing* 65(1): 2-16 (2010).
21. J.P. Arroyo-Mora, M. Kalacska, R. Soffer, G. Ifimov, G. Leblanc, E.S. Schaaf, and O. Lucanus. Evaluation of phenospectral dynamics with Sentinel-2A using a bottom-up approach in a northern ombrotrophic peatland. *Remote sensing of environment* 216: 544-560 (2018).
22. F. Di Palma, F. Amato, G. Nolè, F. Martellozzo, and B. Murgante. A SMAP supervised classification of landsat images for urban sprawl evaluation. *ISPRS International Journal of Geo-Information* 5(7): 109 (2016).
23. E. Hussain, and J. Shan. Object-based urban land cover classification using rule inheritance over very high-resolution multisensor and multitemporal data. *GIScience and Remote Sensing* 53(2): 164-182 (2016).
24. S.A.P. Bentir, A.K.D. Balan, A.H. Ballado, and J.B. Lazaro. Optimization of object—based image segmentation in classifying water region. *In 3rd International Conference on Control and Robotics Engineering (ICCRE)*. IEEE, pp. 249-253 (2018).
25. M. Rana, and S. Kharel. Feature Extraction for Urban and Agricultural Domains Using Ecognition Developer. *International Archives of the Photogrammetry, Remote Sensing and Spatial Information Sciences* 42: 609-615 (2019).
26. C. Munyati. Optimising multiresolution segmentation: delineating savannah vegetation boundaries in the Kruger National Park, South Africa, using Sentinel 2 MSI imagery. *International Journal of Remote Sensing* 39(18): 5997-6019 (2018).
27. J. Fethers. Remote Sensing of Eelgrass using Object Based Image Analysis and Sentinel-2 Imagery. M.Sc. Thesis. *Aalborg University, Copenhagen, Denmark* (2018).
28. L.A. Ruiz, J.A. Recio, P. Crespo-Peremarch, and M. Sapena. An object-based approach for mapping forest structural types based on low-density LiDAR and multispectral imagery. *Geocarto International*

33(5): 443-457 (2018).
29. V. Lebourgeois, S. Dupuy, E. Vintrou, M. Ameline,S. Butler, and A. Bégué. A combined random forest and OBIA classification scheme for mapping smallholder agriculture at different nomenclature levels using multisource data (simulated Sentinel-2 time series, VHRS and DEM). *Remote Sensing* 9(3): 259 (2017).
30. R.L. Lawrence, S.D. Wood, and R.L. Sheley. Mapping invasive plants using hyperspectral imagery and Breiman Cutler classifications (Random Forest). *Remote Sensing of Environment* 100(3): 356-362 (2006).

Proceedings of the Pakistan Academy of Sciences: A Physical and Computational Sciences 61(1): 51-59 (2024)

ISSN (Print): 2518-4245; ISSN (Online): 2518-4253
https://doi.org/10.53560/PPASA(61-1)830

Pakistan Academy of Sciences

Research Article

Development of Pervious Concrete with Enhanced Skid Resistance using Waste Tires Particles

Muhammad Rizwan Anwar, Naqash Ahmad, Anwar Khitab*, and Raja Bilal Nasar Khan

Department of Civil Engineering, Mirpur University of Science and Technology (MUST), Mirpur-10250, (AJ&K) Pakistan

Abstract: Rubber tires are excessively increasing with the advancement in transportation technologies. It is difficult to dispose off the tires and as such they cause environmental threats to the on-land and aquatic lives. In this work crumb rubber is used as a fractional replacement of sand in concrete at 5%, 10% and 15% by mass. The aim is to produce a porous concrete with acceptable mechanical strength and high skid resistance. The workability and fresh density of the concrete decreased with the crumb rubber. Similar reduction in mechanical strength was also noticed, however, 5% replacement showed mechanical properties similar to those of the control units. The crumb rubber enhanced the porosity of the material. The study as a whole suggests that a lightweight concrete with enhanced porosity and skid resistance can be produced by recycling crumb rubber as a partial replacement of sand. The porous concrete with good skid resistance is a useful pavement material as it allows the infiltration of rainwater through it and thus has the capacity to reduce runoff during heavy rainfalls. It can additionally help reduce the accidents due to higher skid resistance in wet conditions.

Keywords: Concrete, Crumb Rubber, Skid Resistance, Mechanical Properties, Rigid Pavement.

1. INTRODUCTION

The recycling of waste materials as a replacement of the ingredients of concrete is being practiced all around the globe. This replacement is in accordance with the sustainable development goals of the United Nations and serves a dual purpose; it reduces the environmental hazards posed by the waste, and it provides a hybrid type of concrete that incorporates a lesser quantity of natural resouces (cement, sand or coarse aggregates). Sand is an important ingrdient of concrete; it is not only used in construction but also in electronic appliances. It is a source of silicon, an important ingrdient of electronic appliances. Its huge utilization will lead to the scarcity in future and many intellectuals are of the view that the world will face a shortage of this natural source [1]. Several studies are available on partial replacement of sand by rubber and other waste materials. In all these studies, rubber particles were either directly incorporated in cementitious mixes or pre-treated/soaked in water/alkaline solutions before their incorporation in the cementitious mixes. Some important studies are described here:

Safan *et al*. [2] studied the effect of crumb rubber on properties on concrete. The authors have reported a 37% decrease in compressive strength with 15% substitution of sand by untreated crumb rubber. When crumb rubber was pre-treated with NaOH, the concrete recovered the strength by 13%. Choudhary *et al.* [3] have reported a decrease in workability of mortar with crumb rubber; the authors attributed the decrease to water retention capabity of rubber particles. Sharma *et al.* [4] used crumb rubber as additive to bitumenous mixes. The authors claimed that the modified bitumen possessed lesser flexibility but higher resistance against rutting. Saifuddin *et al.* [5] examined the effect of crumb rubber on concrete performance. The authors have reported that the concrete containing rubber had a smoother surface and higher flexibility. The rubber particles enhanced the resistance to water (impermeability) and the compressive strength increased up to 5% partial replacement. Eltayeb *et al.* [6] used crumb rubber in place of fine aggregates in the range of 0-50% in concrete. The authors evaluated the modified concrete in terms of resistance to bullets, blast, impact and collision loads. The concrete outperfomed the conventional

Received: July 2023; Revised: December 2023; Accepted: March 2024
*Corresponding Author: Anwar Khitab; anwar.ce@must.edu.pk

concrete in the dynamic parameters as mentioned above. Deshpande *et al.* [7] used treated and untreated rubber particles as fractional substitute of sand in concrete. The authors have reported that the concrete containing treated rubber particles had higher strength than that of the concrete containing untreated particles. Kashani *et al.* [8] studied the performance of lightweight cellular concrete (LCC) employing waste crumb rubber as a filler. Crumb rubber was soaked in NaOH solution prior to the mixing in concrete matrix. The acoustic and thermal insulation, as well as the water absorption capacities of LCC got improved with crumb rubber addition. The treatment also improved the ITZ (Intersticial Transition Zone) of the mix. Khan *et al.* [9] utilized crumb rubber particles as partial substitute of sand for making sustainable concrete mixes.The performance of the specimens was evaluated in terms of physical, mechanical and durability properties using standard destructive and non-destructive techniques. They have mentioned that the rubber particles reduce the weight and strength but enhance the thermal insulation of the material.

Automotive industry is growing in Pakistan. With the growth of the industry, the number of waste tyres are also growing. In each city of Pakistan, the discarded waste tyres are stored and dumped in improper way as shown in Figure 1. Most unformtunate part of this story is that these waste tyres are also used as fuel, which emits toxic gases into the atmosphere. Present study focusses on the use of grinded waste local tyres as partial substitute of fine aggregates in normal concrete and concrete pavements. The emphasis is not only to promote the recycling of local waste tyre rubber in building and pavement materials but also to produce a concrete with enhanced porosity and skid resistance; both these charateristics are helpful in rainfall or moonson season as they not only allow the infiltration of water and thus decrease the surface runoff and flooding but also provide enhanced skid resistnace to the moving tyres. This study was formulated in accordance with the sustainable development goals of the United Nations, which stress for sustainable cities and responsible consumption and production.

2. MATERIALS AND METHODS

Concrete was designed, mixed, prepared and cured as per ASTM (American Society for Testing and Materials) standards in the controlled laboratory environment. The machine mixing was carried out with the help of the concrete mixer.

Fig. 1. Waste rubber tyres store.

The materials used for the reasearch work are shown in Table 1. The properties of coarse aggregates, fine aggregates and crumb rubber are given in the Table 2, Table 3 and Table 4, respectively. These properties were determined by using the ASTM standards.

The concrete's composition is shown in the Table 5. Crumb rubber was used as fractional replacement of sand by mass; the percentages were fixed as 5%, 10%, and 15% on the basis of previous studies. All the ingredients were mixed in accordance with ASTM C 685/C685M–17 [10].

The mixing was carried out in a tilting drum concrete mixer. The fresh concrete mix was cast in cylindrical and beam moulds. Workability of the fresh concrete was determined according to the ASTM C 143 method [11]. Similarly the fresh density of concrete was found out by ASTM C 138 [12]. The compressive strength and flexural strength of the specimens were evaluated as per standard ASTM C 39/C 39M [13] and ASTM C 78 [14] methods, respectively. Skid resistance test was carried on the slabs after the slabs were cured for 28 days; the test was carried out by following the standard ASTM E2340/E2340M method [15]. Thermal conductivity of the concrete was measured by employing ASTM C1045–07 and ASTM C177-13 standard methods [16, 17]. Fourier's law was applied for calculating the thermal conductivity of the cores. Finally, the porosity in concrete was measured through standard ASTM water absorption test in the hardened state [18].

Table 1. Description of the materials used.

Sr. No.	Material	Description
1	Coarse aggregates	Obtained from Margalla crush plant near Islamabad
2	Fine aggregates	Lawrencepur Sand (Well-documented river sand)
3	Cement	Bestway Cement (A well-known Pakistani Brand)
4	Crumb rubber	Obtained by grinding the waste tires of vehicles in district Mirpur Azad Kashmir, Pakistan

Table 2. Properties of coarse aggregates.

Sr. No.	Properties	Value Obtained
1	Water absorption (%)	0.46
2	Fineness Modulus (FM)	7.71
3	Specific Gravity	2.64
4	Bulk Density (kg/m^3)	1598
5	Flakiness Index (%)	26.616
6	Elongation Index (%)	11.838

Table 3. Properties of fine aggregates.

Sr. No.	Properties	Value Obtained
1	Specific Gravity	2.69
2	Bulk Density (kg/m^3)	1500
3	Dry Density (kg/m^3)	1850
4	Fineness Modulus	3
5	Water Absorption (%)	3.88
6	Moisture Content (%)	2.01

Table 4. Properties of crumb rubber.

Sr. No.	Properties	Value Obtained
1	Specific Gravity	1.62
2	Fineness Modulus	3.5
3	Color	Black color due to carbon content
4	Surface	Moderately Rough surface

Table 5. Concrete's composition.

Sr. No.	Mix design	Mix criteria	Cement (Kg)	w / c ratio	Water (Kg)	Sand (Kg)	CR (Kg)	Crush (kg)	No of specimens	No of slabs
1	1:2:4	CR0	36	0.55	19.8	72	0	144	9	1
2	1:2:4	CR5	36	0.55	19.8	68.4	3.6	136.8	12	1
3	1:2:4	CR10	36	0.55	19.8	64.8	7.2	129.6	9	1
4	1:2:4	CR15	36	0.55	19.8	61.2	10.8	122.4	9	1

3. RESULTS AND DISCUSSION

3.1 Workability

The slump values of the specimens are presented in Figure 2. In all the cases, a true slump was observed; the slump cone shape of rubberized concrete (10%) is shown in Figure 3. From Figure 2, it can be observed that the workability decreased with the quantity of crumb rubber. There are two reasons for the reduction. Firstly, the rubber particles have good shock absorbing characteristics; the compaction

efforts are not effective in expelling air, which reduces the slump [19, 20]. Secondly, the rubber particles act as fibres and keep the concrete matrix intact; this makes the mix more cohesive [9]. The workability was reduced but a cohesive true slump took place. The least value of slump (22.5 mm) was recorded with 15% fractional replacement. It is expected that further increment in the crumb rubber content will make the concrete mix less workable.

Concrete with a low slump is preferred in rigid pavements. The low slump allows the pavement not to deform, once the machinery is removed. This deformation also affects the concrete surface. A higher workability may also allow the segregation of the cement paste from the aggregates. For these reasons, the workability of the rigid pavements is purposely kept low (0-75 mm) [21]. The slump values as obtained during this study lie within the range of 0-75 mm; moreover, the true slump as shown in Figure 3 depicts that the concrete is cohesive and is free from segregation.

3.2 Fresh Density

The variation of fresh density with rubber content is shown in Figure 4. Crumbed rubber particles are lighter in weight than the sand particles. The specific gravity of crumb rubber is 1.62 against that of 2.69 for sand. Therefore, with the increase in crumbed rubber proportion the mass of concrete samples is reduced; hence, the density of fresh concrete decreases with the increase in rubber content. Secondly, after the incorporation of crumb rubber, voids are generated in concrete, which causes loss of weight of the sample per unit volume.

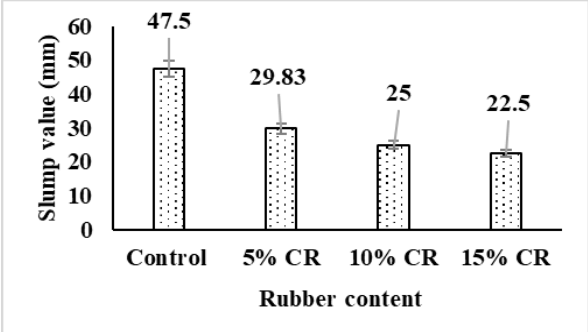

Fig. 2. Variation of slump with rubber content.

Fig. 3. True slump in rubberized concrete containing 10% crumb rubber.

The crumb rubber particles hinder the compaction efforts due to shock absorbing characteristics of the rubber particles; the air gets trapped within the matrix. Therefore, the results are closely linked to the slump test results. The basic principle that lies behind the making of a light-weight concrete is the induction of air [19]. For this purpose, various admixtures are added. Thus, the rubber particles act as admixtures and reduce the weight of the concrete. Light weight concrete pavements are advantageous in the situations, where roads are constructed over a weak soil. The heavyweight pavements tend to settle down in such situations, whereas, a lightweight pavements perform relatively better [22].

3.3 Compressive Strength

The variation of compressive strength with rubber content is shown in Figure 5. The control unit showed the maximum compressive strength. As the sand was fractionally replaced with the crumb rubber, the bonding between concrete mix got disturbed and this made the loss of strength in compression. The crumb rubber decreased the compressive strength of the concrete because it entrapped the air and generated free spaces that resulted in the air void production in the concrete mix. The compressive

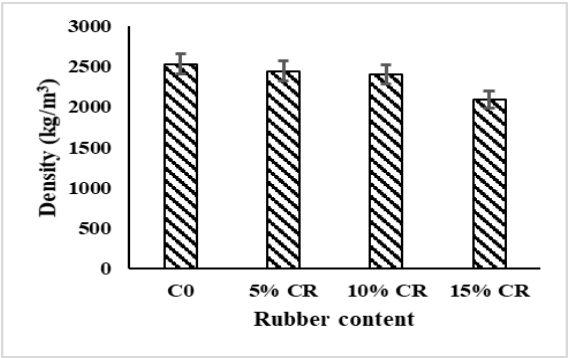

Fig. 4. Variation of fresh density with rubber content.

strength is directly related to the density of the material [23]. This also shows that the stiffness of the crumb rubber is lesser to sustain the same loads as the control unit does. The incorporation of the rubber particles as a partial replacement of sand, introduces air voids. These voids/pores decrease the strength, increase the porosity and therefore decrease the density. The results are consistent and are inter-linked. The microstructure and concrete specimen texture are shown in Figure 6 [9] and Figure 7, respectively. The compressive strength although is specified for concrete pavements, but is not usually considered a critical parameter for road performance. However, it is determined because the test is simple and commonly available and the result values are closely related to flexural strength, tensile strength, density and permeability [24]. Typical compressive strength for road pavements range from 20 MPa to 40 MPa [21]; whereas, higher compressive strengths lead to shrinkage cracks.

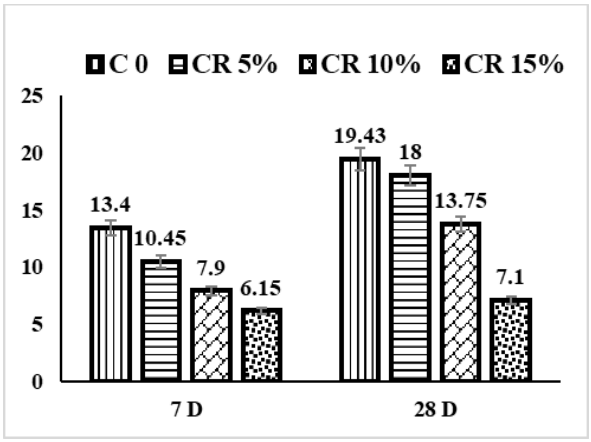

Fig. 5. Variation of compressive strength with crumb rubber.

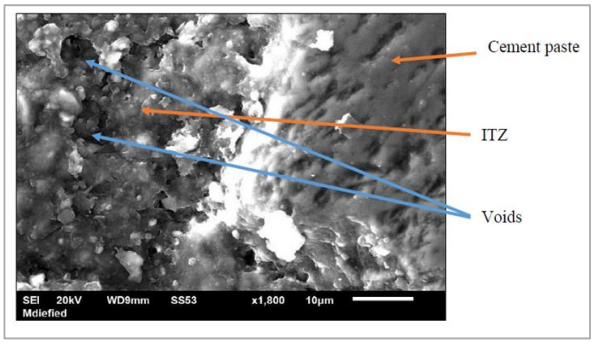

Fig. 6. Microscopic view showing the formation of higher number of voids at 15% replacement level.

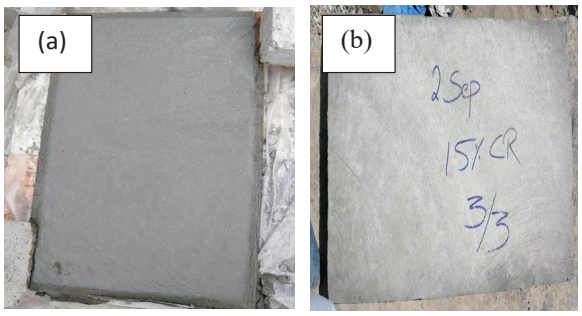

Fig. 7. Smooth surface of CR 15 sample (a) fresh form, (b) cured form.

3.4 Flexural Strength

The flexural strength is an important indicator of the performance of the concrete pavement. The variation of flexural strength with rubber content is shown in Figure 8. The control unit showed the maximum strength of all the specimens. The specimens containing the crumb rubber showed a linear decrease. The control unit shows a strength of 6.3 MPa and 9.1 MPa at 7 and 28 days, respectively. These values are suitable for concrete pavements as per international standards [21].

For ordinary concrete, the flexural strength varies as 10-20% of the compressive strength [25, 26]. The flexural strength is more than 20% of the compressive strength in the present case. Although, flexural strength is usually considered to be directly linked to the compressive strength; as a matter of fact, the two parameters depend on different variables. While, compressive strength is dependent on the density of the material, the flexural strength is more dependent on the cohesion of the material. Since, rubber particles may act as fibres,

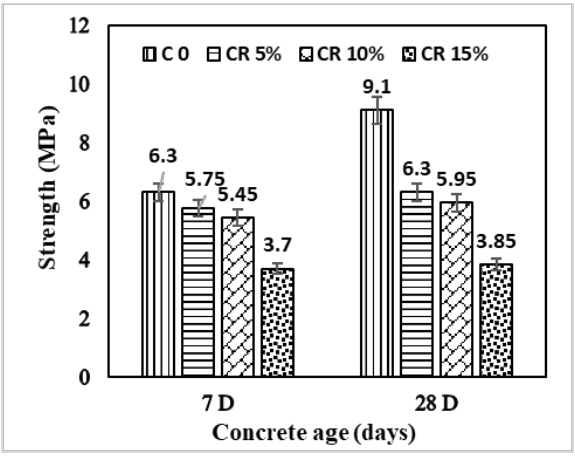

Fig. 8. Flexural strength of concrete as a function of %age replacement of CR.

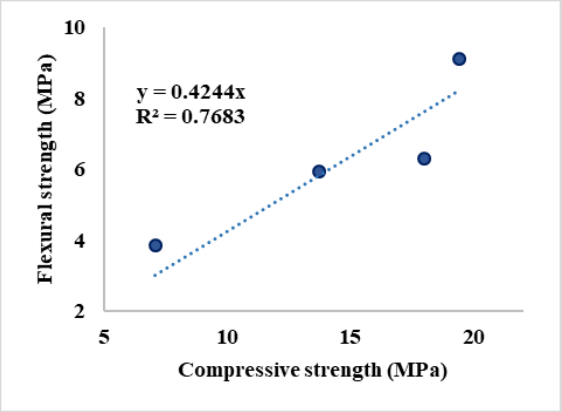

Fig. 9. Relationship between flexural and compressive strengths.

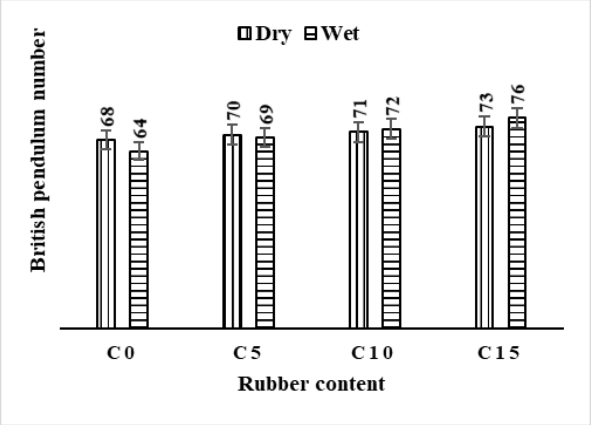

Fig. 10. British pendulum number of concrete as a function

interconnecting the concrete particles, they have the capacity to enhance the flexural strength [19, 27]. The minimum flexural strength requirement for a concrete pavement is mostly designated as 4 − 4.5 MPa at 28 days of age in various codes [21, 28] pavement aggregates, applied load characteristics, and climate. Various sub-grade condition and concrete slab flexural strength values results on the pavement design thickness that have a direct impact on the cost construction. In this study, the rigid pavement design of an apron with various sub-grade condition and concrete flexural strength values are presented. As a reference, the Federal Aviation and Administration (FAA; thus the rubber concrete while having low compressive strength, exhibits comparatively good flexural strength. The relationship between the compressive strength and the flexural strength is given in the form of the equation (1) and diagrammatically shown in Figure 9. The curve shows that flexural strength is directly proportional to the compressive strength:

$$f_f = 0.42.f_c' \quad (1)$$

Where, f_f is the flexural strength and f_c' is the compressive strength (both in MPa).

3.5 Skid Resistant Test

Figure 10 shows a comparison of skid resistances of dry and wet surfaces of control units and rubberized slabs. The skid resistance of the control unit is greater on dry surface than on wet surface of the pavement.

Higher value of the British Pendulum Number shows a good surface of the concrete pavement. It indicates the strong resistance for fast traffic flows. For concrete pavements with 5% rubber content, the value of skid resistance on dry and wet surfaces is almost same, however, the rubber improves the resistance of the concrete. The slab with 10% replacement of sand with crumb rubber shows different behaviour than control sample and 5% CR slab; its skid resistance on wet surface is greater than that on the dry surfaces. This behaviour exhibits an improved adhesive nature of crumb rubber after contacting with water. The skid resistance of the concrete with 15% rubber content is higher on wet surface than on the dry one. This is because of the rough texture of the crumb rubber that improves the resistance when in contact with the water.

3.6 Thermal Conductivity

Figure 11 shows the variation of thermal conductivity with the rubber content. Thermal conductivity decreases as the rubber content of the concrete increases. The results are analogous to those of compressive strength and density. The results demonstrates that the concrete has air voids, which reduce the thermal conductivity.

According to US Department of Transportation, the thermal conductivity of the pavement materials normally varies from 0.8 Watts/m-K to 2.0 Watts/m-K [29]. In the present study, the thermal conductivity of the control material lies within the range. The low thermal conductivities are advantageous in normal as well as in pavement concretes. The lower thermal conductivities keep the temperature low within the pavements and ensure high-temperature stability of the pavements [30].

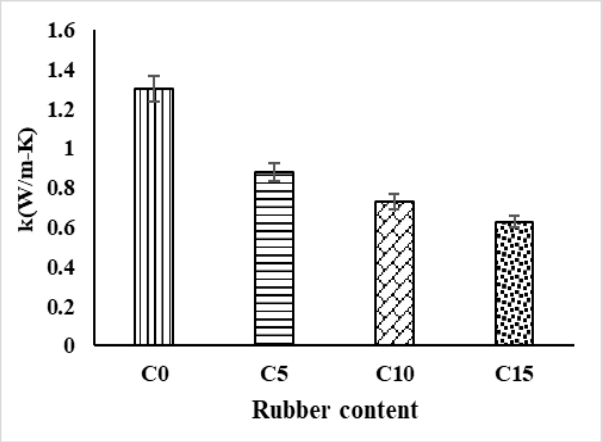

Fig. 11. Variation of thermal conductivity with rubber content.

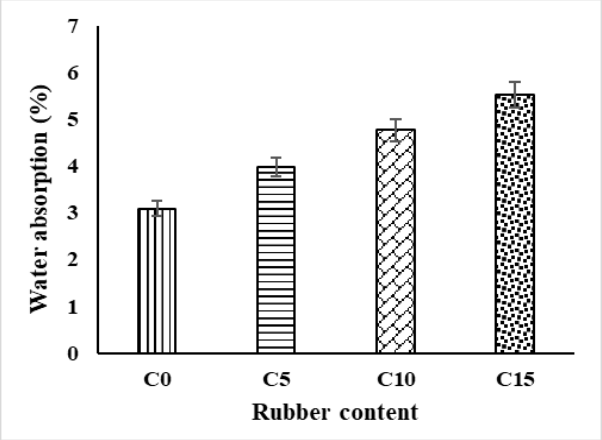

Fig. 12. Enhancement of water absorption with rubber content.

3.7. Porosity (Water Absorption Test)

The effect of rubber content on porosity was confirmed through water absorption test [18]. Figure 12 shows the variation of the water absorption of control unit and the others incorporated with crumb rubber at 5%, 10% and 15% levels. Porosity of the concrete was evaluated by dipping the cores of the specimens into the water and by recording the dry and wet masses before and after dipping the cores in water. As the rubber content increases in the concrete, the voids also increase. The increase in voids leads to higher water absorption; this is an indicator of higher porosity with rubber content. Higher porosities make the concrete pervious. The pervious concrete in pavements is advantageous in today's life, especially, during the Monson season as it has higher capacity to absorb water. It also allows rain water to infiltrate through it. Pakistan is frequently facing surface runoff during these days and the rubber content helps enhance the water absorption capacity of the rigid pavements.

The relationship between the porosity and thermal conductivity is given by the equation (2) and graphically shown in Figure 13.

$$k = 5.17.w^{-1.25} \qquad (2)$$

Where k is the thermal conductivity in W/m-K and w is the water absorption in percentage.

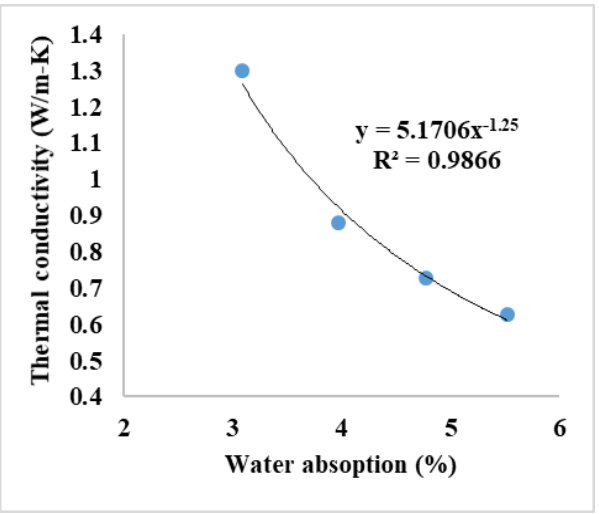

Fig. 13. Variation in thermal conductivity with porosity.

4. CONCLUSIONS

This work describes the benefits and drawbacks of using rubberized concrete for road pavements. The material was evaluated through some physical, mechanical and durability parameters. Based on the experimental work, following conclusions are drawn:

1. Rubber content reduces the workability. The compaction efforts are not effective in expelling air due to shock absorbing characteristics of the rubber particles. This in turn also reduces density, mechanical strength, and enhances porosity and thermal insulation.
2. The reduced workability and true slump indicate that the concrete containing rubber particles is suited for rigid pavements.
3. The lightweight pavements are suited if the pavements are to be laid over weak soils.
4. Rubber particles enhance the skid resistance of concrete both in wet and dry conditions. This shows that the rubber particles enhance the surface roughness of the pavement.
5. Present day urbanization is resulting in floods/

surface runoff in cities. Rubber particles enhance the perviousness of concrete and thus allow the passage of water through it. The use of rubberized concrete for low-to-average-volume traffic roads/streets can be a viable solution in flood-affected areas.

6. Rubber content reduces thermal conductivity. This will maintain stable temperature levels within the pavement.
7. The enhancement of the skid resistance in wet conditions demonstrate that the rubberized concrete pavements can increase the friction between the tyres and the pavement and thus add to the safety of the vehicles in rainy seasons.

5. ACKNOWLEDGEMENT

The authors are grateful to their colleagues in the civil engineering department MUST for the assistance, which enabled them to complete this work in time.

6. CONFLICT OF INTEREST

The authors declare that they have no conflict of interest.

7. REFERENCES

1. X. Zhong, S. Deetman, A. Tukker, and P. Behrens. Increasing material efficiencies of buildings to address the global sand crisis. *Nature Sustainability* 5: 389–392 (2022).
2. M. Safan, F.M. Eid, and M. Awad. Enhanced Properties of Crumb Rubber and Its Application in Rubberized Concrete. *International Journal of Current Engineering and Technology* 7: 1784-1790 (2017).
3. R. Choudhary, J. Khatti, and K.S. Grover. Effect on Water Retention of Different Mortar Mix with Different Percentage of Fine Crumb Rubber. In: International Conference on Advancements in Computing & Management. *Jagannath University, Jaipur, India* (2019).
4. S. Sharma and A. Goel. A study on fractionalreplacement of bitumen with crumb rubber. *International Journal of Civil Engineering and Technology (IJCIET)* 10: 1487-1495 (2019).
5. M. Saifuddin, P.D. Maneeth, and S. Brijbhushan. An experimental investigation of partially replaced crumb rubber with fine aggregates in concrete. *International Journal of Scientific & Technology Research* 8: 1-5. (2019).
6. E. Eltayeb, X. Ma, Y. Zhuge, J. Xiao, and O. Youssf. Dynamic performance of rubberised concrete and its structural applications – An overview. *Engineering Structures* 234: 111990 (2021).
7. N. Deshpande, S.S. Kulkarni, T. Pawar, and V. Gunde. Experimental investigation on strength characteristics of Concrete using tyre rubber as aggregates in concrete. *International Journal of Applied Engineering Research and Development (IJAERD)* 4: 97-108 (2014).
8. A. Kashani, T.D. Ngo, P. Mendis, J.R. Black, and A. Hajimohammadi. A sustainable application of recycled tyre crumbs as insulator in lightweight cellular concrete. *Journal of Cleaner Production* 149: 925-935 (2017).
9. A. Khitab and R.B.N. Khan. Suitability of concrete incorporated with scrubbed rubber tire particles: assessment based on destructive and non-destructive testing. *Pakistan Journal of Engineering* 1: 6-22 (2022).
10. ASTM C685. Standard Specification for Concrete Made by Volumetric Batching and Continuous Mixing. *West Conshohocken, PA, 19428-2959 USA* (2018).
11. ASTM C143/C143M. Standard Test Method for Slump of Hydraulic-Cement Concrete. *West Conshohocken, PA, 19428-2959 USA* (2015).
12. ASTM:C138/C138M-13. Standard Test Method for Density (Unit Weight), Yield, and Air Content (Gravimetric). *West Conshohocken, PA, 19428-2959 USA* (2013).
13. ASTM C39. Standard Test Method for Compressive Strength of Cylindrical Concrete Specimens. *West Conshohocken, PA, 19428-2959 USA* (2016).
14. ASTM C78/C78M. Standard Test Method for Flexural Strength of Concrete (Using Simple Beam with Third-Point Loading). *West Conshohocken, PA, 19428-2959 USA* (2018).
15. ASTM E2340. Standard Test Method for Measuring the Skid Resistance of Pavements and Other Trafficked Surfaces Using a Continuous Reading, Fixed-Slip Technique. *West Conshohocken, PA, 19428-2959 USA* (2021).
16. ASTM C1045-07. Standard Practice for Calculating Thermal Transmission Properties Under Steady-State Conditions. *West Conshohocken, PA, 19428-2959 USA* (2013).
17. ASTM C177-13. Standard Test Method for Steady-State Heat Flux Measurements and Thermal Transmission Properties by Means of the Guarded-Hot-Plate Apparatus. *West Conshohocken, PA, 19428-2959 USA* (2013).
18. ASTM C1585-20. Standard Test Method for Measurement of Rate of Absorption of Water by Hydraulic-Cement Concretes. *West Conshohocken, PA, 19428-2959 USA* (2020).
19. R.B.N. Khan, and A. Khitab. Enhancing Physical, Mechanical and Thermal Properties of Rubberized Concrete. *Engineering and Technology Quarterly Reviews* 3(1): 33-45 (2020).
20. M. Kluczyk, A. Grządziela, M. Pająk, Ł. Muślewski,

and A. Szeleziński. The Fatigue Wear Process of Rubber-Metal Shock Absorbers. *Polymers* 14: 1186 (2022).

21. D.S. Lane. Evaluation of concrete characteristics for rigid pavements, Report VTRC 98-R24, *Virginia Transportation Research Council*, *Virginia, USA* (1998).
22. M. Maher, and J. Hagan. Constructability Benefits of the Use of Lightweight Foamed Concrete (LFCF) in Pavement Applications. In: Resiliant Infrastructure. *Canadian Society for Civil Engineering, Ontario, Canada* pp. 1354 (2016).
23. U. Safeer, R.B.N. Khan, and A. Khitab. Performance enhancement of concrete by employing composite mixture of ceramic and brick powders in place of cement. In: Advances in Civil and Construction Engineering 2022 (ACCE 2022) *University of Management and Technology Lahore, Pakistan* (2022).
24. R. Arif, A. Khitab, M.S.Kırgız, R.B.N. Khan, S. Tayyab, R.A. Khan, W. Anwar, and M.T. Arshad. Experimental analysis on partial replacement of cement with brick powder in concrete. *Case Studies in Construction Materials* 15: e00749 (2021).
25. Q. Bashir, R.B.N. Khan, and A. Khitab. Effect of steel slag on concrete having varying amount of cement. In: Conference on Sustainability in Civil Engineering (CSCE'22). *Capital University of Science and Technology (CUST) Islamabad, Pakistan* (2022).
26. Z.U. Abdin, and A. Khitab. Effect of Pine Needle Fibers on Properties of Cementitious Mortars : Pine Needles-Reinforced Mortars. *Proceedings of The Pakistan Academy of Sciences: A. Physical And Computational Sciences* 57: 33-46 (2021).
27. A. Khitab, M.T. Arshad, N. Hussain, K. Tariq, S.A. Ali, S.M.S. Kazmi, and M.J. Munir. Concrete reinforced with 0.1 vol% of different synthetic fibers. *Life Science Journal* 10: 934-939 (2013).
28. M.D.W. Ardana, and A.Ariawan. The significance of concrete slab flexural strength inference variation based on its compression strength characteristics in apron pavement analysis and design. *MATEC Web of Conferences* 276: 934-939 (2019).
29. FHWA-HIF-15-002. Toward Sustainable Pavement Systems: A Reference Document. *Federal Highway Administration (FHWA) Washington, DC, USA* (2017).
30. J. Wang, Z. Zhang, D. Guo, C. Xu, and K. Zhang. Study on Cooling Effect and Pavement Performance of Thermal-Resistant Asphalt Mixture. *Advances in Materials Science and Engineering* 2018: 6107656 (2018).

Proceedings of the Pakistan Academy of Sciences: A Physical and Computational Sciences 61(1): 61-69 (2024)

ISSN (Print): 2518-4245; ISSN (Online): 2518-4253
https://doi.org/10.53560/PPASA(61-1)793

Pakistan Academy of Sciences

Research Article

Experimental Implementation and Analysis of Microwave Power Dividers and Directional Couplers

Imad Ali[1*], and Nasir Saleem[2]

[1]Department of Computer Science, University of Swat, Pakistan
[2]Department of Electrical Engineering, Faculty of Engineering and Technology, Gomal University, Dera Ismail Khan, Pakistan

Abstract: In radio technology, directional couplers and power dividers play a vital role. These devices have well-established theories; however, their performance is not studied under diverse input voltages (and frequencies). This article analyzes the aforementioned devices via extensive laboratory hardware experiments under various input voltages and frequency band settings. The splited power is measured and examined at detectors and ports, while additional parameters, including Insertion Loss and Directivity, are used. The experimental analysis of microwave devices is examined for the power split over a band of frequencies. Our experimental results over a frequency band of 2.0 to 3.0 GHz (with a step size of 0.1 GHz) show that transmitted power at low frequencies is equal and is slightly affected at higher frequencies while the power splitting characteristic over a band of frequencies matches their theories.

Keywords: Microwave Devices, Power Dividers, Directional Couplers, Insertion Loss, Directivity.

1. INTRODUCTION

In radio technology, directional couplers (DCs) and power dividers (PDs) play a vital role [1]. A certain amount of the electromagnetic (EM) power in the transmission line is linked via these devices that can be used in other circuits [2]. The EM power can only be coupled to an isolated port [3]. A DC is used when there is a desire to equalize power. It consists of two linked transmission lines designed so that EM power in one line in a given direction is linked to the other line, propagating only in one direction but not in another, which is a vital characteristic of the DCs [4]. The description of coupling, coupling properties, and directivity can be explained with the help of Figure 1. Figure 1(A) shows the EM power incidents (carried by electromagnetic waves) at the port 1, and power appears at the coupled port, port 3. No decoupled power appears at port 4. Likewise, when the EM power incidents at the port 2, the power appears at the coupled port, port 4, and no decoupled power appears at port 3, as shown in Figure 1(B). Therefore, such coupling is directional. The coupling coefficient of the DC can be defined as:

$$\kappa = \frac{\text{Port}_3}{\text{Port}_1} \tag{1}$$

Assuming all ports are matched, the coupling is usually expressed in dB and is given as:

$$C_{\text{OUPLING}} = 10\log_{10}\left(\frac{P_3}{P_1}\right) = 20\log\left(\frac{P_3}{P_1}\right) \tag{2}$$

Directivity is used as a measure of coupling properties and can be defined as the ratio of the power to a decoupled port to the power at the coupled port, given by the formula:

$$D_{\text{IRECTIVITY}} = 10\log_{10}\left(\frac{P_4}{P_3}\right) = 20\log\left(\frac{P_4}{P_3}\right) \tag{3}$$

The insertion loss can be calculated from the following formula:

$$I_{\text{nsertion}}L_{\text{oss}} = 20\log_{10}\left(\frac{P_2}{P_1}\right) \tag{4}$$

On the other hand, power dividers (PD) divide

Received: October 2022; Revised: November 2023; Accepted: March 2024
*Corresponding Author: Imad Ali <imadali@uswat.edu.pk>

the input EM signals into two in-phase EM signals [5]. The PDs can also be used to combine power. The common port is the output port, whereas the other two ports are exploited as the input ports. Necessary design provisions for the PDs contain insertion loss, amplitude, and phase balance between arms and return losses. Intended for the power combining of uncorrelated EM signals, the most vital design specification is the isolation, that is, the insertion loss from one equal power port to another. Figure 2 shows the Wilkinson PD with two parallel uncoupled quarter-wavelength transmission lines (λ/4 length). The input is provided to two corresponding lines, and the outputs are ended with matching impedance. To avoid coupling, both the lines must be kept spaced; and must get back together at outputs. The impedances at all ports must be the same as the microwave system's characteristic impedance (normally,70 Ω) [6].

Similarly, the rat-race hybrid ring coupler (RHRC) [7], is a four-port device with a transmission line of the mean circumference of 3/4λg with four pots spaced, as shown in Figure 3. The EM power supplied at one port to the RHRC splits equally to the two head-to-head ports, and no EM power appears at the remaining port. The characteristic impedance of the ring line is matched when it is equal to $\sqrt{2}Z_O$. Thus, for a 50 Ω system, $\sqrt{2}Z_O$ = 70.7 Ω. The operation of the RHRC is illustrated in Figure 3**,** where the input EM power at ports 1 appears at ports 2 and 4. Ignoring the power losses, the output EM powers are 3dB down (i.e., half-power) compared to the incident EM power, but these are in phase by 180 degrees due to a half-wavelength difference in their parts through the ring [8]. No power appears at port 3 since waves following path 1 Ø 2 Ø 3 travel $1/2\lambda_g$. Whilst those traveling 1 Ø 4 Ø 3 cover λ_g and hence the path difference is $1/2\lambda_g$. The two components are thus in anti-phase and cancel.

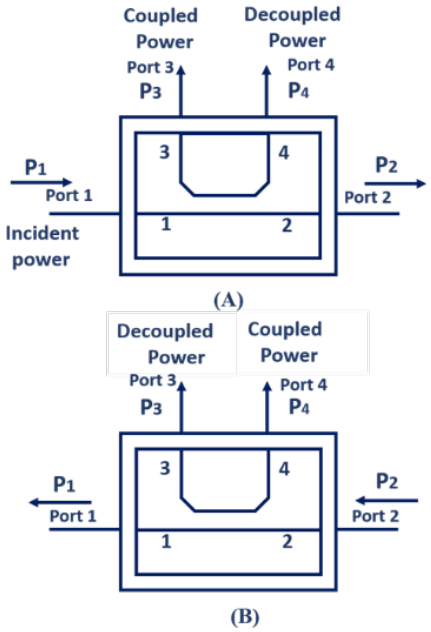

Fig. 1. Schematic diagram of directional coupler transmission properties: (A) Port 1 incident power, (B) Port 2 incident power.

In the past, microwave components like equal PDs, Quadrature Hybrid Couplers, and Rat Race Hybrid Ring couplers were designed for their isolation and matching properties but hinting at the potential for high symmetry and bandwidth enhancement [9]. Studies on Wilkinson power dividers demonstrated their capacity to split power into equiphase segments with isolation between output ports, achieving -27dB isolation and favorable VSWR values [10]. A proposed 90˚ hybrid coupler showcased a compact design with an 18.2% bandwidth enhancement [11]. An Evolutionary Algorithm demonstrated competence in a slot-coupled 3-dB hybrid coupler [12]. Exploration of stub-loaded transmission lines for Wilkinson

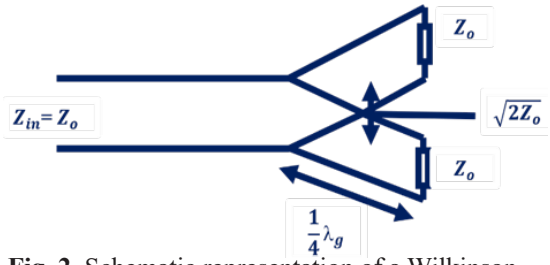

Fig. 2. Schematic representation of a Wilkinson Power Divider.

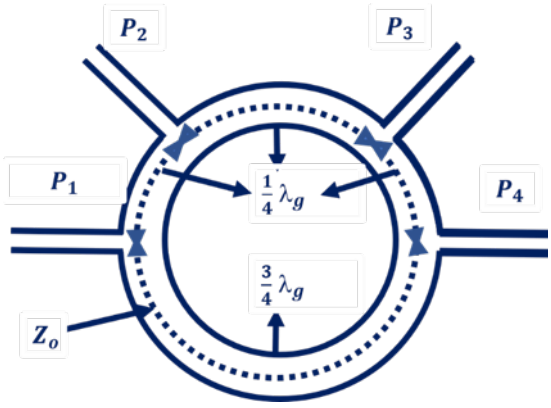

Fig. 3. Illustration depicting a Rat-Race Hybrid Ring Coupler.

PDs demonstrated adaptability for unequal power divisions [13]. Microstrip designs achieved size reduction, and harmonic suppression, maintaining traditional PD features [14]. Capacitive loading in planar Wilkinson PDs improved efficiency, resulting in miniaturized dividers with superior performance [15]. Various methods for 6-dB coupler realization, including rat-race and ring couplers, were explored, acknowledging limitations such as low isolation and specific frequency range constraints [16].

These devices have well-established theories; however, their performance is not studied under diverse input voltages (and frequencies). This article analyzes the aforementioned devices via extensive laboratory hardware experiments under various input voltages and frequency band settings. The primary contribution of this paper lies in the rigorous experimental analysis of microwave power dividers and directional couplers under conditions not extensively explored in existing literature. While prior studies have established the theoretical foundations of these devices, our research provides a practical examination of their performance, particularly focusing on power-splitting characteristics over a broad spectrum of frequencies. In contrast to earlier works that may have limited their investigations to specific frequency ranges or neglected the impact of varying input voltages, our experiments reveal nuanced insights. We address the gap in the literature by demonstrating that transmitted power is only slightly affected at higher frequencies, and the power splitting characteristic holds true across diverse frequency bands.

The present research aimed to address and overcome some of the limitations identified in the previous works. The proposed study conducts extensive laboratory experiments under various input voltages and frequency bands, providing a comprehensive analysis of microwave power dividers and directional couplers. By exploring a broader range of operating conditions, the present research seeks to enhance the understanding of these devices and uncover potential performance variations not covered in previous studies. Moreover, the proposed work delves into the experimental analysis of power splitting characteristics over a band of frequencies, evaluating parameters such as Insertion Loss and Directivity. It may allow to assess the behavior of the devices beyond their specified frequency bands, providing valuable insights into their practical applicability. The experimental results showed that transmitted power is slightly affected at higher frequencies while the power splitting characteristic over a band of frequencies matches their theories.

2. EXPERIMENTS DESIGN

This section outlines various experiments conducted to assess directional couplers (DCs) and power dividers (PDs) across a range of frequencies and VCO voltages. The experiment includes: (a) investigating and measuring directional properties and determining the Coupling, Directivity, and Insertion Loss of DCs, (b) investigating the power division characteristics over a band of frequencies, and (c) investigating how power splits in the branch line coupler. The details about the hardware implementation used to perform the experiments mentioned above are given in Table 1.

For power splitting**,** microwave power dividers and directional couplers are designed to split the input power into multiple outputs. The coupling properties are fundamental to their operation. The coupling coefficient, as defined in Equation (1) in the paper, is a crucial parameter. It quantifies the ability of the device to split power between different ports. The paper conducts extensive laboratory hardware experiments under various input voltages and frequency band settings. By measuring the power at different ports and detectors, the experimental results provide insights into the actual power-splitting characteristics of the devices. These results are crucial for validating the theoretical expectations and understanding how the devices perform in practical scenarios.

The impact of higher frequencies on transmitted power is considered in the paper, where transmitted power may vary with increasing frequencies. Through the hardware experiments, the paper analyzes the stability of transmitted power at higher frequencies. By varying the input frequency and measuring the transmitted power, the experimental results reveal the device's performance under different frequency bands. This experimental evidence is essential for understanding how the devices handle transmitted power across a spectrum of frequencies.

Table 1. Hardware description used in experiments.

S. No.	Module	Description
1	Microstrip Base	Voltage Controlled Oscillator: Tunable over range 2GHz to 4GHz, RF Detector: Input +5 dBm and Power Range: -45dBm ~ -5dBm
2	Directional Coupler	Microstrip components with Directional Transmission, properties used to measure Power Reflection Coefficient, Return loss.
3	3dB Attenuator	Microstrip attenuator producing a transmission loss of 3 dB
4	Hybrid Coupler	Microstrip component designed to couple incident power at one port equally to two other ports but provide isolation between the incident and a fourth port.
5	Wilkinson Power Divider	Microstrip component designed to split incident microwave power equally to its two output ports.
6	Rat race Hybrid Coupler	Microstrip component designed to couple incident power at one port equally to two other ports but provide isolation between the incident and a fourth port.
7	Three Port Circulator	Ferrite circulator mounted in Microstrip used for its non-reciprocal transmission properties widely used as an isolator, diplexer, and channel separator

Directivity and Insertion loss are critical parameters in microwave devices. These parameters have been defined in Equations (3) and (4), respectively. Insertion loss quantifies the power loss between the input and output ports, while directivity measures the ability of the device to couple power to a specific port while minimizing power to other ports. The experimental analysis in the paper includes measurements of insertion loss and directivity. These measurements provide practical insights into how the devices perform in terms of power loss and coupling efficiency. The experimental results are compared with the theoretical expectations, enhancing the understanding of the devices' real-world behavior.

2.1. Directional Properties, Directivity, and Insertion Loss

In the first experiment, the results are obtained to show coupling, directivity, and insertion loss of the DC over the range of 2.0 GHz to 3GHz band. Figures 4 and 5 show the experimental setup. P1 is measured using the circuit in Figure 5, where a 3-port circulator is used as an isolator for the voltage-controlled oscillator (VCO) microwave source with low transmission from port1 to port2. The coupled power P3 is measured. Ports 2 and port 4 are matched with a characteristic impedance. The crystal detector is used for a suitable match at port 3. The Power P4 to the decoupled port is measured, whereas port 2 and port 3 are terminated with a 50Ω matched load. Finally, transmission power P2 is measured, whereas port 3 and port 4 are terminated with a 50Ω matched load. The use of a 3-port circulator as an isolator for the VCO helped reduce transmission losses from port 1 to port 2. The use of a 3-port circulator as an isolator for the VCO helped reduce transmission losses from port 1 to port 2. The transmission coefficient (S_{21}) can be expressed as:

$$S_{21} = e^{-j\beta l} \tag{5}$$

where β is the propagation constant and l is the length of the transmission line. Additionally, ports 2 and 4 were matched to the characteristic impedance (Z_0) to optimize energy transfer. The reflection coefficient (ΓΓ) at a matched load can be given by:

$$\Gamma = \frac{Z_L+Z_0}{Z_L-Z_0} \tag{6}$$

where Z_L is the load impedance.
The crystal detector at port 3 ensured a suitable match, contributing to minimizing losses. The power transfer coefficient (T) for a matched load can be expressed as:

$$T = 1 - |\Gamma|^2 \tag{7}$$

Terminating ports 2 and 3 with a 50Ω matched load further assisted in containing energy losses, ensuring that the incident and transmitted powers are efficiently transferred.

2.2 Power Splitting Characteristics over Band of Frequencies

A critical characteristic that determines the superiority of a microwave PD is the degree to which the input EM power is divided [9]. Thus,

Fig. 4. Experimental layout with hardware connection in the laboratory.

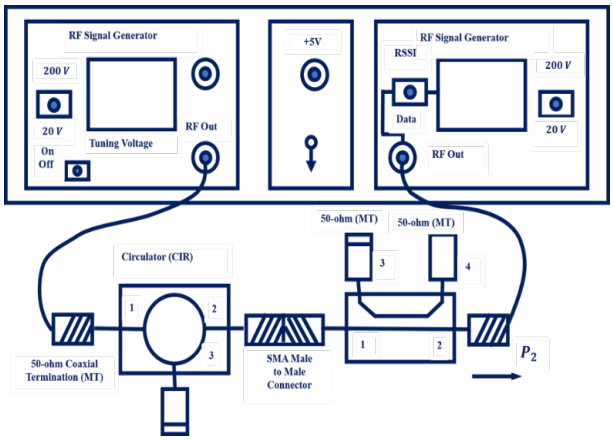

Fig. 5. Schematic detailing the hardware connections for an experimental setup in the laboratory.

when lines are matched, the EM power splits equally between the two output lines. The input VSWR and isolation between the output lines are also important. We have investigated the splitting potential of the Wilkinson PD and the RHRC. The equipment setup is shown in Figures 4 and 5**,** with the third PD port terminated with a 50Ω load to match this port. Directional Couplers (DCs) and Power Dividers (PDs) operate within the microwave range (2.0 GHz to 3 GHz) and undergo analysis with a step size of 0.1 GHz. Using the voltage frequency calibration data supplied, set the VCO to 2.0 GHz. Energy losses in the directional coupler (DC) were minimized using a 3-port circulator as an isolator, matched ports, and 50Ω load termination and in assessing power splitting characteristics over a frequency band, energy loss mitigation involved VCO calibration and careful port termination with matched loads for optimized energy transfer. The power P2 emerging from port 2 at the input RF signal generator is measured. Repeated the power measurement at 0.1GHz intervals through the band up to 3 GHz and recorded the results. A 50 Ω termination is connected to port P2 and connected port P3 to the RF input of the signal detector, so Power P3 at port 3 can be measured with port 2 matched. The power emerging at port 3 is measured and recorded the results from 2 GHz to 3GHz.

3. RESULTS AND DISCUSSION

Tables 2-4 present a detailed analysis of detector voltage, incident and transmitted power, coupled and decoupled powers, directivity, and insertion loss. The following elaboration provides a nuanced interpretation of the presented results.

3.1. Coupled and Decoupled Power Analysis

Table 2 provides a comprehensive analysis of coupled and decoupled power for different frequencies (GHz) and corresponding VCO voltages.

The decoupled power (P4) represents the power that is isolated from the system, while the coupled power (P3) indicates the power that is influenced by the system. As the frequency increases, the decoupled power initially rises but eventually becomes negative, signifying a shift towards the system's influence. The coupled power demonstrates a consistent decrease, indicating the diminishing impact of the system. This table serves as a valuable reference for understanding the intricate relationship between frequency, VCO voltage, and the distribution of coupled and decoupled powers in the presented analysis.

Table 2. Coupled and decoupled power.

Fr (GHz)	VCO (Volts)	Decoupled Power P4 (dBm)	Coupled Power P3 (dBm)
2.0	2.01	2.082911	0.069211
2.1	2.70	1.783967	-0.11366
2.2	3.30	1.554624	-0.28249
2.3	4.10	1.378552	-0.3365
2.4	4.90	1.206401	-0.29147
2.5	5.70	0.788282	-0.55594
2.6	6.60	0.440315	-0.71481
2.7	7.41	-0.03481	-0.96354
2.8	8.31	-0.05227	-0.73369
2.9	9.30	-2.32677	-2.90174
3.0	10.0	-4.49507	-4.64205

Table 3. Incident power and transmitted power analysis after passing three detectors.

Fr (GHz)	VCO (Volts)	Incident Power P1 (dBm)	Detector Volts V1	Detector Volts V2	Detector Volts V3	Detector Volts V4	Transmitted Power P2 (dBm)
2.0	2.01	4.65	1.71	1.70	1.00	1.27	4.62
2.1	2.70	4.45	1.67	1.67	0.98	1.22	4.45
2.2	3.30	4.30	1.64	1.64	0.96	1.19	4.33
2.3	4.10	4.30	1.64	1.63	0.96	1.17	4.29
2.4	4.90	4.19	1.62	1.62	0.96	1.14	4.20
2.5	5.70	4.08	1.60	1.59	0.93	1.09	3.94
2.6	6.60	3.99	1.58	1.58	0.92	1.05	3.81
2.7	7.41	4.16	1.61	1.60	0.89	0.99	3.98
2.8	8.31	3.85	1.55	1.55	0.91	0.99	3.75
2.9	9.30	3.37	1.47	1.44	0.71	0.76	3.19
3.0	10.0	1.99	1.23	1.25	0.58	0.59	1.88

3.2. Incident Power and Transmitted Power Analysis

Table 3 delves into incident power, detector voltages, and transmitted power after passing three detectors. The results showcase a consistent trend where incident power decreases with increasing VCO voltage. Simultaneously, the transmitted power demonstrates a similar pattern. This behavior highlights the impact of VCO voltage on both incident and transmitted powers, providing valuable insights for optimizing power transmission efficiency [9].

3.3. Directivity and Insertion Loss Analysis

Table 4 focuses on directivity and insertion loss analysis. The coupling, directivity, and insertion loss are computed from hardware readings, revealing intriguing patterns. The directivity remains relatively stable across frequencies, indicating consistent isolation between ports. Additionally, the insertion loss, though minimal, displays slight variations. This emphasizes the need for careful consideration of insertion loss in practical applications, especially at higher frequencies.

3.4. Power Tracking Analysis of Wilkinson Power Divider

The power tracking analysis results, presented in Table 5 offers a comprehensive overview of power distribution across different ports of the Wilkinson Power Divider (PD). The results suggest an effective power division at lower frequencies, with a slight deviation at higher frequencies. This behavior is mirrored in the detected voltages at these ports, affirming the splitting capabilities of the Wilkinson PD.

3.5. Rat-Race Hybrid Ring Coupler Investigation

Table 6 provides the details of the investigation of the Rat-Race Hybrid Ring Coupler (RHRC). The powers at ports 1 and 3 exhibit similarity at lower frequencies, with a gradual difference emerging at higher frequencies. This trend aligns with the detected voltages at these ports, emphasizing the frequency-dependent behavior of the RHRC.

Table 4. Directivity and insertion loss analysis.

Fr (GHz)	Coupling (P1-P3) dB	Directivity (P4-P3) dB	Insertion Loss (P1-P2) dB
2.0	4.59	2.01	0.035
2.1	4.57	1.89	0.005
2.2	4.62	1.83	0.005
2.3	4.63	1.71	0.010
2.4	4.48	1.49	-0.010
2.5	4.64	1.34	0.043
2.6	4.70	1.15	-0.016
2.7	5.13	0.92	0.081
2.8	4.59	0.68	0.000
2.9	6.27	0.57	0.184
3.0	6.44	0.14	-0.181

Table 5. Wilkinson Power Divider power tracking analysis.

Fr (GHz)	VCO (Volts)	Detector Volts V2	Power at P2 (dBm)	Detector Volts V3	Power at P3 (dBm)
2.0	2.0	1.67	4.45	1.67	4.45
2.1	2.5	1.64	4.34	1.64	4.33
2.2	3.5	1.62	4.21	1.62	4.21
2.3	4.5	1.60	4.08	1.60	4.09
2.4	5.5	1.55	3.85	1.56	3.86
2.5	6.5	1.53	3.73	1.53	3.69
2.6	7.5	1.46	3.34	1.46	3.31
2.7	8.5	1.31	2.37	1.31	2.40
2.8	9.5	1.15	1.23	1.15	1.26
2.9	10.5	0.95	-0.39	0.95	-0.44
3.0	11.5	1.07	0.62	1.08	0.69

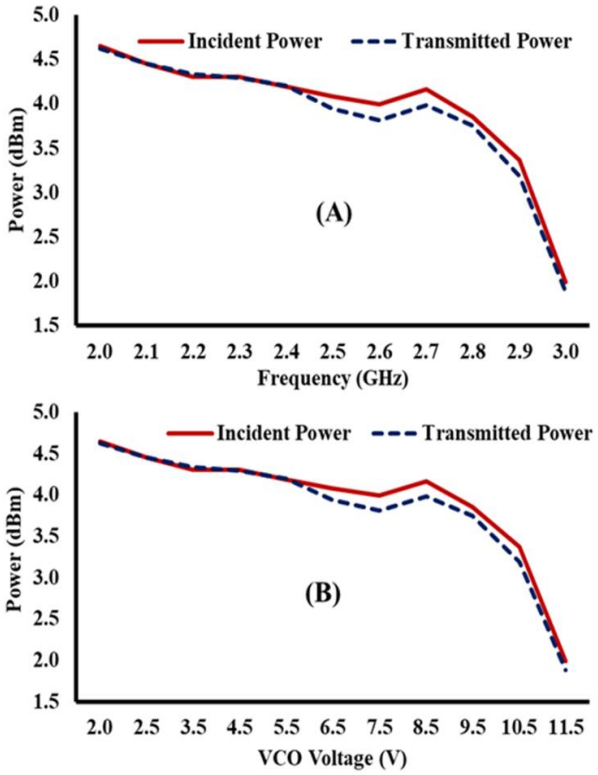

Fig. 6. Incident and transmitted power analysis of frequency band (A) with respect to the input voltage for a Voltage-Controlled Oscillator (B).

3.6. Power Analysis Regarding VCO Input Voltage and Frequency Band

The analysis of incident and transmitted power for frequency band is illustrated in Figure 6 (A), while the same analysis concerning input voltage in a VCO is shown in Figure 6(B). Figure 6 provides a visual representation of power analysis concerning VCO input voltage and the frequency band. The power tracking trends affirm the consistent behavior observed in the tables, further validating the stability and reliability of the proposed devices within their designed frequency bands.

3.7. Theoretical Validation and Frequency-Dependent Losses

The results obtained in these experiments align with theoretical expectations within the designed frequency bands [9]. The observed losses at higher frequencies underscore the importance of assessing device performance in practical settings, where deviations from designed frequency bands can impact overall efficiency. This analysis provides a crucial understanding of the practical implications of the proposed devices, informing future design considerations and applications.

The results obtained from the present experiments match with the theories at the designed frequency bands [9]. The reason for the slight difference at higher frequencies is that these devices are fabricated and designed for particular frequencies (or certain bands). When they operate in the designed frequency bands, their losses are minimal. However, their losses increase when they are used at different frequency bands. Thus, it is crucial to find the losses associated with it in practical settings, as analyzed in this article. In summary, the comprehensive results and their detailed interpretation enhance our understanding of the proposed devices' performance characteristics, offering valuable insights for both theoretical advancements and practical applications.

Table 6. Rat-Race Hybrid Ring coupler investigation.

VCO (Volts)	Detector Volts V1	Power at P1 (dBm)	Detector Volts V2	Power at P2 (dBm)	Detector Volts V3	Power at P3 (dBm)
2.0	1.69	4.58	1.66	4.43	1.66	4.41
2.5	1.66	4.44	1.64	4.34	1.63	4.28
3.5	1.64	4.31	1.62	4.21	1.62	4.21
4.5	1.62	4.19	1.59	4.05	1.59	4.07
5.5	1.58	4.00	1.55	3.84	1.56	3.87
6.5	1.56	3.91	1.52	3.65	1.54	3.78
7.5	1.53	3.74	1.38	2.80	1.46	3.28
8.5	1.40	2.97	1.35	2.63	1.30	2.30
9.5	1.25	1.97	1.42	3.08	0.99	-0.00
10.5	1.11	0.96	1.13	1.06	0.67	-3.36
11.5	1.25	1.93	1.20	1.61	0.81	-1.79

4. SUMMARY AND CONCLUSIONS

This article presents an intense analysis of microwave PDs and DCs regarding the splited power, detector voltage, and frequency bands. The experiments and analysis are performed by hardware implementations. Wilkinson PDs, DCs, and Rat-RHRC are used in experiments. During the experiments, PDs and RHRCs are analyzed for different input VCO voltages and bands of frequencies. The split power is then measured and examined at detectors and ports. In the case of the DCs, additional parameters, including Insertion Loss and Directivity. The experimental analysis of microwave devices has shown how power splits in microstrip systems. After practical experiments, it is analyzed that the transmitted power is somehow affected at higher frequencies. Moreover, the PDs showed equal power splitting at different ports. The splitting characteristics over a band of frequencies are observed according to theoretical discussions.

5. CONFLICT OF INTEREST

The authors declare no conflict of interest.

6. REFERENCES

1. X. Guan, H. Wu, Y. Shi, L. Wosinski, and D. Dai. Ultracompact and broadband polarization beam splitter utilizing the evanescent coupling between a hybrid plasmonic waveguide and a silicon nanowire. *Optics Letters* 38(16): 3005-3008 (2013).
2. A. Collado, and A. Georgiadis. Conformal hybrid solar and electromagnetic (EM) energy harvesting rectenna. *IEEE Transactions on Circuits and Systems I: Regular Papers* 60(8): 2225-2234 (2013).
3. X. Hu, and F. Xu. A six-port network based on substrate substrate-integrated waveguide coupler with metal strips. *IET Microwaves, Antennas & Propagation* 16(1): 18-28 (2022).
4. D.A. Letavin, Y.E. Mitelman, and V.A. Chechetkin. Compact microstrip branch-line coupler with unequal power division. *11th IEEE European Conference on Antennas and Propagation (EUCAP)* 1162-1165 (2017).
5. A.I. Omi, M.H. Maktoomi, M.A. Maktoomi, and P.K. Sekhar. Miniaturized Wideband Three-Way Power Dividers with Arbitrary Band Ratio Using a New Analytical Design Technique. *IEEE Access* 11: 72148-72158 (2023).
6. A.J. Alazemi, and F.H. Almesri. Analysis and Simulation of a Wideband Dual-Band Balanced-to-Unbalanced Gysel Power Divider Using Coupled Lines. *Journal of Engineering Research* 11(1A): 170-183 (2023).
7. Y. Kim. Analysis method for a multi-section rat-race hybrid coupler using microstrip lines. *Journal of Electromagnetic Engineering and Science* 22(2): 95-102 (2022).
8. C. Herrojo, P. Velez, J. Munoz-Enano, L. Su, P. Casacuberta, M.G. Barba, and F. Martin. Highly sensitive defect detectors and comparators exploiting port imbalance in rat-race couplers loaded with step-impedance open-ended transmission lines. *IEEE Sensors Journal* 21(23): 26731-26745 (2021).
9. M.G.E. Kalpanadevi, M.K.N. Nishaw, E. Priyamalli, V. Radhika, and V.S. Priyanga. Design and analysis

of Wilkinson power divider using microstrip line and coupled line techniques. *IOSR Journal of Electronics and Communication Engineering (IOSR-JECE)* 34: 34-40 (2017).

10. D. Wang, X. Guo, and W. Wu. Wideband unequal power divider with enhanced power dividing ratio, fully matching bandwidth, and filtering performance. *IEEE Transactions on Microwave Theory and Techniques* 70(6): 3200-3212 (2022).
11. S. Shelar, and N. Kolhare. Design and Analysis of Hybrid Coupler. *International Journal of Engineering Research & Technology (IJERT)* 3(5): 1217-1220 (2014).
12. S. Y. Zheng, N. Kolhare, A. Gupta, Y.N. Jadhav, and H.G. Prabhakar. Design of broadband hybrid coupler with tight coupling using jumping gene evolutionary algorithm. *IEEE Transactions on Industrial Electronics* 56(8): 2987-2991 (2009).
13. N. Zhang, X. Wang, L. Zhu, and G. Lu. A novel unequal power divider with general isolation topology: Design and verification. *IEEE Microwave and Wireless Technology Letters* 33(1): 19-22 (2022).
14. M. Hayati, M.A. Sattari, S. Zarghami, and S.M. Shah-ebrahimi. Designing ultra-small Wilkinson power divider with multi-harmonics suppression. *Journal of Electromagnetic Waves and Applications* 37(4): 575-591 (2023).
15. C. Qingquan, Z. Yujin, and C. Yong. Miniaturized Wilkinson Power Divider Based on Capacitive Loading and Coupled Microstrip Line. *2022 IEEE International Conference on Microwave and Millimeter Wave Technology (ICMMT) Harbin, China* pp. 1-3 (2022).
16. I.A. Mocanu, N. Codreanu, and M. Pantazică. Design and analysis of hybrid couplers using lumped elements and microstrip topology. *2022 IEEE 28th International Symposium for Design and Technology in Electronic Packaging (SIITME) Bucharest, Romania* pp. 100-103 (2022).

Proceedings of the Pakistan Academy of Sciences: A Physical and Computational Sciences 61(1): 71-80 (2024)

ISSN (Print): 2518-4245; ISSN (Online): 2518-4253
https://doi.org/10.53560/PPASA(61-1)818

Pakistan Academy of Sciences

Research Article

The Research Growth Rate (2019-2020) of Forty Countries in the Field of the Earth and Planetary Science Research

Waseem Hassan*, Sajid Rahman, and Amina Ara

Institute of Chemical Sciences, University of Peshawar, Peshawar 25120, Khyber Pakhtunkhwa, Pakistan

Abstract: The project is designed to explore the research output of the world's top forty countries in the field of Earth and Planetary Sciences from 2010 to 2020. The data in the field of earth and planetary sciences for each country was retrieved from Scopus. Based on the number of publications (in 2020), the top three most productive countries are China (n = 39236), United States (n = 27889), and United Kingdom (n = 10784). However, based on the growth rate (for 2019-2020), the top three countries are Pakistan (n = 38.86), Indonesia (n = 31.36), and Finland (n = 22.00). In 2013-14 and 2010-11, Pakistan was on the 3rd position. While for the years (2015-2018) Pakistan have occupied the 2nd position. This motivated us to decode the research productivity of Pakistan since independence (1947). The total number of publications were found to be 4972, where 8814 authors and 10445 institutes significantly contributed. The University of Peshawar was the most productive university with 584 publications. Pakistan produced 90.50 % (n = 4500) publications in the 21st century (after 2000). The astonishing growth could be attributed to several reasons for example, the establishment of Higher Education Commission (HEC), Islamabad, Pakistan, increase in total expenditure on higher education, increase in international collaboration, etc. At the same time (in 2020), Pakistan has a meagre global share of only 0.178 % (total global production is 2,790,854). This confirms that significant measures are needed to increase the overall productivity (both the number and quality of research publication.

Keywords: Earth and Planetary Sciences, Research Progress, Growth Rate, Forty Countries, Pakistan.

1. INTRODUCTION

Bibliometric analysis involves statistical and mathematical examination of published literature such as research documents, books, or book chapters to identify emerging trends in various fields. This method sheds light on the most productive researchers, research institutes, and countries [1-3]. Typically, data for bibliometric analysis is gathered from one or more databases and then quantitatively analyzed based on specific bibliometric indicators [4]. The significance of bibliometric studies is increasingly recognized worldwide and is utilized by various agencies and universities for diverse purposes [5].

Numerous studies have examined research progress, both in terms of quantity and growth rate, across different countries. For instance, recent research has delved into Australia's science and technology output, analyzing collaboration patterns and research domains [6]. Another study focused on contributions from China, Japan, South Korea, and Taiwan in transplantation research, exploring correlations between GDP and research output [7]. Singapore's national scientific output has also been scrutinized using bibliometrics, analyzing 83,439 papers published between 2000 and 2009 [8]. Similarly, extensive bibliometric analysis has been conducted on Brazilian scientific production in building and construction technologies, as well as on collaboration patterns between Brazil and Spain in medical research [9, 10]. Furthermore, a comprehensive study was conducted [11] on the engineering development of BRICS countries (Brazil, Russia, India, China, and South Africa).

Similarly, there have been several studies focusing on Pakistan's progress across various fields. For example, Bajwa and Yaldram [12]

Received: May 2023; Revised: January 2024; Accepted: March 2024
*Corresponding Author: Waseem Hassan <waseem_anw@yahoo.com>

examined the development of biotechnology research in Pakistan from 1980 to 2011, while Siddique *et al.* [13] analyzed research in library and information science in Pakistan from 1957 to 2018. Additionally, our group reported on Pakistan's chemistry [14] and material sciences [15] research output.

To the best of our knowledge this is the 1st study, to explore the research productivity of Pakistan in Earth and Planetary Sciences from 1947 to 2020. According to Scopus, the following subjects are classified under the title of "Earth and Planetary Sciences".

1. Earth and Planetary Sciences (all)
2. Earth and Planetary Sciences (miscellaneous)
3. Atmospheric Science
4. Computers in Earth Sciences
5. Earth -Surface Processes
6. Economic Geology
7. Geochemistry and Petrology
8. Geology
9. Geophysics
10. Geotechnical Engineering and Engineering
11. Oceanography
12. Palaeontology
13. Space and Planetary Sciences
14. Stratigraphy

The aim of this study is to comprehensively analyze the research output of the top forty countries in the field of Earth and Planetary Sciences over the decade spanning from 2010 to 2020. Specifically, the study aims to:

1. Identify the most productive countries in terms of research publications in 2020.
2. Determine the growth rates of research publications for each country from 2010 to 2020.
3. Investigate the research productivity of Pakistan since its independence in 1947.
4. Highlight factors contributing to Pakistan's research productivity, particularly its significant growth in the 21st century.
5. Assess Pakistan's global share of research production in the field of Earth and Planetary Sciences and propose measures to enhance its overall productivity.

The scope of this study encompasses a detailed examination of various aspects related to research output in Earth and Planetary Sciences, with a particular focus on Pakistan. The scope includes, but is not limited to:

1. Retrieval and analysis of data from Scopus, a leading database in the field, to obtain comprehensive information on research publications.
2. Identification of the most productive countries based on the number of publications in 2020, as well as the top countries with the highest growth rates from 2019 to 2020.
3. Exploration of Pakistan's research productivity since its independence in 1947, including trends in publication output and its position in global rankings over the years.
4. Examination of factors contributing to Pakistan's research productivity, such as the establishment of the Higher Education Commission (HEC), increased investment in higher education, international collaborations, and the growth of educational institutions.
5. Analysis of publication and citation clubs to present the contributions of authors and institutes in Pakistan, with a focus on highlighting the University of Peshawar as the most productive university.
6. Presentation of detailed data on publications and citations for all authors and institutes (from Pakistan) involved in the study, provided in supplementary files.
7. Emphasis on the significant growth in Pakistan's research productivity in the 21st century, with a comparison of publications before and after the year 2000.
8. Evaluation of Pakistan's global share of research production in Earth and Planetary Sciences, indicating areas for improvement and proposing measures to enhance both the quantity and quality of research publications.

Overall, the study aims to provide valuable insights into the research landscape of Earth and Planetary Sciences on a global scale, with a specific focus on Pakistan. In our study, two major indicators, i.e., number of published articles and the growth rate were determined for the top forty (n = 40) countries. For simplicity, the manuscript is divided in following parts.

Part-1: In this part, based on the number of publications (for the year 2020), the ranking of

forty countries is established.
Part-2: In 2nd part, based on the growth rate (for the year 2019-2020), the rankings details of forty countries are provided.
Part-3A: Since, Pakistan has the highest growth rate (in 2019-2020), therefore we retrieved the publication output of Pakistan since independence (1947-2020).
Part-3B: Based on the number of publications, University of Peshawar (UOP), Peshawar, KP-Pakistan is the top ranked University in Pakistan. We will explore the per year publications of UOP.

2. MATERIALS AND METHODS

2.1. Data Sources

The data was retrieved in March-April 2021 from Scopus. The database is one of the largest in world and hosted by Elsevier. It provides data of peer-reviewed articles published in the life, social, physical, and health sciences. In advance search option, we selected the physical sciences as the major domain and later we selected "Earth and Planetary Sciences" [SUBJAREA (EART)]. Based on the number of publications (in 2020) we selected the top forty (n = 40) countries. Next, we retrieved their per year publications data from 2010 to 2020. Furthermore, we calculated their per year growth rates. It's important to note that we only focused on research articles and reviews. The publications of 2021 were ignored in analysis.

2.2. VOSVeiwer Analysis

We used VOSviewer version 1.6.9 for viewing and analyzing the authors, institutes and countries [16].

3. RESULTS AND DISCUSSION

Part-1: Ranking based on number of publications (for the year 2020)

Based on the number of publications, it can be confirmed that the USA and China are arguably the top two global superpowers in the current research publications. According to National Science Foundation report published in 2018, USA has occupied the top rank as the leading producer of science and engineering (S&E) research. United States produced 393,979 S&E publications in 2008, which increased to 422,808 in 2018. While China produced 249,049 publications in 2008 and published extensively in 2018 (i.e., 528,263) [17]. The average annual growth rate 2008–18 (%) for USA was lower (n = 0.71) than China (n = 7.81). Similarly, the nature ranking also confirmed that China is the global leader in high quality chemistry research. This is exactly we observed in the present study. From 2010 to 2014, USA was the top producer with highest number of publications, i.e., 23833, 23527, 21861, 21709 and 20746, respectively. However, from 2015, China has overtaken USA. The per year publications (of China) for the last six years are 2015 (n = 39236), 2016 (n = 35210), 2017 (n = 31773), 2018 (n = 28293), 2019 (n = 27588) and 2020 (n = 26894). In fact, China has astonishingly produced 30.96%, 30.14%, 28.61%, 27.07%, 26.75% and 27.03% research publications for the stated years, respectively.

China's ascent in scientific contributions can be attributed to its substantial investment in research and development (R&D). In 2018 alone, the country allocated approximately $554 billion towards R&D spending in education, reflecting a robust commitment to advancing scientific endeavors. Although, the United States retains its position as the leading R&D nation, its 2018 spending saw a more modest increase, rising by only 5% to approximately $581 billion. Gross domestic spending on R&D encompasses the total expenditure, including both current and capital, on research and development conducted by resident companies, research institutes, universities, government laboratories, and other entities within a country.

Moreover, China's investment in its universities has experienced remarkable growth from 2000 to 2018, multiplying by 10.2 times during this period. In contrast, expenditures in the United States grew at a much slower rate, increasing by only 1.8 times over the same timeframe. The National Science Foundation (NSF) has compiled data from various reputable sources, including the United Nations Educational, Scientific and Cultural Organization (UNESCO) Institute for Statistics database and the Organization for Economic Co-operation and Development (OECD) to corroborate these findings. Additionally, data from the National Bureau of Statistics of China, as presented in the China Statistical Yearbook, further affirm this trend.

1. From 2004 onwards China awarded more

Bachelor's degree in S&E fields.

2. From 2006 onwards China awarded more Doctoral degrees in S&E fields.
3. From 2005 onwards, China has more estimated number of researchers as compared with USA.

The publications data of all forty countries from 2010 to 2020 is provided in supplementary Table S1. While, the data for the year 2020 is presented in Table 1. We can also represent the country-wise data in different regions or continents.

From Europe nineteen countries contributed to research publications. The top five countries from this region are United Kingdom (n = 10784), Germany (n = 10429), France (n = 7783), Russian Federation (n = 6942) and Italy (n = 6620). From Asia eight countries were involved in publications. The highest contribution was offered by China (n = 39236), India (n = 6523), Japan (n = 5135), South Korea (n = 2428) and Taiwan (n = 1295). From North America, three countries have significantly contributed, i.e., United States (n = 27889), Canada (n = 6021), Mexico (n = 1454). Australia (n = 6558), New Zealand (n = 1171) contributed from Oceana, Brazil (n = 3932), Chile (n = 1992), and Argentina (n =1380), from South America; Iran (n = 3344), Saudi Arabia (n = 930) and Israel (n = 894) from Middle East, while South Africa (n = 1843) and Egypt (n = 1049) were the top contributors from Africa.

While, irrespective of the region (in 2020), the top ten countries are China (n = 39236), United States (n = 27889), United Kingdom (n = 10784), Germany (n = 10429), France (n = 7783), Russian Federation (n = 6942), Italy (n = 6620), Australia (n = 6558), India (n = 6523) and Canada (n = 6021). In fact, from 2010-the top two countries are China and USA. Some of the common features of these ten countries are the high-ranking research institutions, rising interest in new fields of science, increase in international collaborations and last but not the least, the increase in government funding. From world bank we also retrieved the per year research and development (R&D) data (from the year 2010 to 2018) for the top ten countries as shown in Table 2 [18]. We will also highlight that based on the number of publications (for the year 2020), Pakistan was ahead of some of the prominent countries. For

Table 1. Number of publications (NOP) of the top forty countries for the year 2020.

S. No.	Country	Total Documents	S. No.	Country	Total Documents
1	China	39236	21	Chile	1992
2	United States	27889	22	South Africa	1843
3	United Kingdom	10784	23	Turkey	1689
4	Germany	10429	24	Belgium	1646
5	France	7783	25	Austria	1507
6	Russian Federation	6942	26	Mexico	1454
7	Italy	6620	27	Denmark	1435
8	Australia	6558	28	Argentina	1380
9	India	6523	29	Portugal	1370
10	Canada	6021	30	Taiwan	1295
11	Japan	5135	31	Czech Republic	1285
12	Spain	5054	32	Finland	1281
13	Brazil	3932	33	New Zealand	1171
14	Iran	3344	34	Egypt	1049
15	Netherlands	3318	35	Greece	1001
16	Switzerland	2918	36	Saudi Arabia	930
17	Poland	2482	37	Hong Kong	897
18	South Korea	2428	38	Israel	894
19	Sweden	2119	39	Indonesia	867
20	Norway	2077	40	Pakistan	854

Table 2. R&D (% of GDP) data of the top ten countries from 2010 to 2020 [18].

Country Name	2010	2011	2012	2013	2014	2015	2016	2017	2018
Germany	2.71	2.80	2.87	2.82	2.87	2.91	2.92	3.04	3.09
United States	2.74	2.77	2.68	2.71	2.72	2.72	2.76	2.82	2.84
France	2.18	2.19	2.23	2.24	2.28	2.27	2.22	2.21	2.20
China	1.71	1.78	1.91	2.00	2.03	2.07	2.12	2.15	2.19
United Kingdom	1.66	1.66	1.59	1.64	1.66	1.67	1.68	1.70	1.72
Canada	1.83	1.79	1.78	1.71	1.72	1.70	1.73	1.67	1.57
Italy	1.22	1.21	1.27	1.31	1.34	1.34	1.37	1.38	1.40
Russian Federation	1.13	1.01	1.03	1.03	1.07	1.10	1.10	1.11	0.99
India	0.79	0.76	0.74	0.71	0.70	0.69	0.67	0.67	0.65
Australia	2.38	2.24	NA	2.18	NA	1.92	NA	1.87	NA

example, Malaysia (n = 802), Ireland (n = 686), Hungary (n = 643), Ukraine (n = 625), Vietnam (n = 558), Thailand (n = 540), Singapore (n = 486), Romania (n = 398), Morocco (n = 384), Slovakia (n = 370), Croatia (n = 338), Bangladesh (n = 312), Slovenia (n = 286), Serbia (n = 274), Iceland (n = 234), Philippines (n = 189), Bulgaria (n = 148), Lithuania (n = 138), Sri Lanka (n = 101), Georgia (n = 99), Lebanon (n = 99), Oman (n = 98), Qatar (n = 76), Luxembourg (n = 66) and Belarus (n = 62).

Part-2: Ranking based on growth rate (for the year 2019-2020)

Based on the growth rate (GR) (for the year 2019-2020), Pakistan is the top ranked country (GR = 38.86), followed by Indonesia (n = 31.36), New Zealand (n = 22.00), Mexico (n = 16.97), Argentina (n = 15.71), Turkey (n = 15.67), Finland (n = 15.66), Taiwan (n = 15.38), India (n = 14.32) and Switzerland (n = 14.12). We further calculated the growth rate for Pakistan and other thirty-nine countries for the last ten years. The data is presented in supplementary Table S2. It is interesting to note that for the years, 2018-19, 2017-18, 2016-17 and 2014-15, Pakistan occupied the 2nd position, for 2013-14 and 2010-11, Pakistan was on 3rd position. The details for the 2019-2020 is presented in Table 3.

Part-3A: Pakistan

This motivated to explore its overall research productivity since independence (from 1947). In total Pakistan published 4972 research documents in earth sciences. The highest documents are published in 2020 (n = 854), followed by 2019 (n = 615), 2018 (n = 492), 2017 (n = 383), 2015 (n = 347), 2016 (n = 333), 2014 (n = 271), 2013 (n = 214), 2012 (n = 178) and 2011 (n = 174). The per year publications details is provided in Table 4.

3.1A. Subject Area or Domains

Scopus categorized the publications in different subject areas, e.g., earth and planetary sciences (n = 4972), environmental science (n = 1493), physics and astronomy (n = 928), engineering (n = 838), agricultural and biological sciences (n = 836), mathematics (n = 454), materials science (n = 369), computer science (n = 256), chemical engineering (n = 204), chemistry (n = 189) and energy (n = 174), to name a few.

3.2A. Authors

Its worthy to note that in all publications (n = 4972), 8814 authors have significantly contributed. Based on the number of publications, the top ten authors are Sharif M. (n = 156), Khan M.A. (n = 124), Ali A. (n = 108), Ali S. (n = 103), Khan S. (n = 101), Ahmad I. (n = 93), Ahmad S. (n = 81), Ali M. (n = 69), Khan A. (n = 69) and Hussain S. (n = 63). However, the highest citations were recorded for Sharif M. (n = 2036), Khan M.A. (n = 1939), Jan M.Q. (n = 1393), Syed F.S. (n = 1202), Dawood H. (n = 1112), Ashraf M. (n = 1088), Burg J.-P. (n = 1041), Farooq M. (n = 1038), Zubair M. (n = 1004), and Giorgi F. (n = 955).

3.3A. Institutes

10445 institutions are directly involved in all

Table 3. Percent (%) growth rate (GR) of the top forty countries for 2019-2020.

S. No.	Year	2019-20	S. No.	Year	2019-20
1	Pakistan	38.86	21	Spain	9.39
2	Indonesia	31.36	22	Greece	9.28
3	Finland	22	23	Netherlands	9.04
4	Turkey	16.97	24	Mexico	8.18
5	Portugal	15.71	25	Iran	8.08
6	Belgium	15.67	26	Australia	7.74
7	Czech Republic	15.66	27	South Korea	7.29
8	Argentina	15.38	28	Italy	7.14
9	India	14.32	29	Japan	7.14
10	Switzerland	14.12	30	Austria	6.43
11	Brazil	13.87	31	Saudi Arabia	6.29
12	New Zealand	13.58	32	France	6.08
13	Chile	13.05	33	Canada	5.85
14	Israel	12.45	34	United Kingdom	5.37
15	Norway	11.55	35	Germany	5.32
16	China	11.43	36	South Africa	5.13
17	Egypt	10.42	37	Sweden	5.06
18	Hong Kong	10.2	38	Poland	4.81
19	Denmark	10.13	39	United States	4.02
20	Taiwan	10.12	40	Russian Federation	-3.02

publications (n = 4972). The highest number of documents are contributed by Department of Mathematics, University of The Punjab, Quaid-e-Azam Campus, Lahore, 54590, Pakistan (n = 111), followed by National Centre of Excellence in Geology, University of Peshawar, Pakistan (n = 83), University of Chinese Academy of Sciences, Beijing, 100049, China (n = 68), Department of Earth Sciences, Quaid-i-Azam University, Islamabad, Pakistan (n = 67), National Centre of Excellence in Geology, University of Peshawar, Peshawar, Pakistan (n = 55). Institute of Geology, University of The Punjab, Lahore, 54590, Pakistan (n = 44), Department of Earth Sciences, Quaid-i-Azam University, Islamabad, 45320, Pakistan (n = 40), Department of Geology, University of Baluchistan, Quetta, Pakistan (n = 40). Department of Geology, University of Peshawar, Pakistan (n = 40) and Centre of Excellence in Mineralogy, University of Baluchistan, Quetta, Pakistan (n = 36).

However, the highest citations were recorded for Department of Mathematics, University of The Punjab, Quaid-e-Azam Campus, Lahore, 54590, Pakistan (n = 1196), followed by Global Change Impact Studies Centre, Pakistan Meteorological Department, Islamabad, Pakistan (n = 880), National Centre of Excellence in Geology, University of Peshawar, Peshawar, Pakistan (n = 833), Department of Mathematics, University of The Punjab, Quaid-e-Azam Campus, Lahore 54590, Pakistan (n = 761), Center For Atmospheric Physics, Institute of Meteorology, Havana, Cuba (n = 746), Department of Air Pollution and Climate Change, Egyptian Meteorological Authority, Cairo, Egypt (n = 746), Department of Civil Engineering and Environmental Science, Loyola Marymount University, Los Angeles, California, United States (n = 746), Department of Earth Sciences, University of California, Santa Cruz, California, United States (n = 746), Department of Environmental Science, University of California, Berkeley, United States (n = 746), Department of Hydrology and Meteorology, Katmandu, Nepal (n = 746) and Earth Systems Physics Group, The Abdus Salam International Centre for Theoretical Physics, Trieste, Italy (n = 746).

3.4A. Universities

Based on the number of publications the top

Table 4. The per year publications of Pakistan.

Year	Publications	Year	Publications	Year	Publications
1912	3	1976	2	1999	23
1913	1	1977	3	2000	28
1916	3	1978	8	2001	26
1919	2	1979	1	2002	33
1951	1	1980	8	2003	29
1952	1	1981	16	2004	36
1953	1	1982	13	2005	40
1954	1	1983	17	2006	52
1955	3	1984	35	2007	86
1959	2	1985	26	2008	88
1961	3	1986	28	2009	100
1962	1	1987	11	2010	121
1963	3	1988	21	2011	174
1964	1	1989	29	2012	178
1965	1	1990	21	2013	214
1966	2	1991	22	2014	271
1967	3	1992	10	2015	347
1968	2	1993	19	2016	333
1970	3	1994	14	2017	383
1971	2	1995	25	2018	492
1972	2	1996	25	2019	615
1973	4	1997	20	2020	854
1975	3	1998	27		

universities are University of Peshawar (n = 584), University of the Punjab, Lahore (n = 515), COMSATS University Islamabad (n = 488), Quaid-i-Azam University, Islamabad (n = 359), National University of Sciences and Technology, Pakistan (n = 265), University of Engineering and Technology Lahore (n = 231), University of Karachi (n = 223), University of Agriculture, Faisalabad (n = 210), University of Chinese Academy of Sciences (n = 136), Geological Survey of Pakistan (n = 126), Pakistan Institute of Nuclear Science and Technology (n = 116) and University of Baluchistan (n = 109). The list of most productive universities is provided in supplementary Table S3.

3.5A. Citation Details for All Documents

The total citations for all publications (n = 4972) were 62555. However, only two documents received more than six hundred citations, four documents received more than three hundred citations, six documents received more than two hundred citations, fifty seven documents received more than one hundred citations, one hundred and ninety seven documents received between fifty and ninety nine (n = 50-99) citations, one thousand three hundred documents received between ten and forty nine citations (n = 10 to 49), two thousand five hundred and thirteen documents received between one and nine citations (n = 1 to 9), while eight hundred and seventy four documents received zero citations.

3.6A. Sources

All documents were published in 648 sources. Based on the number of publications, the top major sources of Pakistan's publications are Astrophysics And Space Science (n = 292), Arabian Journal of Geosciences (n = 264), European Journal of Scientific Research (n = 209), Journal of Himalayan Earth Sciences (n = 179), International

Journal of Modern Physics D (n = 117), SN Applied Sciences (n = 113), Iranian Journal of Science and Technology Transaction A: Science (n = 112), Environmental Earth Sciences (n = 89), Agricultural Water Management (n = 70) and Journal of Asian Earth Sciences (n = 57).

However, the highest citations were received by Astrophysics and Space Science (n = 3578), Agricultural Water Management (n = 2099), Soil and Tillage Research (n =1996), Atmospheric Environment (n = 1462), Environmental Earth Sciences (n = 1087), Arabian Journal of Geosciences (n = 987), Nature Geoscience (n = 981), Geology (n = 980), Journal of Asian Earth Sciences (n = 967) and Journal of Geochemical Exploration (n = 963).

Part 3B: University of Peshawar (UOP), Peshawar, KP-Pakistan

Since UOP produced the highest number of publications (n = 584) for Pakistan, therefore we also retrieved the research output details. UOP published its 1st document in 1971. The highest number of documents are published in 2019 (n = 74), followed by 2020 (n = 71), 2018 (n = 60), 2016 (n = 56) and 2017 (n = 49). The per year number of publications (University of Peshawar) along with collaboration countries is provided in Table 5.

3.1B. Citation Details for All Documents

The total citations were found to be 7613 for all publications (n = 584). Only one document received more than two hundred citations (n = 200), thirteen documents received between 100-199 citations, twenty documents received between 51 to 99 citations, one hundred and forty-six documents received between 10 to 49 citations, two hundred and ninety nice received between 1 to 9 citations and one hundred and five documents received zero (n = 0) citations.

Table 5. The per year publications and main collaborating countries for University of Peshawar.

Year	Publications	Year	Publications	Collaborating Countries	Publications	Collaborating Countries	Publications
1970	1	1999	5	Pakistan	584	Egypt	3
1973	1	2000	3	China	78	Finland	3
1977	1	2001	3	United States	71	Georgia	3
1978	1	2003	5	United Kingdom	66	Israel	3
1979	1	2004	4	Netherlands	17	Malaysia	3
1981	5	2005	3	Australia	13	Afghanistan	2
1982	4	2006	3	Austria	13	Ireland	2
1983	3	2007	7	Germany	13	Jordan	2
1984	13	2008	6	Canada	11	Kyrgyzstan	2
1985	11	2009	9	Turkey	11	New Zealand	2
1988	3	2010	12	Italy	9	Oman	2
1989	7	2011	13	Iran	8	Taiwan	2
1990	2	2012	17	Japan	8	Tajikistan	2
1991	1	2013	29	Brazil	7	Algeria	1
1992	1	2014	37	France	7	Armenia	1
1993	4	2015	47	Spain	6	Azerbaijan	1
1994	1	2016	56	Thailand	5	Brunei Darussalam	1
1995	2	2017	49	India	4	Estonia	1
1996	7	2018	60	Saudi Arabia	4	Hong Kong	1
1997	1	2019	74	Switzerland	4	Iraq	1
1998	1	2020	71	Denmark	3	Lebanon	1

3.2B. Sources

Total number of sources were 160. The highest documents are published in Journal of Himalayan Earth Sciences (n = 115), followed by Arabian Journal of Geosciences (n = 51), Geological Bulletin, University of Peshawar (n = 21), Journal of Asian Earth Sciences (n = 19), Natural Hazards (n = 12), Journal of Atmospheric and Solar-Terrestrial Physics (n = 11), Journal of Earth System Science (n = 11), Journal of Mountain Science (n = 11), Acta Geologica Sinica (n = 10) and Atmospheric Environment (n = 9).

While the highest citations were received by Palaeogeography, Palaeoclimatology, Palaeoecology (n = 400), Tectonics (n = 362), Special Paper of the Geological Society of America (n = 340), Geology (n = 328), Geomorphology (n = 312), Journal of Asian Earth Sciences (n = 307), Journal of Petrology (n = 284), Journal of the Geological Society (n = 243), Journal of Soils and Sediments (n = 218) and Journal of Himalayan Earth Sciences (n = 195).

3.3B. Authors

Total 1090 authors have contributed in 584 publications. Based on the number of publications, the top ten authors are Khan S. (n = 85), Khan M.A. (n = 52), Jan M.Q. (n = 44), Ahmad S. (n = 42), Hanif M. (n = 36), Ali A. (n = 34), Jan I.U. (n = 34), Shafique M. (n = 31), Shah M.T. (n = 31) and Ahmad I. (n = 27). However, the highest citations were noted for Jan M.Q. (n = 1316), Khan M.A. (n = 1199), Tahirkheli R.A.K. (n = 678), Khan S. (n = 598), Shah M.T. (n = 564), Alam K. (n = 428), Hamidullah S. (n = 390), Shafique M. (n = 294), Ullah S. (n = 235), Ahmad I. (n = 234) and Ali A. (n = 231).

After keeping the minimum number of publications to be five, we also calculated the citation per documents (CPD) for all authors. The highest CPD was noted for Tahirkheli R.A.K. (n = 85), followed by Khattak M.U.K. (n = 41), Jan M.Q. (n = 30), Bibi H. (n = 26), Khan S.F. (n = 25), Bibi S. (n = 25), Khan M.A. (n = 23), Afzal J. (n = 23), Muhammad S. (n = 21) and Sayab M. (n = 19).

The UOP also collaborated with 46 countries. The highest documents are collaborated with China (n = 78), followed by United States (n = 71), United Kingdom (n = 66), Netherlands (n = 17), Australia (n = 13), Austria (n = 13), Germany (n = 13), Canada (n = 11), Turkey (n = 11) and Italy (n = 9).

4. CONCLUSIONS

The substantial growth in Pakistan's scientific output can be attributed to several pivotal factors. A key catalyst was the establishment of the Higher Education Commission (HEC) in Islamabad, Pakistan, on September 11, 2002, which emerged as a major driving force behind this expansion. Notably, Pakistan produced a staggering 90.50% (n = 4500) of its publications in the 21st century (after 2000); whereas, only 9.50% (n = 472) were published from 1947 to 1999. Similarly, the University of Peshawar witnessed a notable shift, with 508 documents published after 2000 compared to only 76 published earlier, with the first document dating back to 1970. The growth of the education sector is evident from the increase in the number of universities, which rose from 74 in 2001-02 to 211 in 2019-20, accommodating a significant increase in both students and faculty members. Public expenditure on education also saw a remarkable surge, escalating from 72.3 billion in 2001 to 315 billion in 2018, reflecting a robust commitment to educational advancement. Notably, the total expenditure on higher education witnessed substantial growth over the years, reaching 44.00 billion in 2009-10. International collaboration in research also experienced a significant upsurge, with collaborations noted with twenty-three countries from 1947 to 1999. Notably, collaborations were primarily with countries such as the USA, UK, and Germany. However, post-2000, a substantial increase in collaboration was observed, with collaborations spanning to 117 countries, with China emerging as Pakistan's most important partner. Despite these significant strides, Pakistan's global share in scientific production remains modest, accounting for only 0.178% of the total global production in 2020. This underscores the need for concerted efforts to further enhance overall productivity in the field of scientific research.

5. CONFLICT OF INTEREST

The authors declare no conflict of interest.

6. REFERENCES

1. J. Hui, L. Wang, R. Liu, C. Yang, H. Zhang, and

A.H.S. Wei. A bibliometric analysis of international publication trends in premature ejaculation research (2008–2018). *International Journal of Impotence Research* 33: 1-10 (2020).
2. P.K. Muhuri, A.K. Shukla, and A. Abraham. Industry 4: A bibliometric analysis and detailed overview. *Engineering Applications of Artificial Intelligence* 78: 218-235 (2019).
3. V. Nunen, K. Li, G. Reniers, and K. Ponnet. Bibliometric analysis of safety culture research. *Safety Science* 108: 248–258 (2018).
4. J.A. Wallin. Bibliometric Methods: Pitfalls and Possibilities. *Basic & Clinical Pharmacology and Toxicology* 97(5): 261–75 (2005).
5. A. Pritchard. Statistical bibliography or bibliometrics. *Journal of Documentation* 25(4): 348-349 (1969).
6. M. Matthews, B. Biglia, K. Henadeera, J.F.D. Hicks, R. Faletic, and O. Wenholz. A Bibliometric Analysis of Australia's International Research Collaboration in Science and Technology: Analytical Methods and Initial Findings. *FEAST Discussion Paper 1/09* (2009).
7. Q.H. Pu, Q.J. Lyu, and H.Y. Su. Bibliometric analysis of scientific publications in transplantation journals from Mainland China, Japan, South Korea and Taiwan between 2006 and 2015. *British Medical Journal Open* 6: e011623 (2016).
8. S. Rana. Bibliometric analysis of output and visibility of science and technology in Singapore during 2000-2009. *Webology* 9(1): 1-12 (2012).
9. P.B. Soares, T.C.J. Carneiro, J.L. Calmon, and O. Castro. Bibliometric analysis of the Brazilian scientific production on Building and Construction Technologies in the Web of Science database. *Ambient Construction* 16: 175-185 (2016).
10. A.A. Arroyo, E.F.T. de Oliveira, M.C.C. Grácio, A. Pandiella, and R.A. Benavent. A bibliometric analysis of collaboration between Brazil and Spain in the field of medical research from 2002 to 2011. *Investigación Bibliotecológica.* 30(69): 198-221 (2016).
11. B. Elango. A bibliometric analysis of literature on engineering research among BRIC countries. *Collection and Curation* 38: 9-14 (2019).
12. R.S. Bajwa and K. Yaldram. Bibliometric analysis of biotechnology research in Pakistan. *Scientometrics* 95(2): 529–540 (2013).
13. N. Siddique, S.Ur. Rehman, M.A. Khan, and A. Altaf. Library and information science research in Pakistan: A bibliometric analysis, 1957–2018. *Journal of Librarianship and Information Science* 53: 89-102 (2021).
14. W. Hassan, M. Khalid, and M.R. Shah. Research Publications Growth Rate of Chemistry and Related Subject Areas in Pakistan and Fifty Countries from 2001 to 2020. *Journal* of the *Chemical Society* of *Pakistan* 2: 144-164 (2021).
15. W. Hassan, S. Rahman, and A. Ara. The Research Publications Growth Rate of Pakistan in the Field of Material Sciences: Comparison with 50 countries: Material Sciences Research in Pakistan: Bibliometric Analysis. *Proceedings of the Pakistan Academy of Sciences: A. Physical and Computational Sciences* 58(3): 1–14 (2021).
16. V.E. Waltman. Software survey: VOSviewer, a computer program for bibliometric mapping. *Scientometrics* 84(2): 523-538 (2010).
17. J. Veysey. National Science Board, National Science Foundation. U.S. Trends and International Comparisons. Science and Engineering Indicators 2020. *NSB-2020-6* (2019). https://www.nsf.gov/pubs/2020/nsb20201/nsb20201.pdf.
18. The World Bank, Research and development expenditure (% of GDP). Code GB.XPD.RSDV.GD.ZS (2024). https://data.worldbank.org/indicator/GB.XPD.RSDV.GD.ZS.

Proceedings of the Pakistan Academy of Sciences: A Physical and Computational Sciences 61(1): 81-88 (2024)

ISSN (Print): 2518-4245; ISSN (Online): 2518-4253
https://doi.org/10.53560/PPASA(61-1)858

Pakistan Academy of Sciences

Research Article

Performance Evaluation of Half-Feed Rice Combine Harvester

Aksar Ali Khan[1], Zia-Ul-Haq[1*], Hamza Muneer Asam[2], Muhammad Arslan Khan[1], Ali Zeeshan[1], Saliha Qamar[1], and Abu Saad[1]

[1]Department of Farm Machinery and Precision Engineering, Faculty of Agricultural Engineering and Technology, PMAS-Arid Agriculture University, Rawalpindi, Pakistan
[2]Center for Agriculture and Bioscience International, Asian Development Bank, Rawalpindi, Pakistan

Abstract: Rice (*Oryza sativa*) is one of the most important cereal grains cultivated on an area of 165 million hectares with approximately 756.7 million metric tons of production in the world. In 2019, Pakistan's area under rice cultivation was about 2.9 million hectares, with 7.5 million tons yield. Rice-wheat cropping system is the most famous, especially in Punjab, Pakistan. Harvesting is presently conducted through manual labor or with the utilization of outdated models of combine harvesters with huge grain quality and quantity losses. Imported half-feed rice combine harvester was introduced and an experiment was planned to evaluate its feasibility. The performance was evaluated at three levels of forward speed (3, 4, and 5 km/h) and cutter bar heights (12, 16, and 20cm) during the harvesting season of 2021 in the district Sheikhupura, Punjab. The machine performance was based on header loss, effective field capacity, broken grains percentage, fuel consumption, and field efficiency. The collected data was analyzed at a 5% level of probability by randomized complete block design (RCBD). The statistical analysis revealed that the machine performed better at the speed S_2 (4 km/h) and cutter bar height H_2 (16cm) with the maximum EFC (0.55 ha/h) and Field Efficiency (75.3%) as well as minimum Grain Losses (24.7 kg/ha) and Grain Breakage (14.2 kg/ha) in standing crop condition. Therefore, this machine is recommended to farmers due to its higher EFC and Field Efficiency as well as lower Grain Losses and Grain Breakage as compared to the conventional methods and obsolete machinery.

Keywords: Combine Harvester, Effective Field Capacity, Field Efficiency, Fuel Consumption, Header Loss.

1. INTRODUCTİON

Rice (*Oryza sativa*) is an important staple food for more than 50% population of the world. It accounts for 15% and 21% of human protein production and collective human calories per capita worldwide [1]. It is an important cash crop in Pakistan, contributing significantly to the country's total economy. It contributes 0.7% of GDP and 2.7% to agriculture. It is Pakistan's second biggest food grain product, and in recent years, it has become a significant source of international exchange reserves. Overall grain production in Pakistan is estimated to be 34 million tons, which exceeded about 33.3 million from the previous year [2]. In the Punjab province of Pakistan, the area between the Ravi and Chenab rivers is famous for rice production and Basmati rice is famous for its aroma all over the world having a huge customer demand. For the year 2021-22, Lahore Division produced a record 5.7 million tons of rice, both basmati and non-basmati, compared to a target of 4.4 million ton, as well as a 1.9% increase in per acre yield over the previous year [3].

Rice-wheat cropping system in Pakistan encompasses 2.1 million hectares, approximately three-fifths of which lies in the Punjab province. Punjab's rice-wheat region comprises districts of Gujranwala, Sheikhupura, and Sialkot. In the rice-wheat cropping system, there is very less time between rice harvesting and wheat sowing. Depending on the time of harvest of the rice crop, wheat conventional tillage requires pre-sowing irrigation on well-drained soils or draining or drying of soil in lowlands followed by one or

Received: July 2023; Revised: February 2024; Accepted: March 2024
*Corresponding Author: Zia-Ul-Haq <zia.ch@uaar.edu.pk>

two disking, two harrowing, and leveling that must be required on time. Late harvesting results in a decrease in the yield of wheat [4].

Delayed rice harvesting results in significant grain and straw losses attributable to over maturity, causing grain breakage as well as delays in seedbed preparation and planting operations [5]. Due to a labor shortage during peak harvest season, farmers are forced to postpone harvesting, resulting in substantial postharvest losses and, in some cases, crop loss due to natural disasters. The demand for agricultural labor has increased dramatically as planting intensity and production of crops have increased [6].

Manual harvesting has been a common practice in the region of South East Asia. Combine harvesters have become an attractive option in many locations in South East Asia as the increased labor cost. This mechanized method consumes less time as compared to manual harvesting, containing; cutting, collecting, sun-drying in the field, and carrying dried paddy to a threshing service. The use of a combine harvester reduces the cost of production and increases the profit. This method also helped reduce the labor shortage and improved rice grain quality [7].

Rice is harvested manually or with the help of combine harvesters. Currently, old models of combine harvesters are being used. These machines are outdated with huge grain quality and quantity losses. To overcome these losses imported half-feed rice combine harvesters were introduced into the rice-wheat cropping system. Keeping in view the above-mentioned problem an experiment was designed to test the feasibility of half-feed rice combine harvester at three different speeds, cutter bar heights and crop conditions.

2. MATERIALS AND METHODS

To retrieve useful information for the farmers of the Rice-Wheat cropping system and to examine the feasibility of the imported machine (Half-Feed Rice Combine Harvester) an experiment was conducted during the rice harvesting season in 2021 at Fatehpur, district Sheikhupura. The average temperature of the experimental area is around 22 °C in the month of October–November and it typically receives about 23.04 millimeters of precipitation and has 49.28 rainy days (13.5% of the time) annually.

2.1. Machine Specifications

The machine specifications are given in Table 1.

Table 1. Machine Specifications of Half-Feed Rice Combine Harvester.

Half-Feed Rice Combine Harvester	
Model name	ER112
Power hp	112 HP
Cutter bar width	7 FT.
Grain tank capacity	800 KG
Fuel tank capacity	85 L

2.2. Experimental Treatments

The performance of the machine was evaluated at three levels of forward speed (S_1 = 3 km/h, S_2 = 4 km/h, and S_3 = 5 km/h) and at three different cutter bar heights (12 cm, 16 cm, and 20 cm).

2.3. Machine Parameters/Performance Indicators

The performance indicators were header loss, effective field capacity, broken grains percentage, fuel consumption, operational time, and field efficiency.

2.3.1. Operational time

The operational time was recorded with the help of a stopwatch. The literature review indicated that this method was previously adopted [8] in which a stopwatch was used to record the amount of time spent on harvesting. The starting and stopping timings were included in the times recorded. The time wasted on turning the combine harvester was also recorded to calculate time losses.

2.3.2. Fuel consumption

Prior to the harvesting operation, the combine harvester was completely refueled. The quantification of fuel consumption was done by gauging the variance in the fuel levels within the tank before and after the operation.

2.3.3. Field efficiency

The field efficiency (FE) of a machine is the ratio of effective field capacity and theoretical field capacity. The FE for a real field procedure was never 100% due to headland turns, machine difficulties, ground surface, and overlapping [9].

The following formula was used to calculate FE:

$$FE = \frac{EFC}{TFC} \times 100 \quad (1)$$

Where,
FE = field efficiency (%)
EFC = effective field capacity (ha/hr)
TFC = theoretical filed capacity (ha/hr)

2.3.4. Adjustment of forward speed

The combine harvester was operated at three different speeds. The speed of the machine was measured by fixing a distance of 20 m and a stopwatch and a measuring tape. A stopwatch was used to record the time to cover the 20 m distance. The average forward speed was estimated using the formula after this operation was conducted three times [10].

$$Speed = \frac{Driven\ Length}{Driven\ Time\ Period} \quad (2)$$

2.3.5. Adjustment of cutter bar height

As per the treatments, the cutter bar heights were set at 12, 16, and 20 cm from the ground in plots consisting of Standing, Lodged, and Standing Cum Lodged Crops. The data was recorded three times in each treatment [11].

2.3.6. Grain losses

The method of measurement of Grain Losses includes the collection of all the grains that were left when the machine operates to harvest in a specific area. Combine harvester operation on an area of 1 m^2 with three replications was selected to calculate the grain losses [12].

Grain losses were found by the following formula,

$$GL = 4047m^2 \times W_L \quad (3)$$

Where,
GL = grain losses
W_L = Weight of lost grains in 1m^2 area
1 acre = 4047 m^2

2.3.7. Damaged grain (%)

Three grains samples of weight 250 g from each treatment were collected. These samples were collected from the grain tank of the combine harvester and each sample was representative of 3 plots. To measure grain damage percentage weight of samples and the weight of broken grain were recorded separately as in previous research [13].
The grain damage percentage was recorded below,

$$GD = \frac{WD}{WS} \times 100 \quad (4)$$

Where,
GD - grain damage (%)
WD – the weight of damaged grain
WS – the weight of the sample

2.4. Statistical Analysis

The experimental data was statistically analyzed by using Randomized Complete Block Design (RCBD) within the "Statistix 8.1" software, applying a significance level of 5%.

3. RESULTS AND DISCUSSION

The performance of the Half-Feed Rice Combine Harvester was evaluated in terms of effective field capacity, field efficiency, grain losses in the field, and grain breakage at three forward speeds and three cutter bar heights. Results for various parameters concerning different treatments are discussed as follows.

3.1. Theoretical Field Capacity (TFC)

TFC of Half-Feed Rice Combine Harvester was measured in standing, standing cum lodged, and lodged crops during the wheat harvesting season of 2022. At speeds, S_1, S_2, and S_3, TFC was measured to be 0.64 ha/h, 0.84 ha/h, and 1.05 ha/h [13].

3.2. Effective Field Capacity (EFC)

In standing crop, statistical analysis has shown that maximum effective field capacity (0.55 ha/hr) was achieved at speed S_3 (5 km/h) and cutter bar height H_3 (20 cm), whereas the lowest field capacity

Table 2. Effect of different Forward Speeds with different Cutter Bar Heights on EFC in Standing Crop.

Speed	H_1	H_2	H_3	Mean
S_1	0.36 c	0.36 c	0.34 c	0.35 c
S_2	0.44 b	0.43 b	0.48 b	0.45 b
S_3	0.52 a	0.53 a	0.55 a	0.53 a
Mean	0.41 a	0.44 a	0.45 a	

*Mean with the same letters are statistically non-significant at a 5% level of probability.

(0.34 ha/hr) was achieved at speed S_1 (3 km/h) and cutter bar height H_3 (20 cm) as shown in Table 2. The statistical results have shown that the mean EFC at different speeds was significantly different while it was non-significantly different at different cutter bar heights at a 5% level of probability. The findings of the current experiment are parallel with the results of [14] who found that the EFC of a Half-Feed Rice Combine Harvester increases from 0.35 to 0.56 ha/hr as speed increases from 3km/h to 5 km/h respectively.

In standing cum lodged crop, statistical analysis showed that maximum EFC (0.52 ha/hr) was observed at speed S_3 (5 km/h) and cutter bar height H_2 (16 cm), and minimum EFC (0.30 ha/hr) was observed and speed S_1 (3 km/h) and cutter bar height H_2 (16 cm) respectively as shown in Table 3. The statistical results have shown that the mean EFC at different speeds was significantly different while it was non-significantly different at different cutter bar heights at a 5% level of probability. The findings of the current experiment are similar to the findings of [14] who suggested that the EFC of a Half-Feed Rice Combine Harvester increases from 0.35 ha/hr to 0.56 ha/hr with an increase in speed from 3 km/h to 5 km/h, respectively.

In lodged crop, statistical analysis has shown that maximum EFC (0.49 ha/hr) was observed at speed S_3 (5 km/h) and cutter bar height H_1 (12 cm) while minimum EFC (0.29 ha/hr) was observed at speed S_1 (3 km/h) and cutter bar height H_2 (16 cm) respectively. The statistical results have shown that the mean EFC at different speeds was significantly different while it was non-significant at different cutter bar heights. The findings of this experiment are more or less similar to the outcomes of [14] who found that the EFC of a Half-Feed Rice Combine Harvester increases from 0.35 ha/hr to 0.56 ha/hr with the increase in speed from 3 km/h to 5 km/h respectively.

Table 3. Effect of different Forward Speeds with different Cutter Bar Heights on EFC in Standing Cum Lodged Crop.

Speed	H_1	H_2	H_3	Mean
S_1	0.32 c	0.30 c	0.33 c	0.31 c
S_2	0.45 b	0.48 b	0.47 b	0.46 b
S_3	0.51 a	0.52 a	0.49 a	0.51 a
Mean	0.44 a	0.45 a	0.41 a	

*Mean with similar alphabets are non-significant statistically at a 5% level of probability.

Table 4. Effect of different Forward Speeds with different Cutter Bar Heights on EFC in Lodged Crop.

Speed	H_1	H_2	H_3	Mean
S_1	0.30 a	0.29 c	0.31 c	0.31 c
S_2	0.35 c	0.37 b	0.39 b	0.37 b
S_3	0.49 a	0.47 a	0.45 a	0.47 a
Mean	0.37 a	0.36 a	0.36 a	

*Similar letters with means are statistically non-significant at a probability level of 5%.

3.3. Field Efficiency

In standing crop, statistical results have shown that maximum field efficiency (75.3%) was observed at speed S_2 (4 km/h) and cutter bar height H_2 (16 cm) whereas the lowest field efficiency (67.6%) was observed at speed S_1 (3 km/h) and cutter bar height H_2 (16 cm) as shown in Table 4. The mean value of field efficiency was significantly different at different cutter bar heights while there was a non-significant difference at different speeds at a 5% level of probability. The findings of the current experiment are parallel with the findings of [15] who found that the Field Efficiency of a Half-Feed Rice Combine Harvester increases from 66% to 74% as speed increases from 3 km/h to 5 km/h, respectively.

Table 5. Effect of Different Forward Speeds with Different Cutter Bar Heights on Field Efficiency in Standing Crop.

Speed	H_1	H_2	H_3	Mean
S_1	70.7 b	67.6 b	71.6 b	69.2 a
S_2	74.3 a	75.3 a	73.8 a	74.2 a
S_3	71.5 ab	72.7 b	74.0 a	72.1 a
Mean	72.1 c	71.8 a	72.7 b	

Table 6. Effect of Different Forward Speeds with Different Cutter Bar Heights on Field Efficiency in Standing Cum Lodged Crop.

Speed	H_1	H_2	H_3	Mean
S_1	67.9 a	62.5 b	66.5 a	69.8 a
S_2	71.8 b	73.3 a	71.3 b	68.8 b
S_3	69.9 a	70.7 a	69.5 a	69.1 a
Mean	65.6 a	72.1 a	70.4 a	

In standing cum lodged crop, statistical results have shown that maximum field efficiency (73.3%) was achieved at speed S_2 (4 km/h) and cutter bar height H_2 (16 cm) whereas the lowest field efficiency (62.5%) was observed at speed S_1 (3 km/h) a cutter bar height H_2 (16 cm). The statistical analysis has shown that the mean value of field efficiency there was a non-significant difference for cutter bar height. The mean findings for field efficiency at different speeds are significantly different at (S_1 and S_2) and (S_2 and S_3) while they are non-significantly different at (S_1 and S_3). The findings of the current experiment are more or less similar to the results of [15] who suggested that the Field Efficiency of a Half-Feed Rice Combine Harvester, increases from 66% to 74% as speed increases from 3 km/h to 5 km/h, respectively.

In lodged crop, statistical results have shown that maximum field efficiency (67.1%) was achieved at speed S_3 (5 km/h) and cutter bar height H_1 (12 cm) whereas the lowest field efficiency (57.7%) was observed at speed S_1 (3 km/h) and cutter bar height H_2 (16 cm). The statistical analysis has shown that the mean-field efficiency was significantly different at different speeds; however, there was a non-significant difference at different cutter bar heights at a 5% level of probability. The results were similar to the findings of [15] who observed that the Field Efficiency of a Half-Feed Rice Combine Harvester increases from 66% to 74% as speed increases from 3 km/h to 5 km/h, respectively.

Table 7. Effect of Different Forward Speeds with Different Cutter Bar Heights on Field Efficiency in Lodged Crop.

Speed	H_1	H_2	H_3	Mean
S_1	61.8 b	57.7 b	59.1 b	59.5 b
S_2	64.8 c	64.2 c	66.3 a	62.9 c
S_3	67.1 a	66.6 a	66.3 a	66.9 a
Mean	69.5 a	65.1 a	66.6 a	

3.4. Grain Losses

In standing crop, maximum Grain Losses (42.5 kg/ha) occurred when the machine was operating at S_3 (5 km/h) and cutter bar height H_3 (20 cm), whereas the minimum grain losses (25.2 kg/ha) occurred at S_1 (3 km/h) and cutter bar height at H_2 (16 cm) as shown in Table 8.

The mean results for grain losses were significantly different at different speeds while they were non-significantly different for different cutter bar heights at a 5% level of probability. The findings of the current experiment are similar to the findings of a previous study [13] in which Grain Losses for Half-Feed Rice Combine Harvester increased from 25.5 kg/ha to 39.8 kg/ha with the increase in speed from 3 km/h to 5 km/h, respectively.

In standing cum lodged crop, maximum Grain Losses (45.4 kg/ha) occurred when the machine was operating at speed S_3 (5 km/h) and cutter bar height H_3 (20 cm) whereas the minimum Grain Losses (24.7 kg/ha) occurred at speed S_2 (4 km/h) and cutter bar height (H_2) as shown in Table 9. The mean Grain Losses of the machine were at significant differences at different speeds while there was a non-significant difference with respect to different cutter bar heights at a 5% level of probability. The findings of the current experiment are less or more similar to the results of [13] who found that Grain Losses for Half-Feed Rice Combine Harvester increased from 25.5kg/ha to 39.8kg/ha with the increase in speed from 3 km/h to 5 km/h, respectively.

In lodged crop, maximum Grain Losses (47.6 kg/ha) occurred when the machine was operating at S_3 (5 km/h) and cutter bar height H_3 (20 cm) whereas the minimum grain losses (27.9 kg/ha) occurred when the machine operates at speed S_2 (4 km/h) and cutter bar height H_2 (16 cm) as shown in Table 10. The mean results for Grain Losses

Table 8. Effect of different Forward Speeds with different Cutter Bar Heights on Grain Losses in Standing Crop.

Speed	H_1	H_2	H_3	Mean
S_1	29.5 b	25.2 b	26.4 c	31.1 b
S_2	25.3 c	23.7 c	33.3 b	26.7 c
S_3	38.3 a	31.2 a	42.5 a	34.1 a
Mean	27.1 b	27.4 b	37.3 a	

Table 9. Effect of different Forward Speeds with different Cutter Bar Heights on Grain Losses in Standing Cum Lodged Crop.

Speed	H_1	H_2	H_3	Mean
S_1	31.4 b	27.2 b	29.0 b	32.9 b
S_2	28.2 c	24.7 c	35.5 c	28.5 c
S_3	39.1 a	33.5 a	45.4 a	36.6 a
Mean	29.2 b	29.5 b	39.3 b	

of the machine were at a significant difference at different speeds while there was a non-significant difference with respect to different cutter bar heights at a 5% level of probability. The findings of the current experiment are parallel to the outcomes of Bawatharani *et al*. [13] in that Grain Losses for Half-Feed Rice Combine Harvester increased from 25.5kg/ha to 39.8kg/ha with an increase in speed from 3 km/h to 5 km/h, respectively.

3.5. Grain Breakage

In standing crop, maximum Grain Breakage (16.3 kg/ha) was observed at speed S_3 (5 km/h) and cutter bar height H_3 (20 cm) whereas the minimum grain breakage (14.2 kg/ha) was found at speed S_2 (4 km/h) and cutter bar height H_2 (16 cm) as shown in Table 11. The mean results of Grain Breakage were at a significant difference at speeds S_1 and S_3 and S_2 and S_3 while there was a non-significant difference at S_1 and S_2. The mean results for Grain Breakage with respect to cuter bar height were non-significantly different at a 5% level of probability. The findings of the current experiment are alike to the conclusions of Da *et al*. [16] who revealed that grain breakage for the machine increased from 13.1 kg/ha to 17.8 kg/ha as the speed increased from 4 km/h to 5 km/h, respectively.

In standing cum lodged crop, maximum grain breakage (16.1 kg/ha) occurred at speed S_3 (5 km/h) and cutter bar height H_3 (20 cm), whereas

Table 10. Effect of different Forward Speeds with different Cutter Bar Heights on Grain Losses in Lodged Crop.

Speed	H_1	H_2	H_3	Mean
S_1	35.1 b	30.2 b	32.1 b	36.7 b
S_2	32.2 c	27.9 c	38.9 c	31.7 c
S_3	43.2 a	37.1 a	47.6 a	39.5 a
Mean	32.4 b	32.9 b	42.6 b	

Table 11. Effect of different Forward Speeds with different Cutter Bar Heights on Grain Breakage in Standing Crop.

Speed	H_1	H_2	H_3	Mean
S_1	14.5 b	14.4 b	14.5 b	14.9 b
S_2	14.5 b	14.2 b	15.2 b	14.5 b
S_3	15.6 a	14.9 b	16.3 a	15.3 a
Mean	14.5 b	14.7 b	15.6 b	

the minimum grain breakage (14.3 kg/ha) was observed at speed S_2 (4 km/h) and cutter bar height H_2 (16 cm) as shown in Table 12. The mean results for Grain Breakage were at a significant difference at different speeds while there was a non-significant difference with respect to different cutter bar heights at a 5% level of probability. The findings of the current experiment are parallel with the findings of Da *et al*. [16] who observed that Grain Breakage for a Half-Feed Rice Combine Harvester increased from 13.1 kg/ha to 17.8 kg/ha as the speed increased from 4 km/h to 5 km/h, respectively.

In lodged crop, maximum Grain Breakage (16.5 kg/ha) was observed at speed S_3 (5 km/h) and cutter bar height H_3 (20 cm), whereas the minimum grain breakage (14.6 kg/ha) occurred at speed S_2 (4 km/h) and cutter bar height H_2 (16 cm) as shown in Table 13.

The mean results for Grain Breakage were at a significant difference at speed S_1 and S_2 or S_2 and S_3 while there was a non-significant difference at

Table 12. Effect of different Forward Speeds with different Cutter Bar Heights on Grain Breakage in Standing Cum Lodged Crop.

Speed	H_1	H_2	H_3	Mean
S_1	15.1 c	14.6 b	14.6 b	15.1 c
S_2	14.7 b	14.3 b	15.1 b	14.7 b
S_3	15.6 a	15.1 b	16.1 a	15.3 a
Mean	14.8 b	14.7 b	15.6 b	

Table 13. Effect of different Forward Speeds with different Cutter Bar Heights on Grain Breakage in Lodged Crop.

Speed	H_1	H_2	H_3	Mean
S_1	15.2 ab	14.8 a	15.1 b	15.3 a
S_2	15.1 b	14.6 a	15.2 b	14.9 b
S_3	15.7 a	15.2 a	16.5 a	15.6 a
Mean	15.1 b	14.9 b	15.8 a	

S_1 and S_3 at a 5% level of probability. The mean results for Grain Breakage were non-significantly different with respect to cutter bar heights at a 5% level of probability. The results of the current experiment are similar to the results of Da *et al.* [16] in which Grain Breakage for Half-Feed Rice Combine Harvester increased from 13.1 kg/ha to 17.8 kg/ha as the speed increased from 4 km/h to 5 km/h, respectively.

4. CONCLUSIONS

For Standing Crops, the maximum values for EFC and Field Efficiency were calculated as 0.55 ha/h and 75.3% at (S_2 and H_2), respectively. The minimum grain losses were observed as 24.7 kg/ha at (S_1 and H_2) and minimum grain breakage was recorded 14.2 kg/ha at (S_2 and H_2) respectively. For Standing Cum Lodged Crop, the maximum values for EFC and Field Efficiency were measured as 0.52 ha/h at (S_3 and H_2), 73.3% at (S_2 and H_2), respectively. The minimum grain losses were recorded as 25.2 kg/ha per hectare at (S_2 and H_2) and minimum grain breakage was observed 14.6 kg/ha at (S_2 and H_2) respectively. For Lodged Crop, the maximum values for EFC and Field Efficiency were found to be 0.49 ha/h at (S_3 and H_1) and 67.1% at (S_2 and H_2), respectively. The minimum grain losses were calculated as 27.9 kg/ha at (S_3 and H_3) and minimum grain breakage was measured as 14.6 kg/ha at (S_2 and H_2). Experimental results have shown that comparatively better performance was observed at forward speed (S_2 = 4 kmh^{-1}) and cutter bar height (H_2 = 16 cm) with maximum efficiency and minimum losses.

Overall machine worked better at speed S_2 (4 km/h) as compared to speed S_1 (3 km/h) and speed S_3 (5 km/h) (Figure 1), and crop with standing condition as considering field efficiency (%), grain losses (kg/ha) and grain breakage (kg/ha) as key performance indicators.

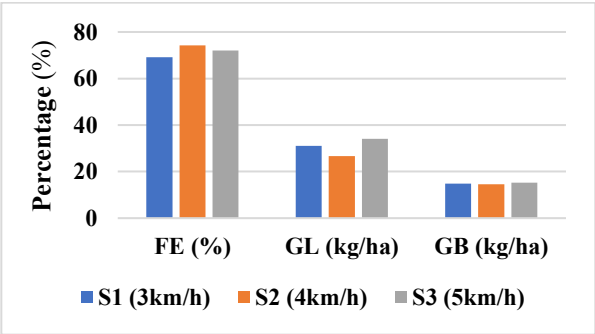

Fig. 1. Abstract Graph of Machine Performance Indicators.

5. FUTURE RECOMMENDATIONS

The performance of this machine can be tested for various rice varieties in different rice growing zones. This machine can also be tested for different soil types and various farm sizes. A knotting unit may be attached at the straw outlet for collecting them in bundles.

6. CONFLICT OF INTEREST

The authors declare no conflict of interest.

7. REFERENCES

1. J. Myszkowska-Ryciak, A.Je. Ishdorj, M. Zewska-Zychowicz, N.A. Mohidem, N. Hashim, R. Shamsudin, and H.C. Man. Rice for Food Security: Revisiting Its Production, Diversity, Rice Milling Process, and Nutrient Content. *Agriculture* 12(6):741 (2022).
2. E. Elahi, Z. Khalid, and Z. Zhang. Understanding Farmers' Intention and Willingness to Install Renewable Energy Technology: A Solution to Reduce The Environmental Emissions of Agriculture. *Applied Energy* 309: 118459 (2022).
3. J.P. Sahoo, A.P. Mishra, and K.C. Samal. The Magical Low Glycaemic Index Rice Staple Truly For Diabetic People. *Agriculture Letters* II(6): 37 (2021).
4. R. Bhatt, P. Singh, A. Hossain, and J. Timsina. Rice-Wheat System in The Northwest Indo-Gangetic Plains of South Asia: Issues and Technological Interventions for Increasing Productivity and Sustainability. *Paddy and Water Environment,* 19(3): 345–365 (2021).
5. D.A. Zuniga-Vazquez, N. Fan, T. Teegerstrom, C. Seavert, H.M. Summers, E. Sproul, and J.C. Quinn. Optimal Production Planning and Machinery Scheduling for Semi-Arid Farms. *Computers and Electronics in Agriculture* 187: 106288 (2020).
6. M. Schmitt-Harsh, K. Waldman, L. Estes, and T. Evans. Understanding Social And Environmental Determinants of Piecework Labor in Smallholder Agricultural Systems. *Applied Geography* 121: 102243 (2020).
7. H. Rahaman, M.M. Rahman, A.K.M.S. Islam, M.D. Huda, and M. Kamruzzaman. Mechanical Rice Transplanting in Bangladesh: Current Situation, Technical Challenges, and Future Approach. *Journal of Biosystems Engineering* 47(4): 417–27 (2022).
8. J. Kershaw, R. Yu, Y.M. Zhang, and P. Wang. Hybrid Machine Learning-Enabled Adaptive Welding Speed Control. *Journal of Manufacturing Processes*

71: 374–383 (2021).
9. R.G. Trevisan. Advanced data analysis methods to optimize crop management decisions. Ph.D. Thesis. *University of Illinois Urbana-Champaign, Urbana, Illinois, USA* (2021).
10. V. Dwivedi, N. Parashar, and B. Srinivasan. Distributed Learning Machines for Solving Forward and Inverse Problems in Partial Differential Equations. *Neurocomputing* 420: 299–316 (2021).
11. R.K. Chaab, S.H. Karparvarfard, H. Rahmanian-Koushkaki, A. Mortezaei, and M. Mohammadi. Predicting Header Wheat Loss in a Combine Harvester, A New Approach. *Journal of the Saudi Society of Agricultural Sciences* 19(2): 179–184 (2020).
12. D. Savickas, D. Steponavičius, L. Špokas, L. Saldukaitė, and M. Semenišin. Impact of Combine Harvester Technological Operations on Global Warming Potential. *Applied Sciences* 11(18): 62-86 (2021).
13. R. Bawatharani, M.H. Bandara, and D.I.E. Senevirathne. Influence of Cutting Height and Forward Speed on Header Losses in Rice Harvesting. *International Journal of Agriculture* 4(2): 1-9 (2016).
14. M.K. Hasan, M.R. Ali, C.K. Saha, M.M. Alam, and M.E. Haque. Combine Harvester: Impact on Paddy Production in Bangladesh. *Journal of the Bangladesh Agricultural University* 17(4): 583–591 (2019).
15. S. Elsoragaby, A. Yahya, M.R. Mahadi, N.M. Nawi, and M. Mairghany. Comparative Field Performances Between a Conventional Combine and Mid-size Combine in Wetland Rice Cultivation. *Heliyon* 5(4): 14-27. (2019).
16. Q. Da, D. Li, X. Zhang, W. Guo, D. He, Y. Huang, and G. He. Research on Performance Evaluation Method of Rice Thresher Based on Neural Network. *Actuators* 11(9): 257 (2022).

Proceedings of the Pakistan Academy of Sciences: A Physical and Computational Sciences 61(1): 89-97 (2024)

ISSN (Print): 2518-4245; ISSN (Online): 2518-4253
https://doi.org/10.53560/PPASA(61-1)828

Pakistan Academy of Sciences

Research Article

Design of Advanced Controllers for Speed Control of DC Motor

Arshad Habib Malik[1*], Feroza Arshad[2], and Aftab Ahmad Memon[3]

[1]Faculty of Engineering, Information and Technology,
Sindh Institute of Management and Technology, Karachi, Pakistan
[2]Department of Information System Division, Karachi Nuclear Power Generating Station,
Pakistan Atomic Energy Commission, Karachi, Pakistan
[3]Faculty of Electrical, Electronic and Computer Engineering,
Mehran University of Engineering and Technology, Jamshoro, Sindh, Pakistan

Abstract: In this research work, an open loop experimental DC motor from National Instruments is investigated for speed control applications in nuclear industry with higher accuracy. For performance analysis, the DC motor is mathematically modeled and advanced control techniques are established. The two design approaches are therefore hardware in loop which is experimental facility and mathematical in nature which is a simulation model. An adequate mathematical model of DC motor is developed using first principle. The hardware realization is accomplished by DC motor experimental setup. Different advanced control algorithms such as PID, SMC and MPC are developed for both models based and hardware-based DC motor research studies. Model development, control synthesis, simulation and analysis are carried out in Simulink and LabVIEW programming environments. Closed loop performance analyses of nonlinear and predictive controllers are evaluated and found much better, smoother and robust than linear controller for speed control of DC motor under different conditions.

Keywords: DC Motor, Speed Control, Linear Control, Nonlinear Control, Predictive Control.

1. INTRODUCTION

The separately excited DC motors is an electrical machine used for wide range of variable speed control drives in industry and power plants. DC motors are widely used in robotics, control and automation industry for high precision position and speed control drives. Therefore, it is desired to investigate the DC motor drive, conduct speed control experiments and device conventional and advanced control schemes. The linear control systems are generally not so accurate and has poor performance against parametric changes and load changes. Therefore, in order to have the improved performance and better robustness, new control schemes are required to introduce. A detailed literature review is conducted to identify the various modeling techniques with different configuration of DC motor. This survey suggests hardware and model-based approaches for DC motor. Different linear, nonlinear, predictive, optimal and robust controllers are studied for either DC motor or similar electrical or other processes. The nonlinear modeling and system identification-based modeling aspects of the DC motor are discussed by Kara and Eker [1]. A DC motor is modeled and simulated using MATLAB script called in LabVIEW environment is evaluated by Patrascoiu [2]. A model based Proportional Integral Derivative (PID) controller is designed for DC motor in LabVIEW by Kumar *et al.* [3]. This study suggests conventional linear controller design methodology for DC motor. Hardware in loop PID controller is attempted for DC motor in LabVIEW by Pradeepa *et al.* [4]. This study is hardware realization of PID control for DC motor. A Linear Quadratic Regulator (LQR) controller is addressed for DC motor by Saiudha *et al.* [5] which is an optimal control design approach. Hardware based Model Predictive Controller (MPC) is synthesized for QNET VTOL takeoff and landing control by Anoop and Sharma [6]. This is similar National Instruments QNET

Received: July 2023; Revised: February 2024; Accepted: March 2024
*Corresponding Author: Arshad Habib Malik <engr.dr.arshad.habib.malik@gmail.com>

hardware but for different application. A detailed performance comparison is analyzed for DC motor using PID, LQR and MPC by Dani *et al.* [7]. This uses a mix linear, state feedback and predictive controllers for DC motor. Speed control of DC series wound motor is conducted using nonlinear Fuzzy Logic Control (FLC) by Ismail *et al.* [8]. This study is basically an intelligent control scheme for a different configuration of DC series motor. A FLC based PID controller is adopted for DC motor by Bansal *et al.* [9]. This is fuzzy logic based nonlinear tuning of PID controller parameters for DC motor. A model based PID controller and nine rules based FLC are designed and compared for separately excited DC motor by Kushwah *et al.* [10] in MATLAB. This study suggests the performance comparison of intelligent and linear controllers for DC motor. Another complex forty-nine rules based Mamdani type FLC is designed for separately excited DC motor by Usoro *et al.* [11]. This FLC design is more robust and complicated as compared to previous one. Another attempt was made for DC motor speed control using predictive MPC and nonlinear FLC by Jibril *et al.* [12] which provides comparison of predictive and fuzzy control techniques. A comparative study was carried out for separately excited DC motor using PID and Artificial Neural Network (ANN) controllers by Hashmia and Dakheel [13] which is a data drive controller design approach. A second order nonlinear Sliding Mode Controller (SMC) is synthesized for DC motor by Huspeka [14]. An investigation is performed for separately excited DC motor using PID and SMC controller by Hashim and Ahmed [15] in MATLAB. Another similar investigation was performed for separately excited DC motor using PID and SMC controller by Jalalu *et al.* [16] in LabVIEW. In these studies, linear and nonlinear controller design schemes are tested in two different simulation platforms. Research is further expanded for the study of hardware in loop PID and SMC controllers design for DC motor by Dumanay *et al.* [17] in LabVIEW. In this study linear and nonlinear controller are configured on hardware. Sliding mode controller is designed for DC motor and controller gains are optimized using Ant Colony algorithm by Jammousi *et al.* [18]. A model predictive control with mini-max scheme is attempted for bioprocess Ant Colony algorithm by Benattia *et al.* [19].

In this research work, two new advanced controllers are attempted to address poor disturbance rejection problem, poor performance of linear controller under parametric and load changes. Sliding mode and predictive control design schemes are adopted. These schemes are configured in two different ways; one closed loop development using hardware in loop while second closed loop development using two distinct simulation platforms. In the present manuscript we present hardware of DC motor drive, mathematical modeling of DC motor, structure of controllers, problem formulation of various controllers, graphical representation of experimental and simulated results and key investigations are discussed in detail.

2. MATERIALS AND METHODS

2.1. Electrical Machine

The electrical machine under consideration in this research work is a separately excited DC motor which is acquired from National Instruments as shown in Figure 1. DC motor design parameters are motor electrical resistance, motor torque constant and moment of inertia. These parameters are estimated using applied voltage of motor, current the motor armature, speed of motor shaft, motor terminal resistance and motor torque constant using tachometer and current sensor. The linear controller design is accomplished by imposing constraints on

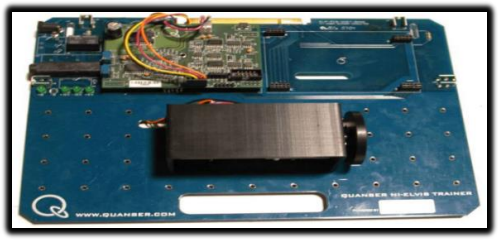

Fig. 1. National Instruments Electrical Machine (DC Motor) Experimental Setup.

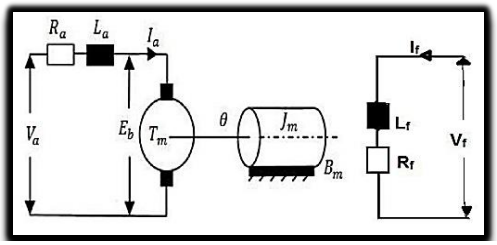

Fig. 2. Schematic Diagram of DC Motor.

the closed loop performance in terms of maximum rise time, overshoot, settling time and steady state error.

2.2. Electrical Machine Modeling

The separately excited DC motor is an electro-mechanical system as shown in Figure 2.

Various parameters/symbols and variables used hereafter in the process of DC motor modeling and controllers are defined in Table 1.

The dynamics of armature current is computed as [7]:

$$\frac{dI_a(t)}{dt} = -\frac{R_a}{L_a} I_a(t) - \frac{K_B}{L_a}\omega(t)\frac{1}{L_a}V_a \qquad (1)$$

The speed of dc motor is computed as [7]:

$$\frac{d\omega(t)}{dt} = -\frac{K_t}{J_m} I_a(t) - \frac{B_m}{J_m}\omega(t) \qquad (2)$$

Table 1. Symbols/parameters of model and controllers.

Parameters	Definitions
V_a	Armature Voltage
E_b	Back emf of Motor
I_a	Armature Current
R_a	Armature Resistance
L_a	Armature Inductance
T_m	Mechanical Torque
J_m	Moment of Inertia
B_m	Friction Coefficient of Motor
ω	Speed of Motor
ω_{ref}	Reference Speed of Motor
K_B	Motor Back emp Constant
K_t	Motor Current Torque Constant
S	Sliding Surface
K_p	Proportional Gain
K_I	Integral Gain = K_p / T_I
a_o	Constant associated with Integral of $e_1$error
a_1	Constant associated with $e_1$error
K	Nonlinear Controller Gain
u(t)	Control Input Signal
PID	Proportional Integral Derivative
SMC	Sliding Mode Control
MPC	Model Predictive Control

Now, equations (1) and (2) are linearized and transformed into standard state-space form as:

$$\frac{dx(t)}{dt} = Ax(t) + Bu(t) \qquad (3)$$

$$y(t) = Cx(t) + Du(t) \qquad (4)$$

2.3. State, Input and Output Vectors

The state vector of state space model of DC motor is given as:

$$x(t) = \begin{bmatrix} \omega(t) & \frac{d\omega(t)}{dt} \end{bmatrix}^T \qquad (5)$$

The input and output variables are defined as:

$$u(t) = V_a(t) \qquad (6)$$

$$y(t) = \omega(t) \qquad (7)$$

2.4. Linear Controller Modeling

The formulation of linear controller is discussed in this section. The linear controller used in the current research work is a Proportional Integral Derivative (PID) controller. This controller configured for DC motor is basically PI controller that can be modeled as [3]:

$$u_{PID}(t) = K_P e(t) + K_I \int e(t)dt \qquad (8)$$

2.5. Nonlinear Controller Modeling

Now, the formulation of nonlinear controller is discussed here. The nonlinear controller used in this research work is a Sliding Mode Controller (SMC). This controller configured for DC motor is basically State Feedback Nonlinear Controller. The error dynamics are defined in equations (9) and (10) while sliding mode surface for the system described in equation (5) is defined in equation (11) and its time domain response is plotted in subsequent section 3.1.

$$e_1(t) = x_1(t) - \omega_{ref} \qquad (9)$$

$$e_2(t) = x_2(t) - \frac{d\omega_{ref}}{dt} \qquad (10)$$

$$s = a_o \int e_1(t)dt + a_1 e_1(t) + e_2(t) \qquad (11)$$

Using the Nonlinear Lyapunov Stability Criteria [17]:

$$s\dot{s} < 0 \qquad (12)$$

The asymptotic stability is guaranteed at the initial state in order to achieve the reachability of the switching plane. A sufficient condition to reach a switching plane is given by Lyapunov function, whose evaluation allows to check the asymptotic stability.

The SMC control law is derived using Lyapunov stability condition mentioned in equation (12) using equation (11) and computed in two parts, one is u_{equ} for speed control and u_{swh} for direction control. The chattering problem is compensated through switching control having a small scaling parameter eta (η) known as tuning parameter. The derived and designed controller model is shown in Figure 4 in the subsequent section. The ultimate control law is given as [17]:

$$u_{SMC}(t) = [f_1(x_1(t) + f_2(x_2(t) - g_1(e_1(t)) - g_2(e_2(t)) - g_3(r)] - h(s,\eta) \quad (13)$$

2.6. Predictive Controller Modeling

In the present section, the formulation of predictive controller is discussed. The predictive controller used in this research work is a Model Predictive Controller (MPC). This controller configured for DC motor is basically nominal MPC, MPC with switching model and Min-Max MPC. Nominal MPC is implemented with fixed model of DC motor. MPC with switching model is implemented with controller that switches between the models according to the DC motor speed.

The Min-Max MPC is implemented using a control input sequence that minimizes cost function with a vector of uncertain parameters in the following form [19]:

$$\hat{u}_k^{k+N_p-1} = \arg\begin{pmatrix}\min \\ u(k)\end{pmatrix}\begin{pmatrix}\max \\ \delta\theta\end{pmatrix} \Pi(x_k, u_k^{k+N_p-1}, \delta\theta) \quad (14)$$

Where, $\hat{u}_k^{k+N_p-1}$ is determined to minimize the output and control tracking errors by considering all trajectories over all possible data scenarios while *Np* is the length of the prediction horizon at the *k*-th sample interval. The cost function is composed of the control input signal (u) with mini-norm and a vector of uncertain parameters (θ) with max-norm determined by nominal parameters vector (θ_{nom}) additive with parameter uncertainties vector ($\delta\theta$) in the prediction domain.

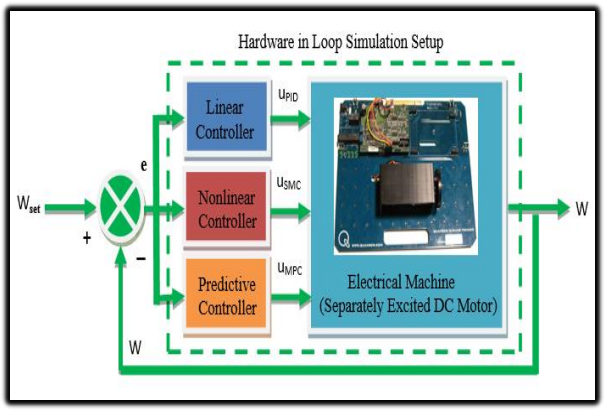

Fig. 3. Block Diagram of DC Motor Speed Control System.

3. RESULTS AND DISCUSSION

The controllers' design, simulation and analysis of DC motor are performed in closed loop framework as shown in Figure 3.

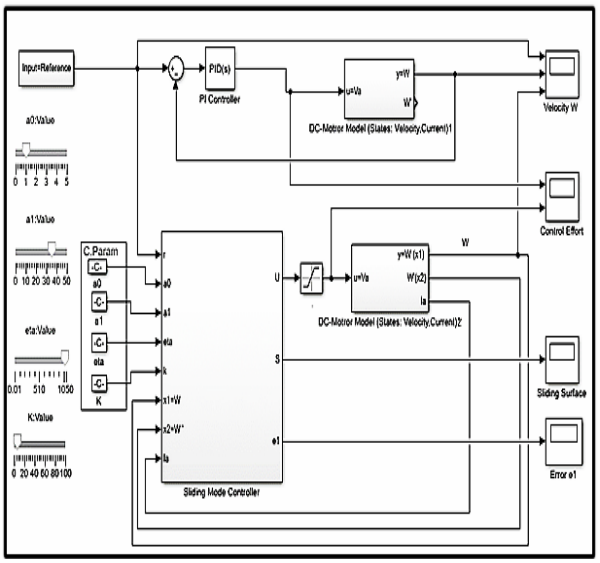

Fig. 4. Simulation Model of Linear and Nonlinear Control of DC motor in Simulink.

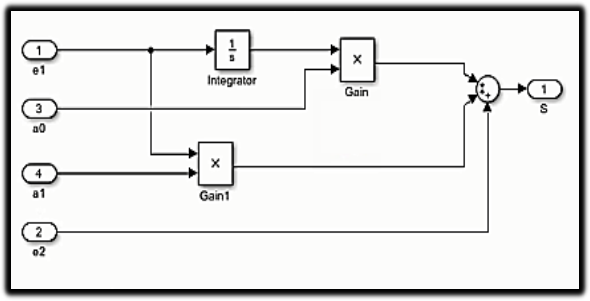

Fig. 5. Simulation Model of Sliding Surface of Nonlinear Controller.

3.1. Performance Analysis of Model based Linear and Nonlinear Electrical Machine Speed Control System in MATLAB Simulink

The PI and SMC controllers modeled in equations (8), (11) and (13) are configured with state space models developed in equations (3) and (4) and programmed in MATLAB Simulink environment as shown in Figures 4 and 5. The control strategy addressed in this research work is designed for the reference tracking mode. Figure 4 shows the design simulation model for tuning of linear and nonlinear controllers and graphical simulations. Figure 5 shows the simulation design model of sliding surface for nonlinear sliding mode controller. The behaviour of the controllers is discussed in Figures 6, 7, 8, 9 and 10.

The response of PI controller in reference tracking mode is shown in Figure 6. The response is fast but it generates a small overshoot in the speed against step reference change. However, the system is stable and no steady state error is observed.

The plot of sliding surface design of nonlinear SMC controller is shown in Figure 7. The response of the sliding surface is quite faster. It minimizes the error dynamics smartly.

The response of nonlinear controller in reference tracking mode is shown in Figure 8. It generates no overshoot in the speed against the step reference change. The closed loop system settles down in around 0.15 second. The system dynamics is quite fast and a very stable output is reached which shows smooth control with SMC.

The closed loop comparison of PI and SMC controllers without parametric variation is shown in Figure 9. The comparison proves that nonlinear controller behavior is better than with linear

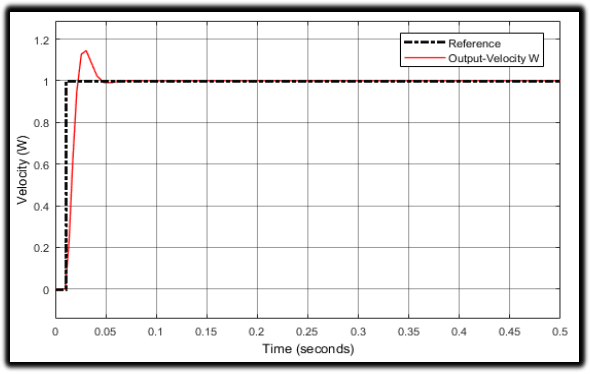

Fig. 6. Reference Tracking Response of DC Motor with Linear Controller

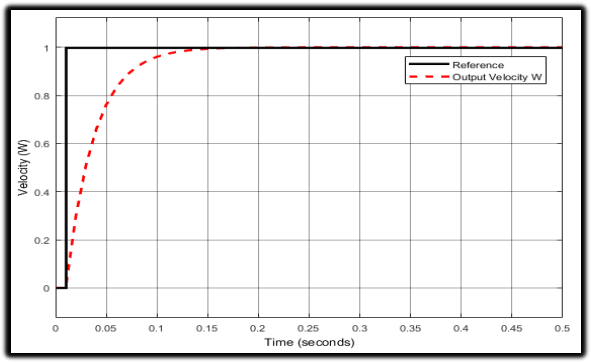

Fig. 8. Reference Tracking Response of DC Motor with Nonlinear Controller.

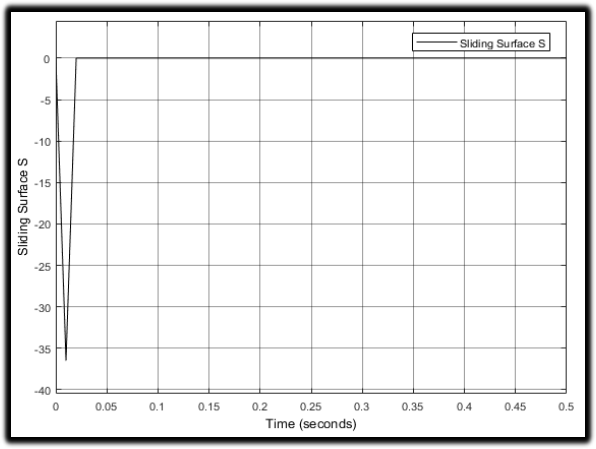

Fig. 7. Response of Sliding Surface of Nonlinear Controller.

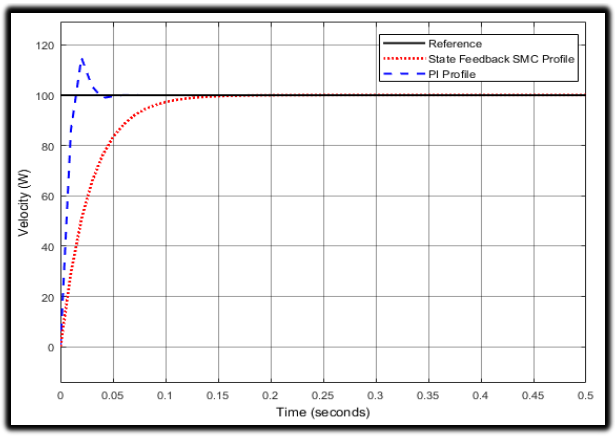

Fig. 9. Closed Loop Simulation of Linear and Nonlinear Control Systems without Parametric Variations.

PID controller. The analysis without parametric variation is basically the closed loop system which is assessed with PI controller and SMC controller with fixed model parameters and there is no role variable structure at all. Such model structure is easier for controllers to handle with.

In this design study, the sliding mode controller is then designed based on variable structure modeling technique using parametric change. This framework is embedded in simulation model as shown Figure 4 and its closed loop performance comparison is graphical represented in Figure 10.

The comparison shows that with parametric change, the PI controller response becomes more oscillatory and takes more time to settle. Therefore, it is obvious that PI controller fails to deal with parametric variation because the controller is not adaptive in nature whereas designed state feedback SMC is insensitive to parametric variations because the controller is nonlinear in nature.

The closed loop gain margin of DC motor speed control system using sliding mode controller is 2 which proves the guaranteed sufficient robustness of the system with remarkable closed loop performance under parametric variations.

3.2. Performance Analysis of Hardware based Linear and Nonlinear Electrical Machine Speed Control System in LabVIEW

The parametric values used in the experimental work are $R_a = 8.7\ \Omega$, $K_t = 0.0334$ N-m, $K_p = 0.0334$ V/(rad/sec), $J_m = 1.8 \times 10^{-6}$ Kg-m^2, $B_m = 1 \times 10^{-5}$ and $L_a = 8.3 \times 10^{-3}$ H.

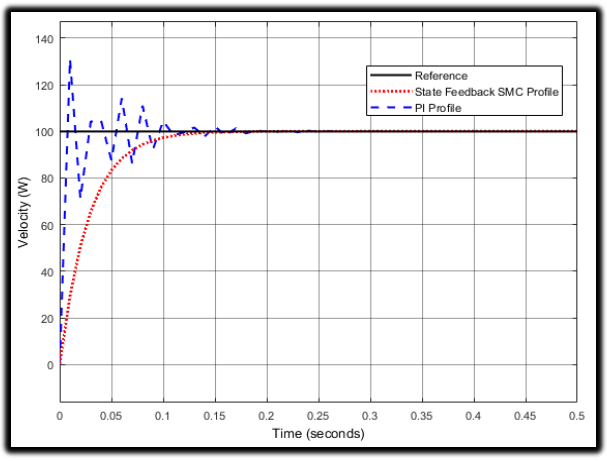

Fig. 10. Closed Loop Simulation of Linear and Nonlinear Control Systems with Parametric Variations.

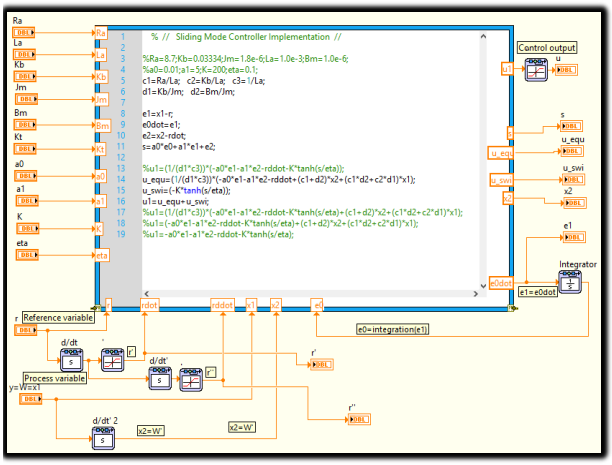

Fig. 12. Simulation Model of Mathscript based Nonlinear Controller in LabVIEW.

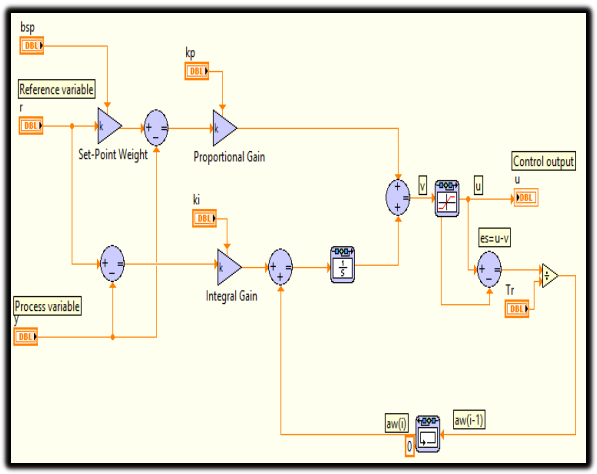

Fig. 11. Simulation Model of Linear Controller in LabVIEW.

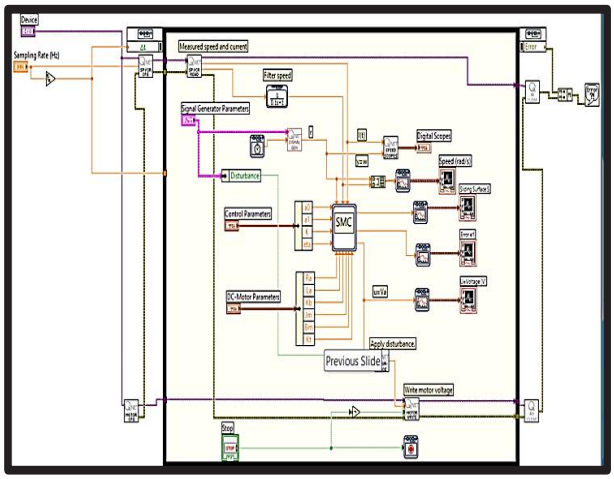

Fig. 13. Hardware in Loop Simulation Model of Linear and Nonlinear Control System in LabVIEW.

The PI and MPC controllers modeled in equations (8), (11) and (13) are configured in hardware in loop framework experimentally and programmed in LabVIEW environment as shown in Figures 11, 12 and 13.

The measured speed of DC motor with linear PID controller experimentally is shown in Figure 14. A sequence of periodic reference behavior is designed and implemented as reference signal and the closed loop system tracks it but with fluctuating dynamics.

The NI instrument-based DC motor speed is measured using nonlinear sliding mode controller as shown in Figure 15. The response reveals that there is very small overshoot with excellent tracking feature, which proves the robust performance of sliding mode controller. The dynamic behavior is much smoother with SMC controller.

It is evident from Figures 14 and 15 that when the linear and nonlinear controllers are implemented on DC motor then its response improves greatly with nonlinear controller and sharp oscillations also decreases.

The measured speed of DC motor is obtained experimentally with linear controller under load disturbance is shown in Figure 16. The fast small fluctuations are the measured values while the sudden dip followed by up spikes are due to motor load torque variations.

The measured speed of DC motor is obtained experimentally with nonlinear sliding mode controller by varying motor load torque as load disturbance. The dynamic response is shown in Figure 17. The sudden fall in motor speed shows the rise in motor load torque.

It is evident from Figure 16 and 17 that when the linear and nonlinear controllers are implemented on DC motor with load disturbances then DC motor speed recovers the desired trajectory quickly. The response with linear PID controller has sharp large overshoots and undershoots while the response with nonlinear sliding mode controller reduces the overshoots and undershoots greatly. Therefore, the state feedback SMC is superior to PI controller in rejecting the external disturbance.

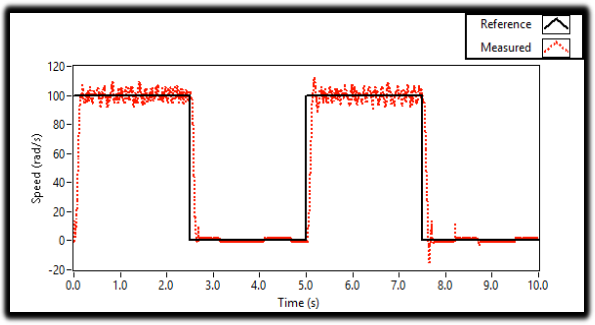

Fig. 14. DC Motor Response with Linear Controller from Hardware.

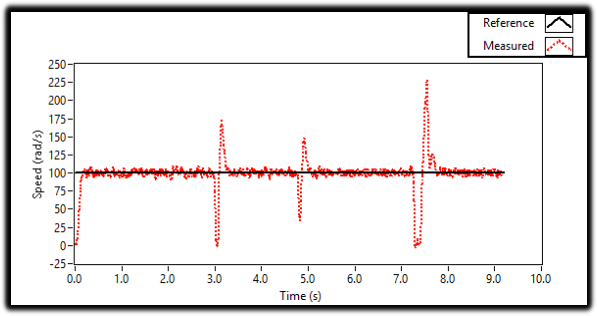

Fig. 16. DC Motor Response with Linear Controller under Disturbance.

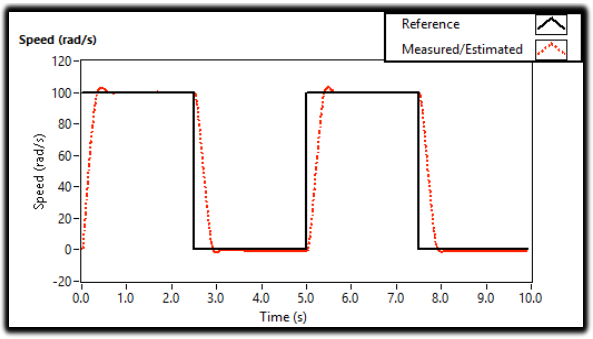

Fig. 15. DC Motor Response with Nonlinear Controller from Hardware.

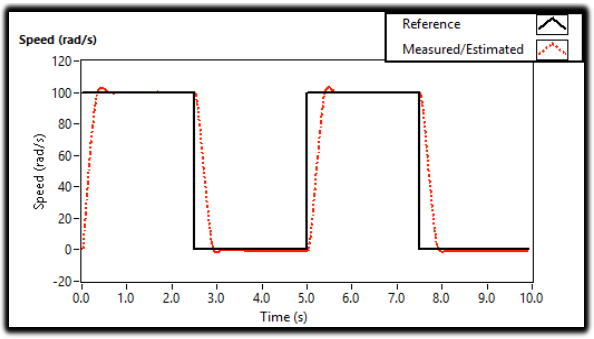

Fig. 17. DC Motor Response with Nonlinear Controller under Disturbance.

3.3. Performance Analysis of Hardware based Linear and Predictive Electrical Machine Speed Control System in LabVIEW

The PI and SMC controllers modeled in equations (8) and (14) are configured in hardware in loop framework experimentally and programmed in LabVIEW environment as shown in Figures 18.

The comparison of predictive behaviors amongst different MPC schemes is shown in Figure 19.

It is evident from Figure 19 that when the MPC with different schemes are implemented on DC motor and tested for reference tracking mode then it is found that MPC with switching model is best in dynamic behavior while the nominal MPC swings around the operating point within a very small steady state error band. Both mini-max MPC and MPC with switching model settles bit quickly in around 1 sec time.

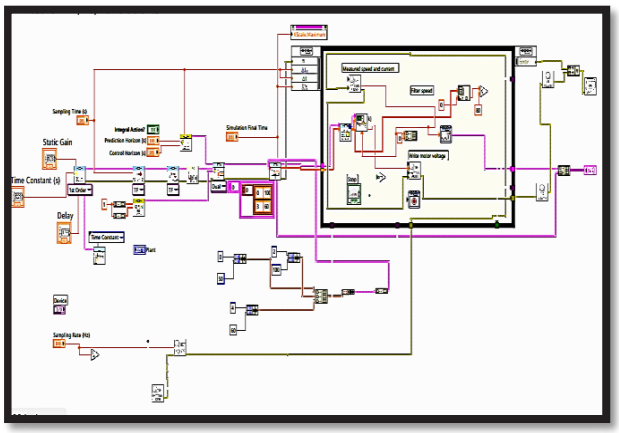

Fig. 18. Simulation Model of Predictive Control System in LabVIEW.

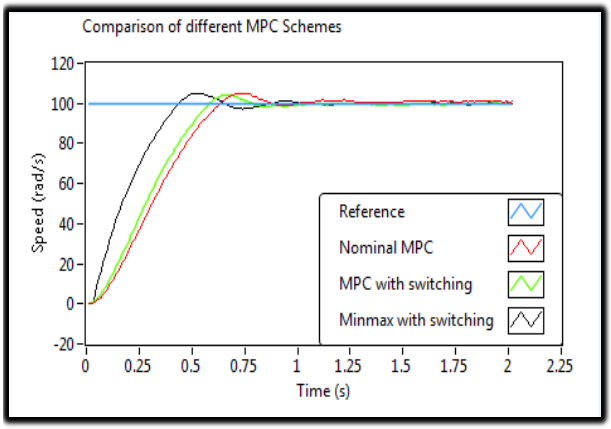

Fig. 19. DC Motor Response with Various Models Predictive Controllers.

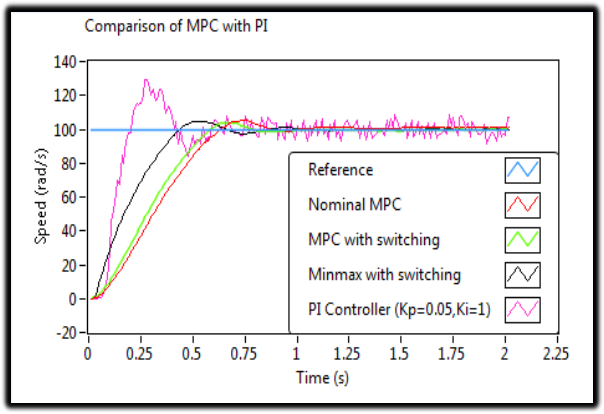

Fig. 20. DC Motor Response with Linear and Various Models Predictive Controllers.

The performance comparison of speed control of DC motor with of PI controller and MPC controller is shown in Figure 20. The comparison shows that the PI controller response becomes fluctuating and more ripples even appear on steady state around the operating point. Therefore, it is obvious that MPC with different schemes are observed with much better performance due to weighted moving average structure.

4. CONCLUSIONS

The separately excited DC motor is formulated in state space form and model parameters are adjusted and fine-tuned in accordance with National Instruments' experimental facility. Simulation experiments are performed to prove the effectiveness of most advanced control design schemes for speed control of DC motor. The designed state feedback SMC has much better performance as compared to PI controller with minimum overshoot and rise time. State feedback SMC is superior in performance as compared to PI controller in rejecting the external disturbances. PI controller fail to deal with parametric variation whereas the designed state feedback SMC is insensitive to parametric variations. MPC with switching scheme is found the best amongst all MPC schemes when compared with PI controller for DC motor. Experimental and simulation experiments proves that successful realization has been achieved for DC motor.

5. ACKNOWLEDGEMENTS

The support of the Mehran University of Engineering and Technology, Sindh Institute of Management and

Technology, Information Support Division of KNPGS is gratefully acknowledged.

6. CONFLICT OF INTEREST

The authors declare no conflict of interest.

7. REFERENCES

1. T. Kara, and I. Eker. Nonlinear Modeling and Identification of a DC Motor for Bidirectional Operation with Real Time Experiments. *Energy Conversion and Management* 45: 1087-1106 (2004).
2. N. Patrascoiu. Modeling and Simulation of the DC Motor using Matlab and LabVIEW. *International Journal of Engineering* 21(1): 49-54 (2005).
3. D. Kumar, M. Hussain, S.V. Tyagi, R. Gupta, and Salim. LabVIEW based Speed Control of DC Motor using PID Controller. *International Journal of Electrical and Electronics Research* 3(2): 293-298 (2015).
4. G. Pradeepa, N.T. Elakkya, J. Jayashree, and S. Madhumitha. Speed Control of DC Motor using LabVIEW. *International Journal of Latest Technology in Engineering, Management and Applied Science* 8(4): 110-113 (2019).
5. V. Saisudha, G. Seeja, R.V. Pillay, and G. Manikutty. Analysis of Speed Control of DC Motor using LQR Method. *International Journal of Circuit Theory and Applications* 9(1): 77-85 (2016).
6. S.K. Anoop, and K.R. Sharma. Model Predictive Control: Simulation Studies for the Implementation on Vertical Take-off and landing Lab Prototype. *Procedia Computer Science* 143: 663-670 (2018).
7. S. Dani, D. Sonawane, D. Ingole, and S.S. Kumar. Performance Evaluation of PID, LQR and MPC for DC Motor Speed Control. *2nd International Conference on for Convergence in Technology, 7th – 9th April 2017, Mumbai India* (2017).
8. N.l. Ismail, K.A. Zakaria, N.S.M. Nasir, M. Syaripuddin, A.S.N. Mokhtar, and S. Thanakdi. DC Motor Speed Control using Fuzzy Logic Controller. *2nd International Conference on Engineering and Technology, 23rd – 24th November 2017, Palm Garden, Putrajaya, Malaysia* (2017).
9. U.K. Bansal, and R. Narvey. Speed Control of DC Motor using Fuzzy PID Controller. *Advance in Electronic and Electronic Engineering* 3(9): 1209-1220 (2013).
10. R. Kushwah, and S. Wadhwani. Speed Control of Separately Excited DC Motor using Fuzzy Logic Controller. *International Journal of Engineering Trends and Technology* 4(6)*:* 2518-2523 (2013).
11. I.H. Usoro, U.T. Itaketo, and M.A. Umoren. Control of a DC Motor using Fuzzy Logic Control Algorithm. *Nigerian Journal of Technology* 36(2)*:* 594-602 (2017).
12. M. Jibril, M. Tadese, and E.A. Tadese. Comparison of DC Motor Speed Control Performance using Fuzzy Logic and Model Predictive Control Method. *International Research Journal of Modernization in Engineering Technology and Science* 2(4): 141-145 (2020).
13. A.L. Hashmia, and S.H. Dakheel. Speed Control of Separately Excited DC Motor using Artificial Neural Network. *Journal of Engineering and Development* 16(4): 349-362 (2012).
14. J. Huspeka. Second Order Sliding Mode Control of the DC Motor. *Proceedings of the 17th International Conference on Process Control, 9th – 12th June 2009,* Štrbské *Pleso, Slovakia* (2009).
15. A. Hashim, and O. Ahmed. Performance Comparison of Sliding Mode Control and Conventional PI Controller for Speed Control of Separately Excited Direct Current Motors. *Journal of Science and Technology* 13(2): 74-80 (2012).
16. G. Jalalu, and P. Rajesh. Design of Sliding Mode Control for DC Motor using LabVIEW. *Journal of Emerging Technologies and Innovative Research* 5(6): 625-629 (2018).
17. A.B. Dumanay, A. Istanbullu, and M. Demirtas. Comparison of PID and SMC Methods in DC Motor Speed Control. *IOSR Journal of Electrical and Electronics Engineering* 2(6): 10-16 (2016).
18. K. Jammousi, Y. Dhieb, M. Yaich, M. Bouzguenda and M. Ghariani. Gain Optimization of Sliding Mode Speed Control for DC Motor. *IEEE International Energy Conference, 28th September to 1st October 2020, Gammarth, Tunisia* (2020).
19. S.E. Benattia, S. Tebbani, and D. Dumur. Linearized Min-Max Robust Predictive Control: Application to the Control of a Bioprocess. *International Journal of Robust Nonlinear Control* 30(1): 1-21 (2019).

Instructions for Authors

Manuscript Format

The manuscript may contain Abstract, Keywords, INTRODUCTION, MATERIALS AND METHODS, RESULTS, DISCUSSION (or RESULTS AND DISCUSSION), CONCLUSIONS, ACKNOWLEDGEMENTS, CONFLICT OF INTEREST and REFERENCES, *and any other information that the author(s) may consider necessary*.

Abstract (font size 10; max 250 words)**:** Must be self-explanatory**,** stating the rationale, objective(s), methodology, main results, and conclusions of the study. Abbreviations, if used, must be defined on the first mention in the Abstract as well as in the main text. Abstract of review articles may have a variable format.

Keywords (font size 10)**:** Three to eight keywords**,** depicting the article.

INTRODUCTION: Provide a clear and concise statement of the problem, citing relevant recent literature, and objectives of the investigation.

MATERIALS AND METHODS: Provide an adequate account of the procedures or experimental details, including statistical tests (if any), concisely but sufficient enough to replicate the study.

RESULTS: Be clear and concise with the help of appropriate Tables, Figures, and other illustrations. Data should not be repeated in Tables and Figures, but must be supported with statistics.

DISCUSSION: Provide interpretation of the RESULTS in the light of previous relevant studies, citing published references.

ACKNOWLEDGEMENTS: (font size 10)**:** In a brief statement, acknowledge the financial support and other assistance.

CONFLICT OF INTEREST: State if there is any conflict of interest.

REFERENCES (font size 10)**:** Cite references in the text **by number only** in **square brackets**, e.g. "Brown et al [2] reported ..." or "... as previously described [3, 6–8]", and list them in the REFERENCES section, in the order of citation in the text, Tables and Figures (not alphabetically). Only published (and accepted for publication) journal articles, books, and book chapters qualify for REFERENCES.

Declaration: Provide a declaration that: (i) the results are original; (ii) the same material is neither published nor under consideration elsewhere; (iii) approval of all authors have been obtained; and (iv) in case the article is accepted for publication, its copyright will be assigned to *Pakistan Academy of Sciences*. Authors must obtain permission to reproduce, where needed, copyrighted material from other sources and ensure that no copyrights are infringed upon.

Manuscript Formatting

Manuscripts must be submitted in Microsoft Word (2007 Version .doc or .docx format); **pdf** files not acceptable. Figures can be submitted in Word format, TIFF, GIF, JPEG, EPS, PPT. Manuscripts, in *Times New Roman*, 1.15spaced (but use single-space for Tables, long headings, and long captions of tables & figures). The text must be typed in a double-column across the paper width. The Manuscript sections must be numbered, i.e., **1. INTRODUCTION, 2. MATERIALS AND METHODS,** and so on… (a) **Title** of the article **(**Capitalize initial letter of each main word; font-size 16; **bold**), max 160 characters (no abbreviations or acronyms), depicting article's contents; (b) Author' first name, middle initial, and last name (font size 12, **bold**), and professional affiliation (i.e., each author's Department, Institution, Mailing address and Email; but no position titles) (font size 12); (c) Indicate the corresponding author with *; (d) **Short running title**, max 50 characters (font size 10).

Headings and Subheadings (font size 11): All flush left

LEVEL-1: **ALL CAPITAL LETTERS; Bold**

Level-2: **Capitalize Each Main Word (**Except prepositions**); Bold**

Level-3: Capitalize each main word (Except prepositions)***; Bold, Italic***

Level-4: *Run-in head*; *Italics*, *in the normal paragraph position. Capitalize the initial word only and end in a colon (i.e., :)*

List of REFERENCES must be prepared as under:

a. Journal Articles *(Name of journals must be stated in full)*

1. I. Golding, J. Paulsson, S.M. Zawilski, and E.C. Cox. Real time kinetics of gene activity in individual bacteria. *Cell* 123: 1025–1036 (2005).
2. W. Bialek, and S. Setayeshgar. Cooperative sensitivity and noise in biochemical signaling. *Physical Review Letters* 100: 258–263 (2008).
3. R.K. Robert, and C.R.L.Thompson. Forming patterns in development without morphogen gradients: differentiation and sorting. *Cold Spring Harbor Perspectives in Biology* 1(6) (2009).
4. D. Fravel. Commercialization and implementation of biocontrol. *Annual Reviews of Phytopathology* 43: 337359 (2005).

b. Books

5. W.R. Luellen. Fine-Tuning Your Writing. *Wise Owl Publishing Company, Madison, WI, USA* (2001).
6. U. Alon, and D.N. Wegner (Ed.). An Introduction to Systems Biology: Design Principles of Biological Circuits. *Chapman & Hall/CRC, Boca Raton, FL, USA* (2006).

c. Book Chapters

7. M.S. Sarnthein, and J.D. Stanford. Basal sauropodomorpha: historical and recent phylogenetic developments. In: The Northern North Atlantic: A Changing Environment. P.R. Schafer, & W. Schluter (Ed.), *Springer, Berlin, Germany*, pp. 365–410 (2000).
8. J.E. Smolen, and L.A. Boxer. Functions of Europhiles. In: Hematology, 4th ed. W.J. Williams., E. Butler and M.A. Litchman (Ed.), *McGraw Hill, New York, USA*, pp. 103–101 (1991).

d. Reports

9. M.D. Sobsey, and F.K. Pfaender. Evaluation of the H2S method for Detection of Fecal Contamination of Drinking Water, Report WHO/SDE/WSH/02.08, *Water Sanitation and Health Programme, WHO, Geneva, Switzerland* (2002).

e. Online references

These should specify the full URL for reference and give the date on which it was consulted. Please check again to confirm that the work you are citing is still accessible:

10. L. Branston. SENSPOL: Sensors for Monitoring Water Pollution from Contaminated Land, Landfills and Sediment (2000). http://www.cranfield.ac.uk/biotech/senspol/ (accessed 22 July 2005)

Tables and Figures

Insert all tables as editable text, not as images. Number tables consecutively following their appearance in the text, Figures should appear in numerical order, be described in the body of the text, and be positioned close to where they are first cited. Each figure should have a caption that describes the illustration, and that can be understood independently of the main text (Caption Table 1. and Fig 1. font size 10; Bold; Captions should be in sentence case; left-aligned). All Figures should have sufficiently high resolution (minimum 1000 pixels width/height, or a resolution of 300 dpi or higher) to enhance the readability. Figures may be printed in two sizes: column width of 8.0 cm or page width of 16.5 cm; number them as **Fig. 1**, **Fig. 2**, … in the order of citation in the text. Parts in a figure can be identified by A, B, C, D, ... and cited as Figure 2A, Figure 2B, Figure 2C. Captions to Figures must be concise but self-explanatory. Laser printed line drawings are acceptable. Do not use lettering smaller than 9 points or unnecessarily large. Photographs must be of high quality. A scale bar should be provided on all photomicrographs.

Tables: with concise but self-explanatory headings must be numbered according to the order of citation (like **Table 1.**, **Table 2.**). *Do not* abbreviate the word "Table" to "Tab.". Round off data to the nearest three significant digits. Provide essential explanatory footnotes, with superscript letters or symbols keyed to the data. Do not use vertical or horizontal lines, except for separating column heads from the data and at end of the Table.

Figures: Figures may be printed in two sizes: column width of 8.0 cm or page width of 16.5 cm; number them as **Fig. 1**, **Fig. 2**, … in the order of citation in the text. Captions to Figures must be concise but self-explanatory. Laser printed line drawings are acceptable. Do not use lettering smaller than 9 points or unnecessarily large. Photographs must be of high quality. A scale bar should be provided on all photomicrographs.

Note: The template of the manuscript is available at http://www.paspk.org/proceedings/; http://ppaspk.org/

Reviewers: Authors may suggest four relevant reviewers, two National and two International (with their **institutional E-mail** addresses).

SUBMISSION CHECKLIST

The following list will be useful during the final checking of an article before sending it to the journal for review.

Ensure that the following items are present:

One author has been designated as the corresponding author with contact details:

• E-mail address (Correct and valid)

• Full address of Institute/organization

• Keywords

• All figure captions

• All tables (including title, description, footnotes)

Further considerations

• Manuscript has been 'spell-checked' and 'grammar checked'

• References are in the correct format for this journal

• All references mentioned in the Reference list are cited in the text, and vice versa

• Permission has been obtained for the use of copyrighted material from other sources (including the Internet)

In case of any difficulty while submitting your manuscript, please get in touch with:

Editor
Pakistan Academy of Sciences
3-Constitution Avenue, Sector G-5/2
Islamabad, Pakistan
Email: editor@paspk.org
Tel: +92-51-920 7140
Websites: http://www.paspk.org/proceedings/; http://ppaspk.org/

PROCEEDINGS OF THE
PAKISTAN ACADEMY OF SCIENCES: PART A
Physical and Computational Sciences

CONTENTS

Volume 61, No. 1, March 2024 **Page**

Research Articles

PAKISTAN ACADEMY OF SCIENCES, ISLAMABAD, PAKISTAN

HEC Recognized; Scopus Indexed

Websites: http://www.paspk.org/proceedings/; http://ppaspk.org